Title
North Pacific Climate, Ocean Circulation, And Productivity Over Millennial And Orbital Timescales

Author
Knudson, Karla Phan

Publication Date
2015

Peer reviewed|Thesis/dissertation

UNIVERSITY OF CALIFORNIA
SANTA CRUZ

NORTH PACIFIC CLIMATE, OCEAN CIRCULATION, AND PRODUCTIVITY OVER MILLENNIAL AND ORBITAL TIMESCALES

A dissertation submitted in partial satisfaction
of the requirements for the degree of

DOCTOR OF PHILOSOPHY

in

EARTH SCIENCES

by

Karla Phan Knudson

December 2015

The Dissertation of Karla Knudson is approved:

____
Professor Ana Christina Ravelo, chair

____
Professor James Zachos

____
Professor Ivano Aiello

____
Tyrus Miller
Vice Provost and Dean of Graduate Studies

Table of Contents

List of Figures

CHAPTER 1

CHAPTER 2

CHAPTER 3

Abstract

North Pacific climate, ocean circulation, and productivity over millennial and orbital timescales

by

Karla P. Knudson

Due to processes that are poorly understood, the arctic/subarctic region is currently warming at approximately twice the rate of the rest of the globe, and these regional changes may in turn have important consequences on global climate. The Bering Sea is an ideal location to study the relationship between sea ice distribution, ocean circulation, and biological productivity, which are all thought to be components of important interactions that both respond to and influence climate changes on regional (North Pacific) to global scales. Geologic records are essential for understanding and predicting future oceanic and climatic changes, but most previous studies of Bering Sea and North Pacific climate and oceanic conditions were limited by short records that only spanned one glacial-interglacial climate cycle (~100 kyr). This dissertation presents new geochemical and sedimentological records of oceanic and climatic conditions over the past 1.2 Myr using sediment cores from Integrated Ocean Drilling Program Site U1342 (54.83°N, 176.92°E, 818 m water depth) in the Bering Sea, providing an unprecedented opportunity to examine trends over multiple glacial-interglacial cycles. Long benthic foraminiferal stable isotope records from Site U1342 provide the first evidence of an important recurring relationship in which extremely cold glacial conditions lead to enhanced Bering Sea ice extent and enhanced local formation of North Pacific Intermediate Water (NPIW), the water mass primarily associated with large-scale North Pacific circulation and heat transport. These results contradict model predictions for weaker NPIW formation during extreme glacial conditions and show that North Pacific and North Atlantic circulation acted in phase on glacial-interglacial timescales. Furthermore, new records of nitrate utilization based on nitrogen isotopes demonstrate that glacial climates were consistently associated with enhanced physical stratification in the Bering Sea, which resulted in increased utilization of nutrients by phytoplankton and a reduction in the carbon dioxide released from the ocean to the atmosphere. Finally, multiple new records that demonstrate high productivity during intervals of laminated sediments, which represent brief anoxic events, indicate that interglacial climates precondition the Bering Sea for rapid oceanic and biological change.

Acknowledgements

Firstly, I am extremely grateful for the support and mentorship from my advisor, Dr. Ana Christina Ravelo, who has provided me with invaluable opportunities and has had tremendous influence in shaping me as a scientist. Working with her, I have increased my "knowledge," but more importantly, I have also increased my ability to think critically, as she has shown me how to identify key scientific problems, how to ask myself the questions that will move me towards finding a solution, and how to provide the strongest and most credible support for my scientific arguments. I feel extremely fortunate to have had the opportunity to work with such a bright, dedicated, and encouraging mentor for the past five years.

I would also like to thank my other Ph.D. committee members, Dr. James Zachos and Dr. Ivano Aiello, who have supported me both professionally and personally over the last five years. Their expertise and insights have been incredibly beneficial to my research. My sincere thanks also goes to my former and current labmates, who have fostered my growth and research through stimulating discussions, moral support, and help in teaching me new laboratory techniques.

Additionally, I would like to thank the entire Integrated Ocean Drilling Program Expedition 323 Shipboard Party, whose efforts led to the collection of the one-of-a-kind sediment cores that are the basis of all three chapters of this thesis. I would particularly like to acknowledge Dr. Kozo Takahashi and Dr. Ravelo, who were co-chief scientists on this research cruise and thus played a lead role in conceiving and executing Expedition 323. Thanks largely to their foresight and ingenuity in pursuing these records, I have been able to address some of the most fascinating questions regarding regional and global climate change, ocean circulation, and biogeochemical cycling.

Furthermore, with over 1,000 samples and multiple types of analyses, this research could not have been completed without the laboratory assistance of several undergraduate workers, who helped to prepare my samples, and Dr. Dyke Andreasen, Chih-Ting Hsieh, Timothy Lambert, and Colin Carney, who worked tirelessly to maintain the several instruments that I used to conduct my research. I particularly thank Dyke for his patience in training me to use the different instruments and teaching me how to robustly analyze the results given instrumental uncertainties.

Last but not the least, I would like to express my deep gratitude to all of my family, friends, and past teachers, professors, and mentors who have inspired my love for the earth sciences and have motivated me to pursue the long road of graduate school. I especially would like to acknowledge the support of my parents, Karl and Clara; my amazing siblings, Christina, Michael, and Jonathan; and my always-encouraging husband, Peter.

The text of this dissertation includes reprints of the following previously published material:

Knudson, K.P., Ravelo, A.C., 2015. North Pacific Intermediate Water circulation enhanced by the closure of the Bering Strait. Paleoceanography (in press), doi:10.1002/2015PA002840.

Knudson, K.P., Ravelo, A.C., 2015. Enhanced subarctic Pacific stratification and nutrient utilization during glacials over the last 1.2 Myr. Geophysical Research Letters (in press), doi:10.1002/2015GL066317.

The co-author listed in these publications (A.C. Ravelo) directed and supervised the research that forms the basis for the dissertation.

Introduction

Background and Motivation

Understanding how climate has behaved in the past and what mechanisms controlled it is critical to our ability to predict how it will respond to ongoing natural and anthropogenic climate forcing. While recent rapid changes have been occurring globally, climate changes within the Arctic/subarctic are of particular interest, as warming in this region has exceeded that of the global average [Screen and Simmonds, 2010; Serreze and Francis, 2006]. This "arctic amplification" affects complicated regional dynamics and climate feedbacks that are still poorly understood, including important interactions between oceanic and atmospheric circulation, heat flux, sea ice, and marine biological productivity. In turn, these dynamic Arctic/subarctic processes may have a significant effect on regional and global climate, as well as regional marine ecosystems.

Of the Arctic/subarctic regions, North Pacific sector is particularly enigmatic, because we have an exceptionally limited understanding of its past behavior and climate interactions. Geological records have the capability to provide evidence of past changes in climatic, oceanic, and biological parameters; however previous paleoceanographic studies from the subarctic Pacific were limited by short piston cores that only extended through the last glacial cycle [Brunelle et al., 2007;

Cook et al., 2005; Okazaki et al., 2005b; Tanaka and Takahashi, 2005]. These records are not long enough to determine whether there are consistent, recurring trends over long timescales or whether there are predictable mechanisms that control rapid changes. Due to these limitations, many fundamental questions about North Pacific climate, ocean circulation, and biological productivity still exist, such as: What is the range of climate variability in this region? Do the regional responses to climate change (e.g. temperature, sea ice, ocean circulation, biological productivity) provide predictable feedbacks that subsequently influence regional and global climate? On what timescales do these processes operate? Does North Pacific circulation display a predictable pattern of change in association with climate variability? Does North Pacific circulation and climate act in phase with the North Atlantic on orbital timescales?

New opportunities to answer these questions have arisen since the Integrated Ocean Drilling Program (IODP) Expedition 323 to the Bering Sea in 2009 drilled several high-resolution, continuous cores that extend through several late-Pleistocene glacial-interglacial cycles. The Bering Sea has high sediment accumulation rates and represents a gateway between the Arctic Ocean and the North Pacific Ocean, making it an ideal location to study the interaction between sea ice distribution, ocean circulation, biological productivity and the high-latitude biological carbon cycle—all feedbacks that generate rapid and long-term climate changes. The Bering Sea is connected to the North Pacific through several deep channels, allowing it to continuously communicate with the largest water mass on earth and record large-scale oceanic changes. At the same time, as the Bering Sea is connected to the Arctic through the shallow (~50 m) Bering Strait, the Bering Sea is a sensitive place to record high-frequency circulation changes due to changes sea level and sea ice. In addition, the Bering Sea is ecologically significant as it is one of the most biologically productive areas in the world [Springer et al., 1996] and represents a region that has gained attention for its potential to influence the carbon cycle [Jaccard et al., 2010].

Overview of Chapters

This dissertation presents new paleoceanographic records from IODP Expedition 323 Site U1342 (54.83°N, 176.92°E, 818 m water depth) to investigate the nature and causes of rapid to orbital-scale changes in North Pacific climate, ocean circulation, biological productivity and nutrient use over the last 1.2 Myr. This work is divided into three chapters, which are briefly described below.

Chapter One: North Pacific Intermediate Water formation enhanced by the closure of the Bering Strait

In Chapter 1, we investigate the basic relationship between large-scale Pacific circulation (i.e. "meridional overturning circulation") and climate over glacial-interglacial timescales. Meridional overturning circulation (MOC) is thought to be very important to regional and global climate, because it is responsible for the redistribution of heat, greenhouse gases, and biologically significant nutrients amongst the world's oceans. The densest water mass formed in the North Pacific is North Pacific Intermediate Water (NPIW), and this is thus the water mass associated with Pacific MOC. While previous studies over the last glacial cycle provided evidence for enhanced NPIW formation during the Last Glacial Maximum [Cook et al., 2005; Horikawa et al., 2010; Matsumoto et al., 2002; Okazaki et al., 2005a; Tanaka and Takahashi, 2005], whether Northern Hemisphere glacial climates were consistently associated with increased NPIW production was still unknown.

Using benthic foraminiferal stable isotopes ($\delta^{18}O$ and $\delta^{13}C$) to reconstruct changes in regional climate and NPIW, we provide the first evidence of for a recurring relationship between climate and NPIW by demonstrating that NPIW was enhanced during each of the extreme glacials associated with the closure of the Bering Strait since 1.2 Ma. Furthermore, our long records of NPIW provide the first opportunity to evaluate whether there is an orbital-scale relationship between NPIW and North Atlantic Deep Water (NADW), the water mass associated with North Atlantic MOC. While several modeling studies predict that the closure of the Bering Strait should cause NPIW formation to weaken and NADW formation to strengthen [Hu et al., 2015; Hu et al., 2010; Okazaki et al., 2010; Saenko et al., 2004; Shaffer and Bendtsen, 1994], our results demonstrate that NPIW and upper NADW both are both enhanced when the Bering Strait is closed. These results therefore provide a new fundamental understanding of the behavior of Pacific MOC on orbital timescales and demonstrate the importance of paleoceanographic data as a test bed for the validation of global ocean-climate models.

Chapter Two: Enhanced subarctic Pacific stratification and nutrient

utilization during glacials over the last 1.2 Myr

In Chapter 2, we investigate the relationship between climate, nutrient utilization, and biological productivity in the Bering Sea. The subarctic Pacific and the Southern Ocean represent the two main high-nutrient, low productivity (or chlorophyll) (HNLC) areas on Earth [Boyd et al., 2007], and some paleoceanographic records have shown that these regions have great potential for enhanced phytoplankton productivity and associated carbon dioxide sequestration [Francois et al., 1997; Galbraith et al., 2007; Haug et al., 1999; Jaccard et al., 2010; Sigman et al., 2010]. There has been significant debate over whether changes in iron supply and/or ocean stratification could explain fluctuations in nutrient utilization and productivity in the subarctic Pacific and Southern Ocean, but previous studies were unable to evaluate these potential mechanisms because they were limited by short records and/or poor age control.

Chapter 2 presents new records of sedimentary nitrogen isotopes from Site U1342, which provide the longest, highest resolution dataset from any polar HNLC area. These records provide the unprecedented opportunity to evaluate variability and recurring trends in nutrient utilization over many glacial-interglacial cycles in order to determine the role that subartic Pacific may play in responding to and influencing climate through changes in regional carbon flux between the ocean and the atmosphere. Our results demonstrate that subarctic Pacific nitrate utilization was enhanced during every previous glacial since 1.2 Ma. Furthermore, we show that physical ocean stratification controlled orbital-scale nutrient utilization and air-sea flux, and that iron fertilization was not a major factor controlling nutrient utilization. As both biological productivity and stratification exert an important control over the ocean-atmosphere exchange of carbon dioxide, these findings are of high importance to our understanding of past atmospheric carbon dioxide concentrations and biogeochemical climate feedbacks.

Chapter Three: Abrupt anoxic events in the Bering Sea caused by enhanced primary productivity

One of the pressing issues concerning global change is understanding how climate variability is related to oceanic oxygen concentrations and biological primary productivity. Climate warming is predicted to result in the loss of dissolved oxygen content (i.e. "deoxygenation") throughout the world's oceans and has already been observed in some locations in the subarctic North Pacific and the tropics over the last few decades [Nakanowatari et al., 2007; Ono et al., 2001; Stramma et al., 2008; Whitney et al., 2007]. Paleoceanographic records can help us to understand the trends and causes of oceanic deoxygenation; however previous North Pacific studies, which were limited to the last glacial cycle, are too short to provide recurring trends that can help us to understand whether the timing and mechanisms of deoxygenation events are predictable.

Chapter 3 examines millennial-scale variability in nitrogen and productivity records from Site U1342 in the Bering Sea, a site which contains several abrupt intervals of laminated sediments representing episodic anoxic events occuring since 1.2 Ma. In doing so, Chapter 3 provides the first high-resolution analysis of abrupt

North Pacific anoxic events over multiple glacial-interglacial cycles and represents the first study to identify some key trends and nuances in the relationship between climate, productivity, and rapid deoxygenation. This chapter builds on the foundation of Chapter 2, which focused on orbital scale glacial-interglacial variations in climate, productivity, and nitrate utilization, and but did not look at higher-frequency variability in nitrate utilization and productivity in detail.

References

Boyd, P.W., Jickells, T., Law, C.S., Blain, S., Boyle, E.A., Buesseler, K.O., Coale, K.H., Cullen, J.J., de Baar, H.J.W., Follows, M., Harvey, M., Lancelot, C., Levasseur, M., Owens, N.P.J., Pollard, R., Rivkin, R.B., Sarmiento, J., Schoemann, V., Smetacek, V., Takeda, S., Tsuda, A., Turner, S., Watson, A.J., 2007. Mesoscale iron enrichment experiments 1993-2005: Synthesis and future directions. Science 315, 612-617, doi:10.1126/science.1131669.

Brunelle, B.G., Sigman, D.M., Cook, M.S., Keigwin, L.D., Haug, G.H., Plessen, B., Schettler, G., Jaccard, S.L., 2007. Evidence from diatom-bound nitrogen isotopes for subarctic Pacific stratification during the last ice age and a link to North Pacific denitrification changes. Paleoceanography 22, doi:10.1029/2005pa001205.

Cook, M.S., Keigwin, L.D., Sancetta, C.A., 2005. The deglacial history of surface and intermediate water of the Bering Sea. Deep-Sea Research Part II-Topical Studies in Oceanography 52, 2163-2173, doi:10.1016/j.dsr2.2005.07.004.

Francois, R., Altabet, M.A., Yu, E.F., Sigman, D.M., Bacon, M.P., Frank, M., Bohrmann, G., Bareille, G., Labeyrie, L.D., 1997. Contribution of Southern Ocean surface-water stratification to low atmospheric CO2 concentrations during the last glacial period. Nature 389, 929-935, doi:10.1038/40073.

Galbraith, E.D., Jaccard, S.L., Pedersen, T.F., Sigman, D.M., Haug, G.H., Cook, M., Southon, J.R., Francois, R., 2007. Carbon dioxide release from the North Pacific abyss during the last deglaciation. Nature 449, 890-U899, doi:10.1038/nature06227.

Haug, G.H., Sigman, D.M., Tiedemann, R., Pedersen, T.F., Sarnthein, M., 1999. Onset of permanent stratification in the subarctic Pacific Ocean. Nature 401, 779-782, doi:10.1038/44550.

Horikawa, K., Asahara, Y., Yamamoto, K., Okazaki, Y., 2010. Intermediate water formation in the Bering Sea during glacial periods: Evidence from neodymium isotope ratios. Geology 38, 435-438, doi:10.1130/g30225.1.

Hu, A.X., Meehl, G.A., Han, W.Q., Otto-Bliestner, B., Abe-Ouchi, A., Rosenbloom, N., 2015. Effects of the Bering Strait closure on AMOC and global climate under different background climates. Progress in Oceanography 132, 174-196, doi:10.1016/j.pocean.2014.02.004.

Hu, A.X., Meehl, G.A., Otto-Bliesner, B.L., Waelbroeck, C., Han, W.Q., Loutre, M.F., Lambeck, K., Mitrovica, J.X., Rosenbloom, N., 2010. Influence of Bering Strait flow and North Atlantic circulation on glacial sea-level changes. Nature Geoscience 3, 118-121, doi:10.1038/ngeo729.

Jaccard, S.L., Galbraith, E.D., Sigman, D.M., Haug, G.H., 2010. A pervasive link between Antarctic ice core and subarctic Pacific sediment records over the past 800 kyrs. Quaternary Science Reviews 29, 206-212, doi:10.1016/j.quascirev.2009.10.007.

Matsumoto, K., Oba, T., Lynch-Stieglitz, J., Yamamoto, H., 2002. Interior hydrography and circulation of the glacial Pacific Ocean. Quaternary Science Reviews 21, 1693-1704, doi:10.1016/s0277-3791(01)00142-1.

Nakanowatari, T., K. I. Ohshima, and M. Wakatsuchi (2007), Warming and oxygen decrease of intermediate water in the northwestern North Pacific, originating from the Sea of Okhotsk, 1955-2004, Geophysical Research Letters, 34(4), doi:10.1029/2006gl028243.

Okazaki, Y., Takahashi, K., Asahi, H., Katsuki, K., Hori, J., Yasuda, H., Sagawa, Y., Tokuyama, H., 2005a. Productivity changes in the Bering Sea during the late Quaternary. Deep-Sea Research Part Ii-Topical Studies in Oceanography 52, 2150-2162, doi:10.1016/j.dsr2.2005.07.003.

Okazaki, Y., Takahashi, K., Katsuki, K., Ono, A., Hori, J., Sakamoto, T., Uchida, M., Shibata, Y., Ikehara, M., Aoki, K., 2005b. Late Quaternary paleoceanographic changes in the southwestern Okhotsk Sea: Evidence from geochemical, radiolarian, and diatom records. Deep-Sea Research Part II-Topical Studies in Oceanography 52, 2332-2350, doi:10.1016/j.dsr2.2005.07.007.

Okazaki, Y., Timmermann, A., Menviel, L., Harada, N., Abe-Ouchi, A., Chikamoto, M.O., Mouchet, A., Asahi, H., 2010. Deepwater Formation in the North Pacific During the Last Glacial Termination. Science 329, 200-204, doi:10.1126/science.1190612.

Ono, T., T. Midorikawa, Y. W. Watanabe, K. Tadokoro, and T. Saino (2001), Temporal increases of phosphate and apparent oxygen utilization in the subsurface waters of western subarctic Pacific from 1968 to 1998, Geophysical Research Letters, 28(17), 3285-3288, doi:10.1029/2001gl012948.

Saenko, O.A., Schmittner, A., Weaver, A.J., 2004. The Atlantic-Pacific seesaw. Journal of Climate 17, 2033-2038, doi:10.1175/1520-0442(2004)017<2033:tas>2.0.co;2.

Screen, J.A., Simmonds, I., 2010. The central role of diminishing sea ice in recent Arctic temperature amplification. Nature 464, 1334-1337, doi:10.1038/nature09051.

Serreze, M.C., Francis, J.A., 2006. The arctic amplification debate. Climatic Change 76, 241-264, doi:10.1007/s10584-005-9017-y.

Shaffer, G., Bendtsen, J., 1994. Role of the Bering Strait in controlling North Atlantic ocean circulation and climate. Nature 367, 354-357, doi:10.1038/367354a0.

Sigman, D.M., Hain, M.P., Haug, G.H., 2010. The polar ocean and glacial cycles in atmospheric CO2 concentration. Nature 466, 47-55, doi:10.1038/nature09149.

Springer, A.M., McRoy, C.P., Flint, M.V., 1996. The Bering Sea Green Belt: Shelf-edge processes and ecosystem production. Fisheries Oceanography 5, 205-223, doi:10.1111/j.1365-2419.1996.tb00118.x.

Stramma, L., G. C. Johnson, J. Sprintall, and V. Mohrholz (2008), Expanding oxygen-minimum zones in the tropical oceans, Science, 320(5876), 655-658, doi:10.1126/science.1153847.

Tanaka, S., Takahashi, K., 2005. Late Quaternary paleoceanographic changes in the Bering Sea and the western subarctic Pacific based on radiolarian assemblages. Deep-Sea Research Part II-Topical Studies in Oceanography 52, 2131-2149, doi:10.1016/j.dsr2.2005.07.002.

Whitney, F. A., H. J. Freeland, and M. Robert (2007), Persistently declining oxygen levels in the interior waters of the eastern subarctic Pacific, Progress in Oceanography, 75(2), 179-199, doi:10.1016/j.pocean.2007.08.007.

Chapter 1

North Pacific Intermediate Water formation enhanced by the closure of the Bering Strait

Abstract

The Bering Strait provides a shallow connection that allows freshwater to flow from the North Pacific into the North Atlantic, but this passage was closed during past glacials when sea level was at least 50 m lower than at present. Climate models investigating Bering Strait closure predict that this mechanism increases the salinity in the North Atlantic and reduces the salinity in the North Pacific, inducing a Pacific-Atlantic seesaw in meridional overturning circulation and poleward heat flux. However, the Pacific circulation response to Bering Strait closure, and thus the seesaw theory, has not been tested by long paleoceanographic records. We present long records of foraminiferal $\delta^{18}O$ and $\delta^{13}C$ from Integrated Ocean Drilling Program Site U1342 in the Bering Sea, which provide the first evidence of enhanced North Pacific Intermediate Water when the Bering Strait was closed during each of the extreme glacials of the last 1.2 Myr. These results suggest that orbital-scale variations in North Pacific Intermediate Water are coherent and in

phase with variations in upper North Atlantic Deep Water, but are unrelated to changes in lower North Atlantic Deep Water. Together, these results provide evidence for systematic, orbital-scale variability in North Pacific Ocean circulation and may challenge the idea of an orbital-scale Pacific-Atlantic seesaw.

1. Introduction

The Bering Strait plays a central role in global climate by acting as a freshwater on-off switch modifying the centers of Northern Hemisphere deep water formation that participate in global meridional overturning circulation (MOC) [Hu et al., 2012a; Hu et al., 2010; Hu et al., 2012b; Saenko et al., 2004; Shaffer and Bendtsen, 1994]. Today, ~1 Sv of the relatively low-salinity North Pacific water that enters the Bering Sea flows through the Bering Strait into the Arctic Ocean before eventually feeding into the more saline North Atlantic [Woodgate et al., 2012]. However, because the Bering Strait sill depth is extremely shallow (50 m), through-flow is highly vulnerable to sea level, and thus global climate. During extreme glacials, such as the Last Glacial Maximum (LGM; ~20 ka), the closure of the Bering Strait isolated the North Pacific from the North Atlantic, which is thought to have had profound implications for deep/intermediate water formation and climate feedbacks in both major ocean basins [Hu et al., 2014; Hu et al., 2012a; Hu et al., 2010; Hu et al., 2012b; Okazaki et al., 2010; Saenko et al., 2004; Shaffer and Bendtsen, 1994].

Many model simulations demonstrate that a strong salinity gradient between the Atlantic and Pacific drives opposed changes, or a seesaw, in subsurface circulation strength between the two basins [e.g. Hu et al., 2014; Hu et al., 2012a; Hu et al., 2010; Okazaki et al., 2010; Saenko et al., 2004]. Models looking at the effect of Bering Strait closure predict that isolating the Atlantic from the Pacific causes saltier North Atlantic surface water, decreased stratification, and enhanced Atlantic MOC (AMOC), while simultaneously causing fresher North Pacific surface waters and weaker Pacific MOC (PMOC) [Hu et al., 2014; Hu et al., 2010]. Consequently, these models predicting seesaw behavior indicate that a closed Bering Strait makes the North Atlantic/North Pacific relatively warm/cool compared to an open strait scenario, and this seesaw behavior is superimposed on, and exists independently from, background conditions [Hu et al., 2014; Hu et al., 2010].

In order to test the seesaw hypothesis maintained by modeling results, we need to assess long geological records of the major water masses associated with Northern Hemisphere MOC: North Atlantic Deep Water (NADW) and North Pacific Intermediate Water (NPIW). However, so far the length and quality of records from the North Pacific has been inadequate for determining recurring trends, and available short records do not provide a clear picture of whether or not there was systematic seesaw behavior during the last glacial periods. Observational records investigating millennial-scale seesaw behavior have been limited to the last ~30 kyr and are contradictory, with some radiocarbon evidence supporting the presence of seesaw behavior during Heinrich Event 1 and the Younger Dryas [Max et al., 2014; Okazaki et al., 2010], and other radiocarbon [Sarnthein et al., 2013] and temperature [Max et al., 2012] evidence supporting in-phase relationships between the Atlantic and Pacific. No records have yet investigated possible orbital-scale seesaw behavior. Moreover, records shorter than one glacial-interglacial (G/IG) cycle cannot determine long-term circulation trends in the context of major climate transitions, nor distinguish how deep and intermediate water masses may differ between weak and strong glacials. Given the importance of understanding how connections through the world's oceans affect regional and global climate, our study aims to use long paleoceanographic records to assess the NPIW-NADW relationship on G/IG timescales. Here we use new, long cores from Integrated Ocean Drilling Program (IODP) Expedition 323 (Figure 1a) in the Bering Sea to generate the first records of orbital-scale changes in NPIW spanning many G/IG cycles over the last 1.2 Myr. These records are then used in comparison with existing orbital-scale records of NADW to reveal observational evidence contradicting the seesaw hypothesis proposed by modeling studies.

2. North Pacific Intermediate Water and the Bering Sea

NPIW, the densest water mass formed in the modern North Pacific Ocean [Talley, 2003], is formed when surface water sinks, carrying atmospherically-equilibrated oxygen into the ocean's interior in a process known as "ventilation." Today, NPIW mostly forms within the Sea of Okhotsk during wintertime sea ice formation, when expelled brine produces extremely dense water masses [Shcherbina et al., 2003; Yasuda, 1997]. The most active regions of brine production occur on the continental shelf within coastal polynyas—open water surrounded by sea ice [Shcherbina et al., 2003; Schumacher et al., 1983].

Evidence for enhanced North Pacific ventilation at shallow to mid-depths during the LGM [Cook et al., 2005; Horikawa et al., 2010; Matsumoto et al., 2002; Okazaki et al., 2005; Tanaka and Takahashi, 2005] has led to the theory that Northern Hemisphere glacial climates are associated with increased NPIW production. The Bering Sea, which has deep connections to the Pacific and was strongly ventilated during the last glacial, has been a suggested source of NPIW [Horikawa et al., 2010; Ohkushi et al., 2003; Rella et al., 2012; Tanaka and Takahashi, 2005]. Trace amounts of deep water recently formed within the Bering Sea demonstrate its potential to supply significant NPIW during glacial periods when sea ice formation and brine rejection were enhanced [Warner and Roden, 1995], and high salinities (up to 35 psu) within Bering Sea polynyas support the feasibility of this mechanism.

3. Study area

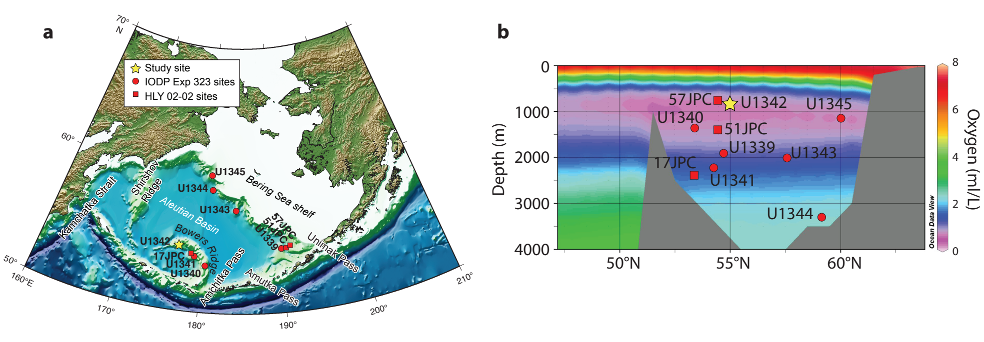

Figure 1. Bering Sea site maps. (a) Locations of IODP Expedition 323 sites in the Bering Sea are marked with red circles (Site U1342 starred), and HLY-02-02 sites

are marked with red squares. **(b)** Bering Sea vertical dissolved oxygen profile along the 180° transect. Site U1342 is located just below modern NPIW, making it ideal for detecting an enhanced and expanded NPIW water mass. Modified from Expedition 323 Scientists [2010].

The Bering Sea exchanges water with the North Pacific through the Kamchatka Strait (~4,000 m sill depth) and the Near Strait (~2,000 m sill depth), which remain open during both glacials and interglacials, allowing the Bering Sea to continuously record changes in North Pacific intermediate and deep water conditions. The focus of our study is the shallowest IODP Expedition 323 site, U1342 (Figure 1a; 818 m water depth), which is ideally situated for detecting changes in NPIW, as it is located near the present-day oxygen minimum zone (~1,000 m; Figure 1b) and the ventilation depth during the last glacial [Horikawa et al., 2010]. Due to its location on the top of Bowers Ridge, Site U1342 also likely benefits from winnowing, which removes organic matter and contributes to excellent foraminifera preservation. The sedimentation rate (4.5 cm/kyr) at this site is high enough to resolve orbital scale variability, but lower compared to other Expedition 323 Bering Sea sites (up to 45 cm/kyr) and other Bowers Ridge sites (12 cm/kyr), allowing longer exposure time of the sediment to the deep water. As a consequence, profiles of interstitial water sulfate, dissolved inorganic carbon, phosphate, and ammonium demonstrate that this site has low rates of anaerobic carbon mineralization [Expedition 323 Scientists, 2011]. Compared to Site U1341 (Figure 1), a deeper site on the flank of Bowers Ridge with much higher sedimentation rates, U1342 displays ammonium concentrations one order of magnitude lower and phosphate concentrations 50% lower [Expedition 323 Scientists, 2011], further demonstrating the low mineralization rates that benefit Site U1342. Thus, even though the Bering Sea is a region of high productivity, Site U1342 has interstitial chemistry that is less altered by aerobic and anaerobic respiration, and better foraminifera preservation, compared to all other sites drilled during Expedition 323 [Expedition 323 Scientists, 2011]. Due to these advantages, benthic foraminiferal stable carbon isotope measurements can be reliably employed to record water mass changes at Site U1342, as we will later discuss in more detail.

4. Materials and Methods

4.1 Benthic Foraminiferal $\delta^{13}C_c$ and $\delta^{18}O_c$

Cores from Site U1342 were sampled at ~1-3 cm intervals, and 1-3 tests of the benthic foraminifera *Uvigerina peregrina* were picked from the >250 µm fraction, sonicated, and analyzed for calcite $\delta^{13}C$ and $\delta^{18}O$ ($\delta^{13}C_c$ and $\delta^{18}O_c$) at the University of California-Santa Cruz (UCSC) Stable Isotope Laboratory using a FISONS Prism mass spectrometer with a common acid bath device and a MAT253 mass spectrometer with an on-line Kiel device. Values are reported in the per mil (‰) notation relative to Vienna Pee Dee Belemnite (VPDB). Reproducibility of in-house standards is 0.07‰ for $\delta^{18}O$ and 0.03‰ for $\delta^{13}C$. In addition, 4-5 individual U. peregrina tests from six different samples representing peak glacials were measured for $\delta^{13}C_c$ and $\delta^{18}O_c$.

4.2 Benthic Foraminiferal Mg/Ca

U. peregrina from three G/IG pairs were analyzed for Mg/Ca ratios. G/IG pairs were selected based on a rapid $\delta^{18}O_c$ transition, large difference in $\delta^{18}O_c$ G/IG values, and foraminifera availability. Prior to analysis, crushed samples were cleaned according to a modified "Boyle protocol" (Boyle and Keigwin, 1985; Lea and Boyle, 1993): samples were rinsed and sonicated in Milli-Q and methanol, cleaned with reductive and oxidative agents, and transferred into 1.5 mL acid-cleaned vials for a weak acid leach and final Milli-Q rinse. Mg/Ca ratios were analyzed at UCSC using a Perkin-Elmer Optima 8300 inductively coupled plasma optical emission spectrometer (ICP-OES). Long-term reproducibility for a liquid consistency standard and foraminifera standards are 0.0254 mmol/mol and 0.176 mmol/mol, respectively.

4.3 Carbonate-free Sediment Stable Isotope Analyses

Sediments for carbonate-free analysis were freeze-dried and crushed by hand using a mortar and pestle, acidified using a buffered solution of glacial acetic acid, and rinsed and centrifuged several times to remove acid. Samples were analyzed for $\delta^{13}C$, wt.%C, and C:N ratio on a Carlo Erba 1108 elemental analyzer interfaced to a Thermo Finnigan Delta Plus XP IRMS, at the UCSC Stable Isotope Laboratory. Carbon mass accumulation rate (CMAR) was calculated as dry bulk density × sedimentation rate × wt.%C.

4.4 Age Model and Spectral Analyses

The U1342 age model, Blackman-Tukey spectral analyses, and cross-phase spectra were completed with AnalySeries 2.0 [Paillard et al., 1996]. The U1342 age model was created using tie points to the LR04 $\delta^{18}O_c$ stack from Lisiecki and Raymo [2005] (Figure 2a and Table A1 in Appendix A), and therefore these records can be compared relative to each other. A discussion of the use of the LR04 stack in tuning the U1342 age model can be found in Appendix A (Text A1).

4.5 Stable Isotope Difference Calculations

To compare $\delta^{13}C_c$ from Site U1342 to Site 849 (0°11'N, 110°31'W; 3,851 m) [Mix et al., 1995], U1342 $\delta^{13}C_c$ values have been converted to the $\delta^{13}C_c$ values of *Cibicidoides wuellerstorfi*, using the standard adjustment of +0.90‰ demonstrated by other studies [Duplessy et al., 1984; Mix et al., 1995]. To better compare the records at Site U1342 and Site 849, slight adjustments were made to update the published Site 849 age model (see Table A2 in Appendix A). $\Delta\delta^{13}C$ and $\Delta\delta^{18}O$ values were calculated based on absolute U1342 $\delta^{13}C_c$ and $\delta^{18}O_c$ values, which were interpolated to the average interval between U1342 samples (~1.4 kyr), averaged over a 3-point running window, and then subtracted from a similarly interpolated record from Site 849. By using this method, high-frequency millennial-scale variability at U1342 was smoothed out, allowing for the comparison of orbital variations between the records at U1342 and lower-resolution records from other sites. To compare North Atlantic sites ODP 982 (57°31'N, 15°53'W; 1,135 m) [Venz et al., 1999] and DSDP Site 607 (41°00'N, 32°58'W; 3,427 m) [Ruddiman et al., 1989] to Site 849, $\Delta\delta^{13}C$ for both datasets was similarly calculated, using an interpolation interval of 1.5 kyr.

4.6 Glacial vs. Interglacial and Open vs. Closed Bering Strait

Where applicable, "glacial" or "interglacial" points were defined as those 1 sigma above or below a 100 kyr moving window of an interpolated three-point running mean of U1342 $\delta^{18}O_c$. Data were further classified according to whether relative sea level (RSL) was above and below -50 m (open vs. closed Bering Strait). RSL from 0-514 ka was assigned from Rohling et al. [2009] and RSL from 515-1200 ka was assigned from Sosdian and Rosenthal [2009]. These RSL estimates are precise enough to capture the general orbital-scale relationship between RSL and water mass distribution, even though the magnitude of local variations in RSL in the Bering Strait region may differ by ~25% [e.g. Clark et al., 2002] from the global RSL variations, depending on local isostatic adjustment and the individual effect of ice sheet volume changes, or "fingerprinting."

5. Stable Isotope Results from U1342

5.1 U1342 $\delta^{18}O$ Stratigraphy and Age Model

The new record of benthic $\delta^{18}O_c$ at Site U1342 was used to create the first published age model for this site (Table A1 in Appendix A) and displays all marine isotope stages (MIS) since 1.2 Ma (Figure 2a). The values of $\delta^{18}O_c$ range from ~2.5 to ~4.5‰, with typical G/IG change of only ~1‰. Comparison with the LR04 benthic stack [Lisiecki and Raymo, 2005]—a compilation of 57 globally-distributed $\delta^{18}O_c$ records used to represent the global average—indicates that the G/IG $\delta^{18}O_c$ range at U1342 (~1‰) is smaller than that of the LR04 stack (~1.5‰) primarily because the glacial (high $\delta^{18}O_c$) values at U1342 are not as extreme (Figure 2a).

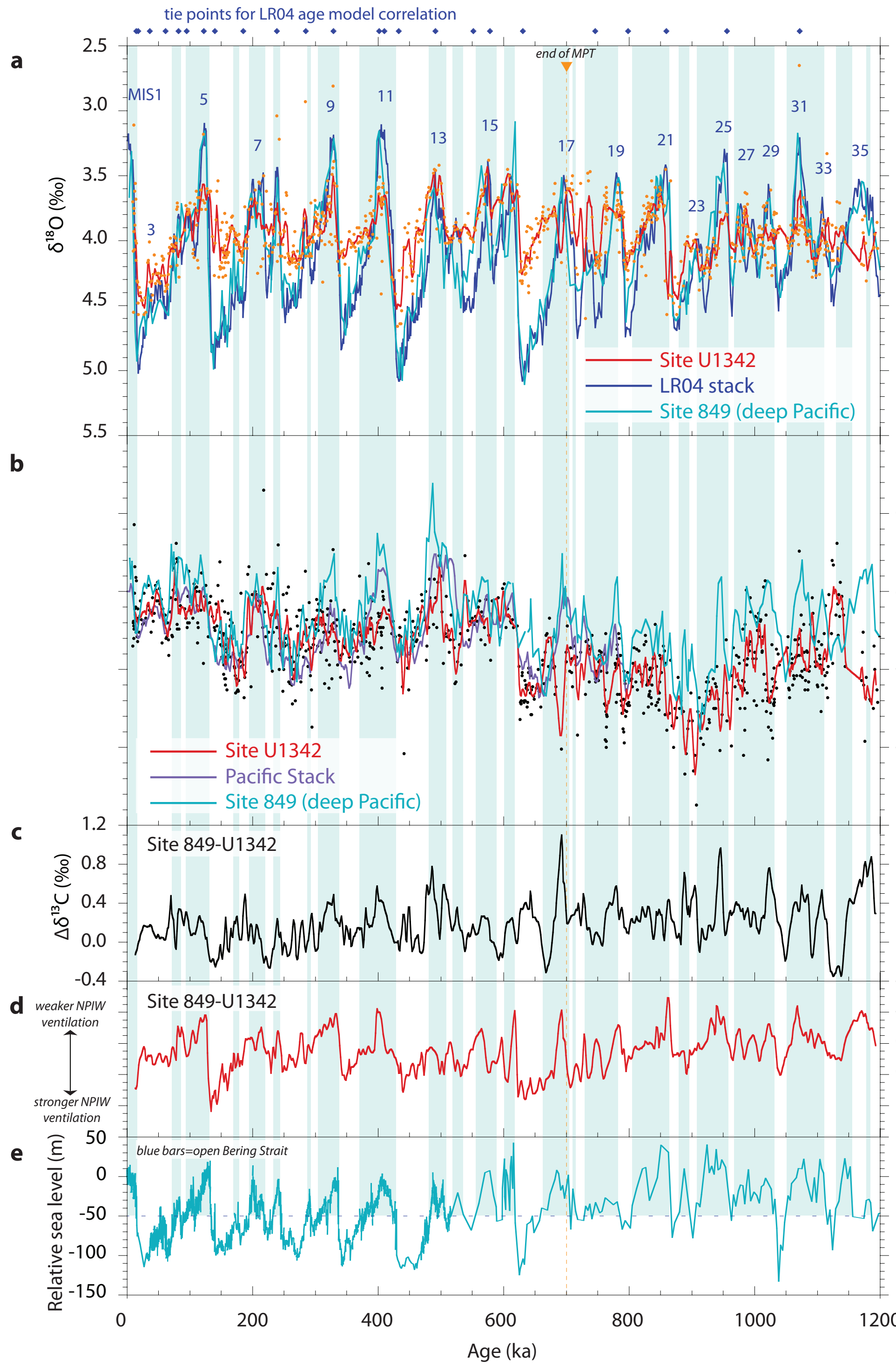

Figure 2. Geochemical records showing changes in climate and NPIW. (a) Benthic foraminiferal $\delta^{18}O_c$ records from Site U1342 (red line indicates three-point

smoothed, interpolated running mean and orange dots indicate original data points), the LR04 stack (dark blue) from Lisiecki and Raymo [2005], and deep equatorial Pacific Site 849 (teal blue) from Mix et al. [1995]. Blue diamonds show tie points used for U1342 age model age correlation with LR04 stack. **(b)** Benthic foraminiferal $\delta^{13}C_c$ of Site U1342 (red line indicates three-point smoothed, interpolated running mean and black dots indicate original data points), compared with Site 849 (teal blue line) and the deep Pacific stack from Lisiecki [2010] (blue line). **(c)** $\Delta\delta^{13}C_{849\text{-}U1342}$ is used here as a proxy for the presence of NPIW. **(d)** $\Delta\delta^{18}O_{849\text{-}U1342}$ is also an indicator of NPIW ventilation. **(e)** Relative sea level: 0-514 ka from Rohling et al. [2009] and 515-1200 ka from Sosdian and Rosenthal [2009]. Blue vertical bars correspond with values above the Bering Strait depth (dashed line; -50 m), indicating open Bering Strait conditions. The end of the Mid-Pleistocene Transition (MPT; 700 ka) is marked by the vertical dotted orange line.

The relatively small G/IG $\delta^{18}O_c$ amplitude at U1342 appears robust, as the quality of the record is supported by high sedimentation rates, continuous recovery, and continuous foraminifera preservation. Additionally, single foraminifer replicates show little $\delta^{18}O_c$ variability (1σ = 0.08 to 0.20‰; Table A3 in Appendix A), indicating that mixing (bioturbation) between G/IG extremes is not responsible for the relatively low-amplitude $\delta^{18}O_c$ variability.

5.2 U1342 $\delta^{13}C$ Stratigraphy

The $\delta^{13}C_c$ record at Site U1342 displays values ranging between about -1.5‰ and 0.7‰, with most of the lowest values occurring in the oldest 250 kyr of the record. Compared to two records that may be taken to represent whole-Pacific records of $\delta^{13}C$, the Lisiecki deep Pacific $\delta^{13}C_c$ Stack [Lisiecki, 2010] and the Site 849 $\delta^{13}C_c$ record from Mix et al. [1995], Site U1342 approximately matches these records during most glacials and has lower (more negative) values during most interglacials (Figure 2b).

6. Evidence for Bering Sea Brine Formation and Ventilation

6.1 Changes in $\delta^{18}O$ Indicate Bering Sea Brine

The finding that the U1342 $\delta^{18}O_c$ record generally displays such a small G/IG change compared to global and regional records is perplexing at first glance and merits explanation. In general, $\delta^{18}O_c$ reflects local water temperature and local $\delta^{18}O$ of seawater ($\delta^{18}O_{sw}$), which is related to global ice volume and also typically to local changes in precipitation and evaporation (and thus salinity). Notably, the G/IG $\delta^{18}O_c$ range at U1342 is roughly equivalent to the change (~1‰) attributed to global ice volume alone [Sosdian and Rosenthal, 2009]. However, given changes in U1342 $\delta^{13}C_c$ discussed later, and suggestions from a short record of neodymium isotopes at a nearby site [Horikawa et al., 2010], it is unlikely that the character of the water bathing Site U1342 was constant throughout the past 1.2 Myr. We posit that the relatively low $\delta^{18}O_c$ amplitude of G/IG variations can be explained by a local water source formed by brine rejection during glacials. Brine rejection increases local salinity without significantly fractionating oxygen isotopes [Brennan et al., 2013; Hillaire-Marcel and de Vernal, 2008; Tan and Fraser, 1976; Tan and Strain, 1996], creating a dense water mass capable of transmitting the extremely low-$\delta^{18}O_{sw}$ Bering Sea surface water to intermediate depths. Thus, the $\delta^{18}O_{sw}$ at U1342 would decrease if the water bathing this site changed from a Pacific source entering the Bering Sea from the south to include a stronger local Bering Sea surface water source. Local brine has been previously implicated to explain negative $\delta^{18}O_c$ excursions in deep North Pacific benthic records [Gebhardt et al., 2008].

To test the idea that glacial brine formation within the Bering Sea resulted in a local low-$\delta^{18}O_{sw}$ glacial influence at U1342, we performed additional analyses in order to quantify G/IG changes in seawater temperature and $\delta^{18}O_{sw}$. In general, anomalously low $\delta^{18}O_c$ glacial values may theoretically be attributed to either bottom water warming or a water mass source with relatively low $\delta^{18}O_{sw}$ values (e.g. Bering Sea brine). To rule out warming as the explanation, we measured U1342 benthic foraminiferal Mg/Ca as a proxy of bottom water temperature and then quantitatively assessed G/IG changes in $\delta^{18}O_{sw}$, based on bottom water temperature measurements and global ice volume data. Mg/Ca results from three selected G/IG pairs are summarized in Table 1 and Table 2, with all data shown in Table A4 in Appendix A. Considering the relationship between $\delta^{18}O_c$ and bottom water temperature (typically -0.23‰/+1°C) [Ravelo and Hillaire-Marcel, 2007], the three G/IG pairs in Table 2 would need to demonstrate ~2-3°C warmer temperature if local $\delta^{18}O_{sw}$ was not lower during the glacials (relative to the interglacials). However, based on the Mg/Ca temperature estimates, local $\delta^{18}O_{sw}$ calculations (Table 2) yield local $\Delta\delta^{18}O_{sw}$ difference values (glacial minus interglacial) that are negative in all three G/IG pairs. These $\delta^{18}O_{sw}$ calculations show that there was a local source of relatively low $\delta^{18}O_{sw}$ during each glacial, in agreement with the mechanism of local brine formation and ventilation.

Table 1. U1342 average benthic foraminiferal $\delta^{18}O_c$ (‰) and Mg/Ca.

	MIS	Average $\delta^{18}O_c$ (‰)	Average Mg/Ca
Interglacial	MIS 1	3.90	0.90
	MIS 5	3.68	0.82
	MIS 9	3.30	0.78
Glacial	MIS 2	4.50	0.79
	MIS 6	4.19	0.90
	MIS 10	4.09	0.73

Table 2. Calculations of glacial minus interglacial bottom water temperature and $\delta^{18}O_{sw}$.

Glacial-Interglacial	$\Delta\delta^{18}O_c$ (‰)	ΔMg/Ca	ΔBottom Water Temperature (°C)*	$\Delta\delta^{18}O_{sw}$ (‰)	$\Delta\delta^{18}O_{sw}$ expected from ice volume (‰)**	$\Delta\delta^{18}O_{sw}$ local (‰)
MIS 2-1	0.60	-0.11	-1.58	0.23	1.00	-0.77
MIS 6-5	0.51	0.07	1.03	0.75	1.06	-0.31
MIS 10-9	0.79	-0.05	-0.70	0.63	0.97	-0.34

*Bottom water temperature calculations based on measured Mg/Ca using the calibration from Bryan and Marchitto [2008]: Mg/Ca=0.86+0.071(T). **$\delta^{18}O_{sw}$ change attributed to glacial ice volume: 0.1‰/-10 m of sea level. Sea level estimates from Rohling et al. [2009].

Salinity changes due to changes in evaporation, precipitation, and runoff cannot explain the low glacials values of $\delta^{18}O_c$ at Site U1342. These processes result in a positive relationship between salinity and $\delta^{18}O_{sw}$ [LeGrande and Schmidt, 2006], and thus the observed relatively low glacial $\delta^{18}O_{sw}$ at U1342, if related to these hydrological processes, would imply relatively low glacial salinity. However, it is implausible for lower salinity water to have occurred at the depth of

Site U1342. In the modern ocean, North Pacific surface salinity is so low that surface waters are not dense enough to sink to appreciable depths, even when temperatures are near freezing [Warren, 1983]. An even lower salinity surface water mass would only create stronger stratification, prohibiting a low $\delta^{18}O_{sw}$ signal from reaching Site U1342.

To demonstrate this point, we use the observed $\Delta\delta^{18}O_{sw}$ (from Table 2) and the North Pacific relationship of $\Delta\delta^{18}O_{sw} = 0.44 \times SSS$ from LeGrande and Schmidt [2006], in which SSS is sea surface salinity (‰), to calculate the theoretical ΔSSS across all three IG/G terminations shown in Table 2. These calculations show ΔSSS ranging from -0.70 to -1.75 psu. Although we argue later that models do not adequately represent brine formation, an important mechanism for NPIW formation, the models provide insight into the open sea convection process. Modeling results from Hu et al. [2012a] show that North Pacific surface water freshening of -0.70 to -1.75 psu would result in reduced open ocean convection, regardless of whether the Bering Strait is open or closed, and another model from Menviel et al. [2012] shows that deep North Pacific convection and deep/intermediate water formation can only arise by increasing surface water salinity. These results show that it would be impossible for surface water with relatively low glacial $\delta^{18}O_{sw}$ values to become dense enough to sink to the depth of site U1342 if that water was of lower salinity. Thus, the relatively low glacial $\delta^{18}O_{sw}$ values must have had anomalously high salinity values, as this would be the only way to explain how water with such low $\delta^{18}O_{sw}$ values could have been dense enough to be recorded at the depth of U1342 during glacials. Therefore, brine rejection from sea ice formation, which can increase salinity and density of surface water without increasing $\delta^{18}O_{sw}$, very likely played an important role in NPIW ventilation in the past.

6.2 Bering Sea Regional Comparison

While there are no other Bering Sea records of $\delta^{18}O_c$ and $\delta^{13}C_c$ of similar length to compare to our stable isotope records from U1342, a regional comparison of shorter records reveals trends consistent with the idea of Bering Sea brine formation during the LGM. A compilation of shorter Bering Sea records (Figure 3, Appendix A Figure A1, and Appendix A Table A5) shows that the amplitude of glacial $\delta^{18}O_c$ is dampened at intermediate depths (<2,000 m) compared to deeper sites (>2,000 m) and to the global average (represented by the LR04 stack). Strong glacial ventilation at intermediate depths (<2,000 m), caused by a relatively high contribution of local Bering Sea surface water relative to deep Pacific-sourced water, is indicated by the relatively high $\delta^{13}C_c$ and low $\delta^{18}O_c$ values during the LGM compared to the Holocene. On the other hand, deep Bering Sea and North Pacific sites display isotopic changes similar to the Lisiecki deep Pacific stack [Lisiecki, 2010] and the LR04 benthic stack, [Lisiecki and Raymo, 2005] indicating little change in circulation in the deep (>2,000 m) Pacific. This comparison, and evidence from the North Pacific during the last deglaciation [Jaccard and Galbraith, 2013], show that intermediate depths were well ventilated from a surface water source, while the deep ocean was not.

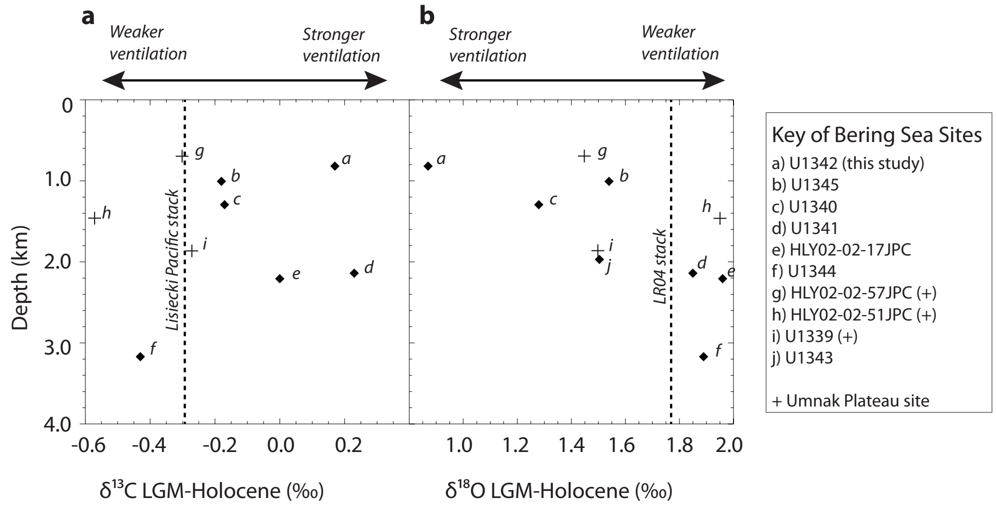

Figure 3. Comparison of ventilation influence on Bering Sea sites. (a) LGM $\delta^{13}C_c$ - Holocene $\delta^{13}C_c$ and **(b)** LGM $\delta^{18}O_c$ - Holocene $\delta^{18}O_c$ for sites HLY02-02-17JPC, HLY02-02-57JPC, and HLY02-02-51JPC; IODP Expedition 323 Sites U1342, U1345, U1340, U1341, U1343, U1344, and U1339. Data is from this study (U1342), Asahi et al. [2014] (U1343), and compiled by M.S. Cook et al. (Tracing Bering Sea circulation with benthic foraminiferal stable isotopes during the Pleistocene, submitted to Deep Sea Research) (all other sites). Sites (g)-(i) are from the Umnak Plateau, remotely located on the western margin of the Bering Sea, where circulation may have been limited (see Figure 1). LGM-Holocene isotopic differences from Bering Sea sites are compared to records of whole-ocean changes from the Lisiecki deep Pacific stack [Lisiecki, 2010] and the LR04 benthic stack [Lisiecki and Raymo, 2005] (dotted lines). The LGM was defined as Marine Isotope Stage 2 based on stratigraphy (maximum $\delta^{18}O_c$).

Furthermore, $\delta^{18}O_c$ data from other oceans shows that the Bering Sea had an unusual water structure profile during the LGM. The difference between $\delta^{18}O_c$ values in the LGM compared to the Holocene for Site U1342 (0.87‰) is less than that of other oceans at intermediate depths, including the North Atlantic (~2‰) [Keigwin, 2004], the South Atlantic (~2‰) [Curry and Oppo, 2005], the South Pacific (~1.5‰) [Herguera et al., 1992], and the Indian Ocean (1.1‰) [Kallel et al., 1988]. Thus, the small LGM-Holocene $\delta^{18}O_c$ difference observed at Site U1342 is a unique feature for intermediate waters and is consistent with the idea of locally formed brine.

Assuming that variability in $\delta^{13}C_c$ and $\delta^{18}O_c$ can be used to examine changes in local ventilation, a compilation of Bering Sea $\delta^{13}C_c$ and $\delta^{18}O_c$ records would, hypothetically and ideally, delineate a regional isotopic water mass structure that reflects the influence of this ventilation. However, our method of looking at the relative changes (LMG-Holocene) in $\delta^{13}C_c$ and $\delta^{18}O_c$ at each site is currently the best method for assessing changes in brine formation during the last glacial, because there are not yet enough comparable datasets from various Bering Sea sites to be able to use absolute values to define regional isotopic water mass structure. Figure 3 and Table A5 in Appendix A provide a comprehensive list of the available $\delta^{13}C_c$ and $\delta^{18}O_c$ Bering Sea records. While there are records from ten Bering Sea sites (including this study), records from seven of those sites cannot be directly compared to Site U1342 due to the use of a different foraminifera species (at 57JPC, U1341, 17JPC, and U1344), an unavailable $\delta^{13}C_c$ record (at U1343), and a remote site location not sensitive to circulation changes (at 51JPC and U1339). Using the three remaining sites (U1342, U1345, and U1340) to assess regional patterns in absolute $\delta^{13}C_c$ and $\delta^{18}O_c$ values is difficult, given their different locations within the basin (shelf vs. ridge; Figure 1), possible variations in age models, and the fact that changes in productivity over time may affect the $\delta^{13}C_c$ at the other two sites more due to their much higher sedimentation rates (up to 30 cm/kyr). Therefore, as described above, using the data that is currently available, the best method for looking at changes in water mass conditions is to calculate relative differences in $\delta^{13}C_c$ and $\delta^{18}O_c$; this approach demonstrates enhancement in local Bering Sea ventilation during the LGM compared to the Holocene. Determining whether the LGM-like pattern of enhanced intermediate water ventilation (NPIW) is a robust and repeated feature of all glacial periods requires long records of $\delta^{13}C_c$ and $\delta^{18}O_c$ at U1342 over the last 1.2 Myr.

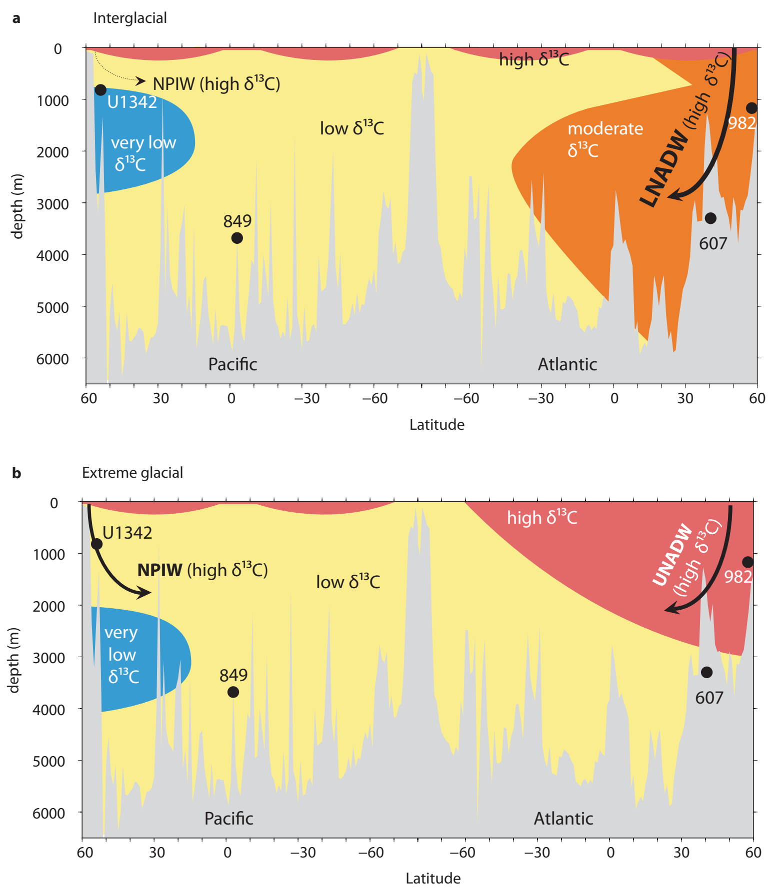

Figure 4. Schematic diagrams of the effect of ventilation on oceanic $\delta^{13}C$. (a) Interglacial scenario, showing ventilation was lower for both the Upper North Atlantic and North Pacific compared to **(b)** extreme glacial conditions, when both NPIW and UNADW formation were relatively strong. Generally, high $\delta^{13}C$ reflects relatively strong ventilation as surface waters sink into the intermediate and deep ocean. Since deep water is produced in the Atlantic but not in the Pacific, Atlantic

Sites 982 and 607 typically have higher $\delta^{13}C$ compared to the Pacific Sites U1342 and 849. Using Site 849 to represent whole-ocean conditions, $\Delta\delta^{13}C_{849\text{-}U1342}$ can be used to measure relative changes NPIW ventilation, and $\Delta\delta^{13}C_{849\text{-}982}$ and $\Delta\delta^{13}C_{849\text{-}607}$ can be used to indicate the relative strength of UNADW and LNADW ventilation. Pacific and Atlantic bathymetry are along 171°W and 30°W longitude, respectively.

7. The Influence of North Pacific Intermediate Water in the Bering Sea

7.1 Proxies of NPIW: $\Delta\delta^{18}O$ and $\Delta\delta^{13}C$

In order to monitor changes in ventilation, inferred to be related to changes in the strength and/or characteristic of NPIW at Site U1342 over multiple G/IG timescales, it is necessary to have proxies that are unencumbered by the effects of whole-ocean chemical changes, which can occur on long timescales. Thus, rather than using absolute values of $\delta^{18}O_c$ and $\delta^{13}C_c$, we have determined two "new" proxies to resolve NPIW orbital-scale variability over the past 1.2 Myr. To subtract the influence of whole-ocean changes and isolate the regional influence of NPIW on the U1342 $\delta^{18}O_c$ and $\delta^{13}C_c$ records, we compare our records to Site 849 [Mix et al., 1995], a deep Pacific site (0°11'N, 110°31'W; 3,851 m) often used to represent global oceanic values. Thus, as proxies of the local influence of NPIW, we calculate $\Delta\delta^{18}O$ values (the $\delta^{18}O_c$ at Site 849 minus the $\delta^{18}O_c$ at U1342) and $\Delta\delta^{13}C$ values (the $\delta^{13}C_c$ at Site 849 minus the $\delta^{13}C_c$ at U1342), rather than using the absolute $\delta^{18}O_c$ and $\delta^{13}C_c$ values from U1342.

Due to temperature and salinity differences, $\delta^{18}O_c$ values at U1342 are presently lower than at Site 849. With enhanced NPIW ventilation, low-$\delta^{18}O_{sw}$ Bering Sea surface waters reaching Site U1342 would further decrease the $\delta^{18}O_c$ recorded here, resulting in higher $\Delta\delta^{18}O$ values. Thus, we interpret relatively high/low $\Delta\delta^{18}O$ values to indicate enhanced/reduced NPIW influence at U1342.

At any given location, the $\delta^{13}C$ of foraminiferal calcite ($\delta^{13}C_c$) reflects the $\delta^{13}C$ of dissolved inorganic carbon ($\delta^{13}C_{DIC}$) in seawater at that site, which is influenced by whole-ocean chemistry, the local balance between photosynthesis and respiration, and local relative mixtures of water masses with distinct $\delta^{13}C_{DIC}$ signatures [Ravelo and Hillaire-Marcel, 2007]. Deep, aged water masses accumulate the respiration products of exported marine organic matter and thus have low $\delta^{13}C_{DIC}$ values, while carbon uptake imparts higher $\delta^{13}C_{DIC}$ values on surface waters. In the modern ocean, deep Pacific water flows northward towards the Bering Sea, progressively aging and acquiring a lower $\delta^{13}C_{DIC}$ signature, and $\Delta\delta^{13}C$ is a relatively large value that reflects this aging process (Figure 4a). However, in an enhanced NPIW scenario, Site U1342 is strongly influenced by a relatively high $\delta^{13}C_{DIC}$ signature from its proximal surface water source, and $\Delta\delta^{13}C$ decreases (Figure 4b). As such, we interpret relatively high/low $\Delta\delta^{13}C$ values to indicate reduced/enhanced NPIW at U1342.

The idea that the two proxies, $\Delta\delta^{18}O$ and $\Delta\delta^{13}C$, are both influenced by changes in NPIW ventilation is supported by strong statistical significance between the two variables ($p<0.0001$). A cross-plot of these two variables (Figure A2 in Appendix A) shows their significant correlation and demonstrates that each time series from U1342 can be used to indicate NPIW prominence. The correlation is not perfect, suggesting other sources of isotope variability exist. For example, there is apparently millennial-scale variability (Figure 2) that may add "noise" to the dataset. We focus here on the orbital G/IG variability; the robustness of our interpretations is reinforced by the mutual agreement of these two NPIW proxies and the length of our records, which allows for the statistical evaluation of many iterations of orbital G/IG cycles (see Section 8.1) in order to determine recurring trends.

7.2 Validation of the $\Delta\delta^{13}C$ NPIW proxy

While the validity of using $\Delta\delta^{18}O$ as an indicator of local brine and NPIW was already discussed (see Section 6.1), some potential complexity with $\delta^{13}C_c$ interpretations makes it necessary to examine the validity of the use of $\Delta\delta^{13}C$ as an NPIW indicator. Specifically, because productivity is high in the Bering Sea [Kim et al., 2011; Riethdorf et al., 2013; Schlung et al., 2013], it is necessary to establish that U. peregrina $\delta^{13}C_c$ is a robust indicator of changes in local bottom water $\delta^{13}C_{DIC}$. Therefore, we performed analyses to rule out the possibility that the record of changes in $\delta^{13}C_c$ of this species is affected by changes in "habitat effects" correlating with the accumulation rate of organic carbon (primary productivity). Changes in habitat effects have been shown in U. peregrina from the eastern

Atlantic, off the coast of northwest Africa, [Zahn et al., 1986] but have not been extensively studied in low-oxygen environments, such as Site U1342.

Our data demonstrate that $\Delta\delta^{13}C$ values are not correlated with primary productivity (Figure 5, Figure 6, and Table 3), indicating that the $\delta^{13}C_c$ of U. peregrina was not strongly influenced by enhanced carbon flux and respiration in the sediment and thus can be interpreted with confidence as a proxy for the $\delta^{13}C_{DIC}$ of bottom water. Carbonate-free sediments from the past ~250 kyr were analyzed for wt.%C and carbon mass accumulation rate (CMAR), two indicators of primary productivity [Meyers and Teranes, 2001; Zahn et al., 1986]. There is a weak correlation of $\Delta\delta^{13}C$ with wt.%C (R=0.11) and CMAR (R=0.24), as shown in Figure 5. Additionally, laminated sediments indicative of high productivity intervals [Schlung et al., 2013] are not associated with excursions of $\Delta\delta^{13}C$ (Figure 5). From these comparisons, it is evident that the $\Delta\delta^{13}C$ record (and therefore the U1342 $\delta^{13}C_c$ record) is not dominantly influenced by primary productivity over the past ~250 kyr. Additionally, while wt.%C and CMAR results are only available for the first ~250 kyr, a strong correlation (Table 3) of these two proxies to density (measured by gamma ray attenuation; GRA) indicates that GRA can be used as a proxy for primary productivity throughout the entire U1342 record.

GRA values show weak correlation to $\Delta\delta^{13}C$ over the 1.2 Myr record (R=-0.15; Figure 6c), in agreement with the results from the last ~250 kyr (Figure 5c). Additionally, a long record of biogenic opal%, another proxy for primary productivity, from nearby Site U1341 [Asahi et al., 2014] shows little correlation to our record of $\Delta\delta^{13}C$ (Figure 6d). Together, this multi-proxy comparison provides confidence that U1342 U. peregrina $\delta^{13}C_c$ is not dominated by the effects of changes in the organic carbon accumulation rates, and thus is not heavily influenced by habitat effects. This conclusion, along with the strong correlation between $\Delta\delta^{13}C$ and $\Delta\delta^{18}O$ (a measurement that is not complicated by habitat effects because U. peregrina calcifies $\delta^{18}O$ in equilibrium with sea water [Shackleton, 1974]), justifies the use of $\delta^{13}C_c$ in calculations of $\Delta\delta^{13}C$ to indicate fluctuations in NPIW.

Additionally, in our study, we are not concerned about the possible effects of air-sea fractionation on the $\delta^{13}C_c$ record. Surface water does not reach the depths of U1342 today [Warren, 1983], meaning that the site was likely buffered from the effects of air-sea $\delta^{13}C$ fractionation during interglacials. During glacials, U1342 was affected by NPIW from a local surface water source containing a relatively high $\delta^{13}C_{sw}$ due to both air-sea and photosynthetic fractionation typical of high-latitude surface waters. Our study focuses on the relative (rather than quantitative) changes in NPIW, and air-sea interactions would merely influence the amplitude but not the direction and pattern of the recorded $\delta^{13}C_c$.

Table 3. Correlation of U1342 proxies of primary productivity and NPIW.

Records compared	Proxy interpretation	Pearson correlation coefficien (R)
Wt.%C vs. $\Delta\delta^{13}C$	Productivity vs. NPIW	0.11
CMAR vs. $\Delta\delta^{13}C$	Productivity vs. NPIW	0.24
GRA vs. Wt.%C	Density vs. Productivity	-0.75
GRA vs. CMAR	Density vs. Productivity	-0.41
GRA vs. $\Delta\delta^{13}C$*	Productivity vs. NPIW	-0.15

*All records compared are from ~250 ka, except for GRA vs. $\Delta\delta^{13}C$ (from 1.2 Ma).

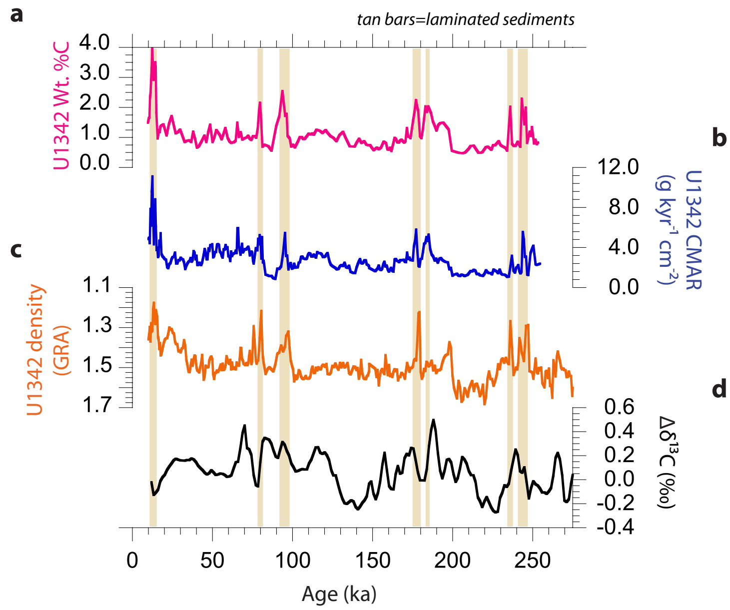

Figure 5. Multiple records of primary productivity are independent of NPIW proxy $\Delta\delta^{13}C$. U1342 proxies of primary productivity, including **(a)** wt.%C, **(b)** carbon mass accumulation rate, and **(c)** sediment density measured by gamma ray attenuation (GRA), show weak correlation compared to **(d)** the NPIW proxy of benthic foraminiferal $\Delta\delta^{13}C_{849\text{-}U1342}$. Tan vertical bars represent low-density laminated sediments representative of high productivity, which are also not well correlated to $\Delta\delta^{13}C$. This multi-proxy comparison indicates that $\Delta\delta^{13}C$ is not dominated by fluctuations in organic carbon, justifying the use of $\Delta\delta^{13}C_{849\text{-}U1342}$ as an NPIW indicator.

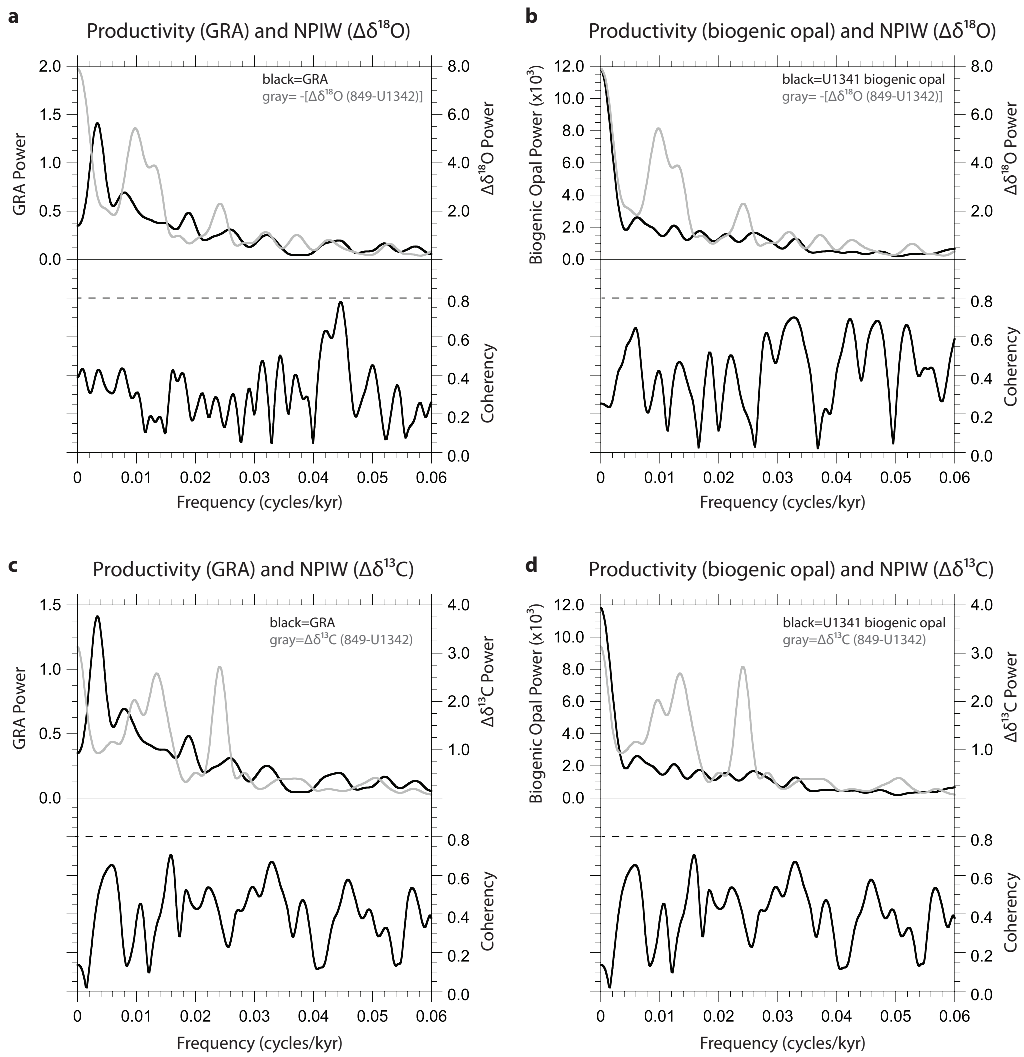

Figure 6. Blackman-Tukey spectral analyses show primary productivity is independent of NPIW proxies. (a) U1342 gamma ray attenuation (GRA, i.e. density) vs. NPIW proxy $\Delta\delta^{18}O_{849\text{-}U1342}$; **(b)** U1341 biogenic opal vs. NPIW proxy $\Delta\delta^{18}O_{849\text{-}U1342}$; **(c)** U1342 GRA vs. NPIW proxy $\Delta\delta^{13}C_{849\text{-}U1342}$; and **(d)** U1341 biogenic opal vs. NPIW proxy $\Delta\delta^{13}C_{849\text{-}U1342}$. Low coherence (<0.8, as marked by dotted line in lower panels) between proxies of primary productivity and NPIW proxies ($\Delta\delta^{13}C$ and $\Delta\delta^{18}O$) demonstrate these two variables are not strongly correlated at U1342, justifying the use of $\Delta\delta^{13}C$ and $\Delta\delta^{18}O$ as NPIW indicators.

8. Changes in NPIW over the last 1.2 Myr

8.1 NPIW Relationship to Climate and the Bering Strait

To assess whether the closure of the Bering Strait has an influence on NPIW, we examine the difference between NPIW proxies during glacials and interglacials, and use relative sea level (RSL) to distinguish glacials with an open Bering Strait (G-OBS) (RSL above -50 m) from glacials with a closed Bering Strait (G-CBS) (RLS below -50 m). G-OBS vs. G-CBS conditions yield significantly different results for both mean $\Delta\delta^{18}O$ (-0.059‰ vs. 0.370‰; $p=7.02\times10^{-19}$) and $\Delta\delta^{13}C$ (0.244‰ vs. 0.106‰; $p=6.21\times10^{-5}$), which all indicate significantly higher levels of ventilation during G-CBS conditions (Table 4; Table A6 in Appendix A). Furthermore, large differences between G-CBS vs. interglacial (IG) values of mean $\Delta\delta^{18}O$ (0.370‰ vs. 0.067‰; $p=9.76\times10^{-11}$) and $\Delta\delta^{13}C$ (0.106‰ vs. 0.244‰; $p=4.65\times10^{-7}$) show that ventilation was considerably stronger during G-CBS compared to IG conditions, while matching values of mean $\Delta\delta^{13}C$ during G-OBS vs. IG conditions (0.244‰ vs. 0.244‰; p=0.987) show that ventilation was similarly weak whenever the Bering Strait was open, regardless of the climate (Table 4; Table A6 in Appendix A). Together, these data indicate that glacial climate alone did not induce more prominent NPIW. Enhanced NPIW in the Bering Sea was only regularly associated with extreme glacial conditions, when sea level cut off circulation through the Bering Strait.

Table 4. Average and standard deviation of NPIW proxies during open and closed Bering Strait conditions from 1.2 Ma[a]

		All glacials	G-CBS	G-OBS	All interglacials
$\Delta\delta^{13}C$ (849-U1342)	Avg.	0.164[b]	0.106[c]	0.244	0.244
	SD	0.212	0.162	0.246	0.211
$\Delta\delta^{18}O$ (849-U1342)	Avg.	0.190[b]	0.370[c]	-0.059	0.067
	SD	0.331	0.253	0.256	0.363

[a]See supporting information Table S6 for t test results. Glacials with a closed Bering Strait (G-CBS) and glacials with an open Bering Strait (G-OBS) are defined as when relative sea level is below or above the Bering Strait sill depth of 50 m.
[b]Average value is statistically different than interglacial value at $p<0.01$.
[c]Average value is statistically different than interglacial value at $p<0.0001$.

Cross-spectral analyses (Figure 7) verify the idea that variations in NPIW are linked to extreme glacial climates when flow through the Bering Strait was cut off. Comparison of NPIW ($\Delta\delta^{13}C$) with the LR04 stack indicates a phase lag whereby maximum glacial conditions precede increases in NPIW by ~4 kyr on 41-kyr cycles (Figure 7a); however, the LR04 record incorporates both temperature and ice volume (sea level) variations, which are not in phase [Shackleton, 2000]. To isolate sea level effects on NPIW, we conducted a cross-spectral analysis using a RSL record from Sosdian and Rosenthal [2009]. These analyses (Figures 7b and 7c) show that variance in the $\Delta\delta^{18}O$ and $\Delta\delta^{13}C$ records, which reflects local changes in NPIW formation, is significantly correlated to (coherence ≥ 0.8), and in phase with (or nearly in phase with) RSL variations at periodicities centered at 41 kyr (for $\Delta\delta^{13}C$) and at 41 kyr and 93 kyr (for $\Delta\delta^{18}O$). The general behavior that these results suggest is that as climate cools, it may take a long time for the sea level to drop below the Bering Strait depth; however, once the strait is closed, the ventilation response within the Bering Sea is immediate.

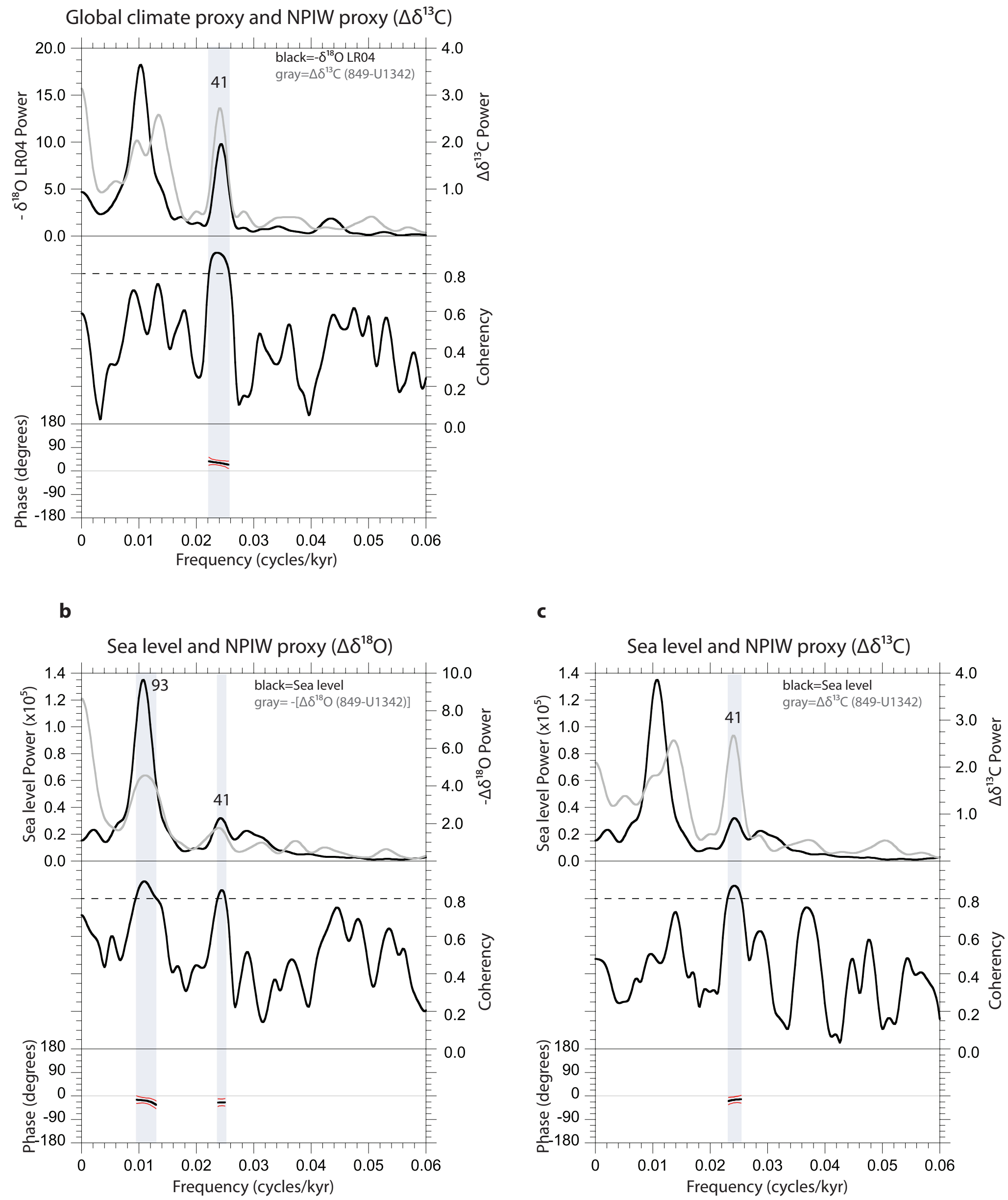

Figure 7. Blackman-Tukey cross-spectral analyses of global climate, sea level, and NPIW. (a) Cross-spectral analysis of -$\delta^{18}O_c$ from the LR04 stack from Lisiecki and Raymo [2005], representing a global record of ocean temperature and ice volume, and $\Delta\delta^{13}C_{849\text{-}U1342}$, representing NPIW presence. **(b)** Relative sea level (RSL) from Sosdian and Rosenthal [2009] compared to -$\Delta\delta^{18}O_{849\text{-}U1342}$, a proxy of NPIW production, **(c)** RSL compared to $\Delta\delta^{13}C_{849\text{-}U1342}$, a proxy of NPIW production. Gray vertical bars highlight frequencies of high coherency (>0.8). Phases (black lines in each bottom panel) were assigned in reference to the first variable in the analysis, and red lines indicate margins of error.

One question that should be addressed is whether other factors associated with extreme glacials (besides the closure of the Bering Strait) could be responsible for the correlation between extreme glacials and enhanced NPIW. Although the relationship between sea level and Bering Strait closure is circumstantial given the available data, modeling results support the idea that the closure of the Bering Strait alone can result in major changes in sub-surface circulation. Modeling results from Hu et al. [2014] showed that regardless of the background climate, changes in freshwater flow through the Bering Strait due to its closure had a prominent effect of strengthening AMOC, changing Arctic sea ice patterns, and altering the temperature in both the North Atlantic and North Pacific. While this model focused on testing the Atlantic circulation response, results from Hu et al. [2014] support the idea that extreme glaciations by themselves (without closing the Bering Strait) do not drive major changes in deep/intermediate circulation. Thus, there is a possible causal relationship between sea level (the closure of the Bering Strait) and enhanced NPIW during extreme glacials.

8.2 Changes in NPIW after the Mid-Pleistocene Transition

The idea of extreme glacials leading to enhanced NPIW is also evident when considering long-term global climate history. The Mid-Pleistocene Transition (MPT; 700-1250 ka) marks a global climatic change from dominant low-amplitude, 40-kyr cycles to high-amplitude, 100-kyr cycles. Results from U1342 (Table 5) show that after the MPT (0-700 ka), average $\Delta\delta^{18}O$ were significantly higher and average $\Delta\delta^{13}C$ were significantly lower compared to before the MPT (700-1200 ka), indicating stronger ventilation during the recent interval of relatively extreme glaciations and frequent episodes of Bering Strait closure.

Table 5. Average benthic stable isotope values before and after the Mid-Pleistocene Transition.

	0-700 ka		700-1200 ka		p-value
	Average (‰)	Standard deviation	Average (‰)	Standard deviation	
$\delta^{18}O$ (U1342)	3.93	0.22	3.97	0.17	<0.001
$\delta^{13}C$ (U1342)	-0.26	0.18	-0.54	0.19	<0.0001
$\Delta\delta^{18}O$ (849-U1342)	0.21	0.33	0.04	0.27	<0.0001
$\Delta\delta^{13}C$ (849-U1342)	0.14	0.21	0.25	0.21	<0.0001

Data for Site 849 (deep equatorial Pacific) is from Mix et al. [1995].

8.3 Evaluating the NPIW-NADW Seesaw Hypothesis

New, long NPIW records from U1342 make it possible for the first time to test if the water mass expansion of NPIW and NADW are inversely related to each other, in order to evaluate the seesaw theory proposed by several modeling studies [Hu et al., 2014; Hu et al., 2012a; Hu et al., 2010; Okazaki et al., 2010; Saenko et al., 2004]. AMOC is associated with North Atlantic Deep Water (NADW), which has two components: lower NADW (LNADW; deeper than 2,000 m) and upper NADW (UNADW; shallower than 2,000 m). North Atlantic sites ODP 982 (57°31'N, 15°53'W; 1,135 m) [Venz et al., 1999] and DSDP Site 607 (41°00'N, 32°58'W; 3,427 m) [Ruddiman et al., 1989] are ideally located to monitor changes in UNADW and LNADW, respectively. While more comparison sites would be preferable for establishing basin-wide changes in ventilation, there are few North Atlantic records of sufficient length for comparison to Site U1342, so we must rely on these two iconic sites for our evaluation. AMOC strength is difficult to quantify with $\delta^{13}C$ and $\delta^{18}O$ data, but changes in the relative contribution of newly formed deep water can be monitored using $\Delta\delta^{13}C$. Thus, to monitor UNADW formation, we use $\delta^{13}C_c$ at ODP 982 to calculate $\Delta\delta^{13}C_{849-982}$ values (Site 849 $\delta^{13}C_c$ - ODP 982 $\delta^{13}C_c$), and to monitor LNADW formation, we use $\delta^{13}C_c$ at DSDP Site 607 to calculate $\Delta\delta^{13}C_{849-607}$ values (Site 849 $\delta^{13}C_c$ - DSDP 607 $\delta^{13}C_c$). The $\delta^{13}C_c$ records from ODP 982 and DSDP Site 607 are shown in Figure A3 in Appendix A, along with the resulting $\Delta\delta^{13}C$ values. These $\Delta\delta^{13}C$ records of UNADW and LNADW can then be compared to our record of NPIW from U1342 ($\Delta\delta^{13}C_{849-U1342}$) to determine whether or not there is an antiphase relationship.

Cross-spectral analyses indicate that NPIW and UNADW variability is coherent and in phase, or nearly in phase (NPIW lags UNADW by ~3 kyr), depending on the periodicity (Figure 8a and 8b). However, NPIW and LNADW variability is uncorrelated (Figure 8c and 8d). Therefore, the relative contributions of NPIW in the Bering Sea and UNADW in the North Atlantic appear to increase and decrease simultaneously, and trends in NPIW and LNADW formation are unrelated. It is possible that these results cannot distinguish between the strength of the UNADW/LNADW water mass and a change in its depth. However, if these records were only affected by a change in water mass position and not ventilation strength, we would expect that the records of LNADW and UNADW would be antiphase, which is not the case (Figure A3 in Appendix A). Regardless of these considerations, we can conclude that these results do not demonstrate an antiphase relationship between NPIW and NADW and therefore challenge the NPIW-NADW

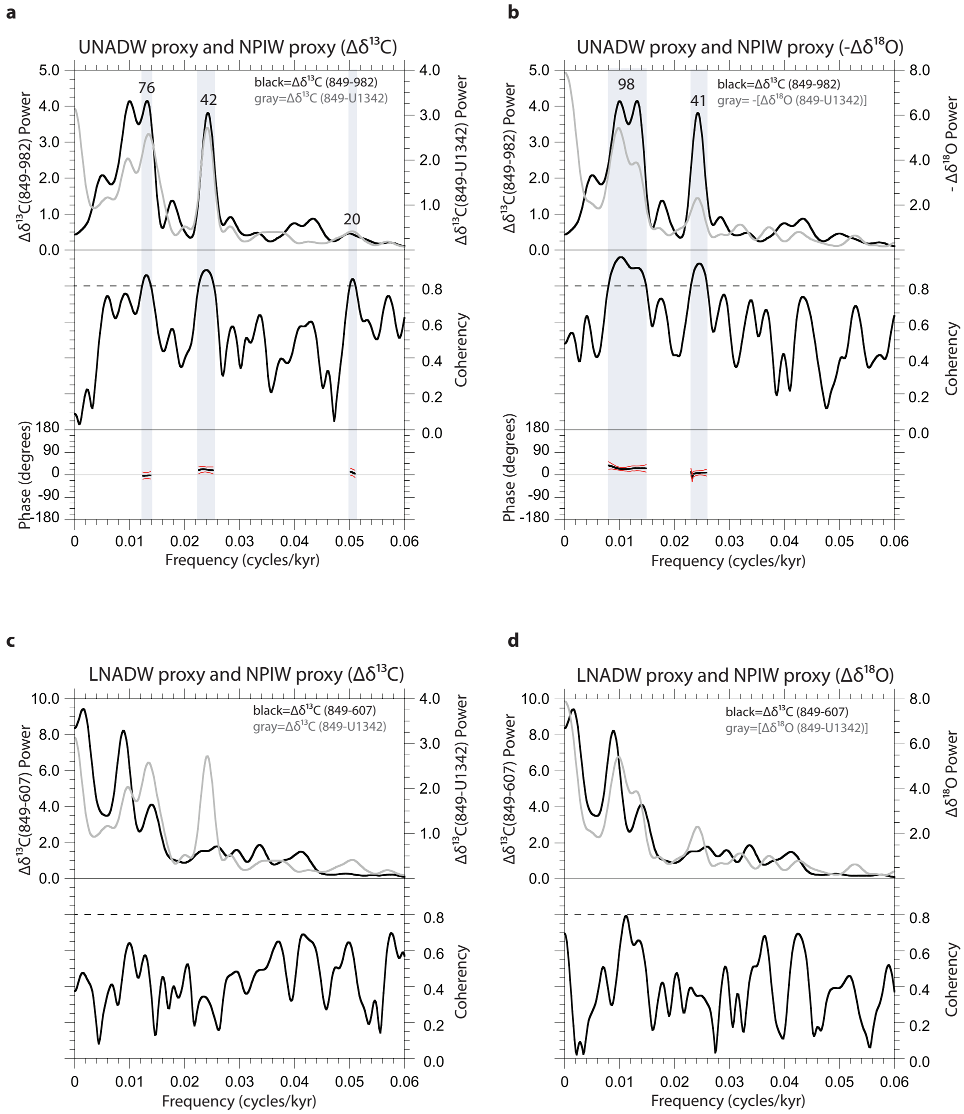

Figure 8. Blackman-Tukey cross-spectral analyses of UNADW and LNADW vs. NPIW do not support an orbital-scale NPIW-NADW seesaw. (a) UNADW proxy $\Delta\delta^{13}C_{849\text{-}982}$ vs. NPIW proxy $\Delta\delta^{13}C_{849\text{-}U1342}$, **(b)** UNADW proxy vs. NPIW proxy $\Delta\delta^{18}O_{849\text{-}U1342}$ **(c)** LNADW proxy $\Delta\delta^{13}C_{849\text{-}607}$ vs. NPIW proxy $\Delta\delta^{13}C_{849\text{-}U1342}$, **d)** LNADW proxy vs. NPIW proxy $\Delta\delta^{18}O_{849\text{-}U1342}$. Gray vertical bars indicate frequencies of high coherency (>0.8; dotted black line), which show (a-b) that UNADW is in phase, or nearly in phase, with NPIW, whereas (c-d) LNADW and NPIW are weakly correlated. Phase (black line in bottom panel) was assigned in reference to UNADW and LNADW, and red lines indicate margins of error. $\delta^{13}C_c$ data used to calculate NPIW, UNADW, and LNADW were from the following sources: Mix et al. [1995] (Site 849; 3,839 m); Venz et al. [1999] (Site 982; 1,145 m); and Ruddiman et al. [1989] (Site 607; 3,427 m).

seesaw theory predicted by models, at least in as much as the theory applies to orbital-scale variations. Because $\delta^{13}C_c$ is not a direct measure of changes in AMOC or PMOC strength, more work is needed to quantify changes in circulation and the mechanisms driving such changes; however, the coherent and in-phase pattern of $\delta^{13}C_c$ variability in NPIW and UNADW provides tentative evidence that the Pacific and Atlantic are linked through a mechanism on orbital timescales that results in in-phase variations in intermediate water circulation, rather than a seesaw.

8.4 Mechanism for NPIW during extreme glacials

Our $\delta^{18}O$ results (Section 6) indicate that brine rejection from enhanced sea ice formation within the Bering Sea is critically important to NPIW formation during extreme glacials of the past 1.2 Myr, and we suggest that Bering Sea brine formation is key to explaining why our data show in-phase NPIW-UNADW coupling while models predict seesaw behavior. Although models include dynamic sea ice processes and convective/open ocean NPIW formation, they do not have high enough resolution to simulate sea ice formation on continental shelves, where brine formation is most critical. Because NPIW formation via brine rejection on shelves is not well represented in current Bering Strait closure models, models may predict weak (rather than strong) NPIW formation during Bering Strait closure.

While the results of this study indicate that Bering Sea brine formation was enhanced when the Bering Strait was closed, the reason for this relationship is less clear. The exact mechanism for the brine formation is outside the scope of our data, but models can offer important insight into parameters (e.g. temperature and atmospheric patterns) that could create conditions amenable for brine formation, even if the models do not adequately simulate brine formation itself. We suggest that one mechanism invoking brine that possibly explains why NPIW is enhanced during glacials, and thus why our data show that NPIW and UNADW formation are nearly in phase, involves the impact of the Bering Strait closure on Bering Sea temperature and sea ice formation. When Bering Strait closure cuts off the freshwater input to the North Atlantic, models show that this results in increased salinity, enhanced UNADW formation, and warming [Hu et al., 2012a]. Concurrently, the modeled seesaw behavior arises from the fact that models predict that closing the Bering Strait and isolating freshwater within the North Pacific results in less saline and colder sea surface temperatures [Hu et al., 2014; Hu et al., 2010], and hence deep convection and NPIW formation in the models is inhibited. Since our data show that NPIW is actually enhanced, there must be a mechanism, which is poorly represented in models, by which colder and less saline sea surface conditions in the Bering Sea promote, rather than inhibit, NPIW formation.

It is possible that the cooler temperatures during intervals of Bering Strait closure were accompanied by major changes in atmospheric conditions that could have enhanced sea ice formation and NPIW via brine formation on/near shelves even while open ocean convection was inhibited. In the modern climate system, very cold North Pacific winters are associated with an easterly shift in the Aleutian Low [Luchin et al., 2002; Rodionov et al., 2007]. This shift may result in more northerly winds over the Bering Sea, moving sea ice southward and extending the polynya growth regions [Rodionov et al., 2007]. Therefore, we propose that an easterly shift in the Aleutian Low during extreme glacials could have enhanced Bering Sea polynya growth, resulting in strong brine rejection; thus, although the North Pacific/Bering Sea surface water may have been fresher on a regional scale, glacial NPIW production would have been promoted in localized areas (polynyas) within the Bering Sea (as it is today within Okhotsk Sea polynyas). This mechanism, which is partially supported by model results that suggest opening/closing the Bering Strait can directly affect the Aleutian Low [Okumura et al., 2009], would most easily explain the increase in Bering Sea brine production, since wind direction is the primary control on sea ice extent within the Bering Sea [Overland and Pease, 1982].

9. Conclusions

New records of foraminiferal $\delta^{18}O$ and $\delta^{13}C$ from Bering Sea Site U1342 provide an unparalleled opportunity to investigate past changes in North Pacific climate and ocean circulation since 1.2 Ma. This study provides the first evidence of reoccurring NPIW ventilation during extreme glacial climates over multiple G/IG cycles and also demonstrates that NPIW ventilation occurred from brine formed locally within the Bering Sea. Due to the unprecedented length and detail of our Bering Sea record, we were able to conduct robust statistical analyses of the orbital-scale variability, which revealed that enhanced NPIW ventilation occurred only during extreme glacial events, in which the Bering Strait was closed (sea level dropped at least 50 m relative to present). Finally, our long records of NPIW provided the first opportunity to evaluate the NPIW-NADW seesaw hypothesis using paleoceanographic data. Our results showed evidence that NPIW was enhanced simultaneously with UNADW on orbital timescales, and NPIW had no relationship to LNADW. These results, which do not demonstrate an orbital-scale antiphase relationship between NPIW and NADW, provide preliminary evidence contradicting seesaw behavior predicted by many models. We suggest that NPIW formation via brine formation on and near continental shelves, which is not adequately simulated in models, may explain data-model discrepancies.

Accurately discerning the behavior of NPIW in relation to NADW is essential to understanding MOC, oceanic heat transfer, and global climate. The effects of closing the Bering Strait are thought to be profound based on modeling results, but these models need to be ground truthed by paleoceanographic data. Some climate models show that the closure of the Bering Strait may result in a ~15% decrease of meridional heat transport, and thus ~1.5˚C cooling in the North Pacific [Hu et al., 2014; Hu et al., 2010] (relative to an open Bering Strait scenario), while others show the opposite response [Okumura et al., 2009]. Additionally, AMOC-PMOC seesaw behavior has been shown to result in buffered Northern Hemisphere cooling during intervals of AMOC shutdown [Okazaki et al., 2010] and is used to explain extreme climatic events of the last deglaciation [De Boer and Nof, 2004; Hu et al., 2012a; Hu et al., 2012b]. Our U1342 records validate the idea of a robust relationship between NPIW prominence and flow through the Bering Strait, but also provide orbital-scale evidence that contradicts modeling studies that demonstrate an NPIW-NADW seesaw with Bering Strait closure. Thus, substantial work is needed both to confirm our data-based results and to understand the source of model-data mismatches. Accurately discerning changes in NPIW and NADW will have significant implications for our understanding of the climate system.

Acknowledgements

This research used samples and data from the Integrated Ocean Drilling Program (IODP). Funding for this research was provided by a Schlanger Ocean Drilling Fellowship from the Consortium for Ocean Leadership and NSF grant OCE0963144. We would like to thank Dyke Andreasen for his help with instrumentation, as well as Ivano Aiello, Mea Cook, Aixue Hu, Axel Timmermann, James Zachos, and anonymous reviewers for their helpful discussions and comments on our manuscript. We also thank several members of the Ravelo Lab for laboratory assistance.

References

Asahi, H., S. Kender, M. Ikehara, T. Sakamoto, K. Takahashi, A. C. Ravelo, C. A. Alvarez Zarikian, B. K. Khim, and M. J. Leng (2014), Orbital-scale benthic foraminiferal oxygen isotope stratigraphy at the northern Bering Sea Slope Site U1343 (IODP Expedition 323) and its Pleistocene paleoceanographic significance, Deep Sea Research Part II-Topical Studies in Oceanography.

Brennan, C. E., K. J. Meissner, M. Eby, C. Hillaire-Marcel, and A. J. Weaver (2013), Impact of sea ice variability on the oxygen isotope content of seawater under glacial and interglacial conditions, Paleoceanography, 28(3), 388-400.

Bryan, S. P., and T. M. Marchitto (2008), Mg/Ca-temperature proxy in benthic foraminifera: New calibrations from the Florida Straits and a hypothesis regarding Mg/Li, Paleoceanography, 23(2).

Clark, P. U., J. X. Mitrovica, G. A. Milne, and M. E. Tamisiea (2002), Sea-level fingerprinting as a direct test for the source of global meltwater pulse IA, Science, 295(5564), 2438-2441.

Cook, M. S., L. D. Keigwin, and C. A. Sancetta (2005), The deglacial history of surface and intermediate water of the Bering Sea, Deep-Sea Research Part II-Topical Studies in Oceanography, 52(16-18), 2163-2173.

Cook, M. S., A. C. Ravelo, A. Mix, I. M. Nesbitt, N. V. Miller, and D. C. McCorkle (in review), Tracing Bering Sea circulation with benthic foraminiferal stable isotopes during the Pleistocene, Deep Sea Research.

Curry, W. B., and D. W. Oppo (2005), Glacial water mass geometry and the distribution of $\delta^{13}C$ of Sigma CO_2 in the western Atlantic Ocean, Paleoceanography, 20(1).

De Boer, A. M., and D. Nof (2004), The Bering Strait's grip on the northern hemisphere climate, Deep-Sea Research Part I-Oceanographic Research Papers, 51(10), 1347-1366.

Duplessy, J. C., N. J. Shackleton, R. K. Matthews, W. Prell, W. F. Ruddiman, M. Caralp, and C. H. Hendy (1984), $\delta^{13}C$ record of benthic foraminifera in the last interglacial ocean: implications for the carbon cycle and the global deep water circulation, Quaternary Research, 21(2), 225-243.

Expedition 323 Scientists, 2011. Takahashi, K., Ravelo, A.C., Alvarez Zarikian, C.A., and the Expedition 323 Scientists. Site U1342. In the Proceedings of the Integrated Ocean Drilling Program, 323 Rep. doi:10.2204/iodp.proc.323.106.2011.

Expedition 323 Scientists, 2010. Bering Sea paleoceanography: Pliocene–Pleistocene paleoceanography and climate history of the Bering Sea. IODP Prel. Rept., 323. doi:10.2204/iodp.pr.323.2010.

Gebhardt, H., M. Sarnthein, P. M. Grootes, T. Kiefer, H. Kuehn, F. Schmieder, and U. Rohl (2008), Paleonutrient and productivity records from the subarctic North Pacific for Pleistocene glacial terminations I to V, Paleoceanography, 23(4).

Herguera, J. C., E. Jansen, and W. H. Berger (1992), Evidence for a bathyal front at 2000 m depth in the glacial Pacific, based on a depth transect on the Ontong Java Plateau, Paleoceanography, 7(3), 273-288.

Hillaire-Marcel, C., and A. de Vernal (2008), Stable isotope clue to episodic sea ice formation in the glacial North Atlantic, Earth and Planetary Science Letters, 268(1-2), 143-150.

Horikawa, K., Y. Asahara, K. Yamamoto, and Y. Okazaki (2010), Intermediate water formation in the Bering Sea during glacial periods: Evidence from neodymium isotope ratios, Geology, 38(5), 435-438.

Hu, A. X., G. A. Meehl, W. Q. Han, B. Otto-Bliestner, A. Abe-Ouchi, and N. Rosenbloom (2015), Effects of the Bering Strait closure on AMOC and global climate under different background climates, Progress in Oceanography, 132, 174-196.

Hu, A. X., G. A. Meehl, W. Q. Han, A. Abe-Ouchi, C. Morrill, Y. Okazaki, and M. O. Chikamoto (2012a), The Pacific-Atlantic seesaw and the Bering Strait, Geophysical Research Letters, 39.

Hu, A. X., G. A. Meehl, B. L. Otto-Bliesner, C. Waelbroeck, W. Q. Han, M. F. Loutre, K. Lambeck, J. X. Mitrovica, and N. Rosenbloom (2010), Influence of Bering Strait flow and North Atlantic circulation on glacial sea-level changes, Nature Geoscience, 3(2), 118-121.

Hu, A. X., et al. (2012b), Role of the Bering Strait on the hysteresis of the ocean conveyor belt circulation and glacial climate stability, Proceedings of the National Academy of Sciences of the United States of America, 109(17), 6417-6422.

Jaccard, S. L., and E. D. Galbraith (2013), Direct ventilation of the North Pacific did not reach the deep ocean during the last deglaciation, Geophysical Research Letters, 40(1), 199-203.

Kallel, N., L. D. Labeyrie, A. Juilletleclerc, and J. C. Duplessy (1988), A deep hydrological front between intermediate and deep water masses in the glacial Indian Ocean, Nature, 333(6174), 651-655.

Keigwin, L. D. (2004), Radiocarbon and stable isotope constraints on Last Glacial Maximum and Younger Dryas ventilation in the western North Atlantic, Paleoceanography, 19(4).

Kim, S., B. K. Khim, M. Uchida, T. Itaki, and R. Tada (2011), Millennial-scale paleoceanographic events and implication for the intermediate-water ventilation in the northern slope area of the Bering Sea duriing the last 71 kyrs, Global and Planetary Change, 79(1-2), 89-98.

LeGrande, A. N., and G. A. Schmidt (2006), Global gridded data set of the oxygen isotopic composition in seawater, Geophysical Research Letters, 33(12).

Lisiecki, L. E. (2010), A simple mixing explanation for late Pleistocene changes in the Pacific-South Atlantic benthic $\delta^{13}C$ gradient, Climate of the Past, 6(3), 305-314.

Lisiecki, L. E., and M. E. Raymo (2005), A Pliocene-Pleistocene stack of 57 globally distributed benthic $\delta^{18}O$ records, Paleoceanography, 20(1).

Luchin, V. A., I. P. Semiletov, and G. E. Weller (2002), Changes in the Bering Sea region: atmosphere-ice-water system in the second half of the twentieth century, Progress in Oceanography, 55(1-2), 23-44.

Matsumoto, K., T. Oba, J. Lynch-Stieglitz, and H. Yamamoto (2002), Interior hydrography and circulation of the glacial Pacific Ocean, Quaternary Science Reviews, 21(14-15), 1693-1704.

Max, L., L. Lembke-Jene, J. R. Riethdorf, R. Tiedemann, D. Nurnberg, H. Kuhn, and A. Mackensen (2014), Pulses of enhanced North Pacific Intermediate Water ventilation from the Okhotsk Sea and Bering Sea during the last deglaciation, Climate of the Past, 10(2), 591-605.

Max, L., J. R. Riethdorf, R. Tiedemann, M. Smirnova, L. Lembke-Jene, K. Fahl, D. Nurnberg, A. Matul, and G. Mollenhauer (2012), Sea surface temperature variability and sea-ice extent in the subarctic northwest Pacific during the past 15,000 years, Paleoceanography, 27.

Menviel, L., A. Timmermann, O. Elison Timm, A. Mouchet, A. Abe-Ouchi, M. O. Chikamoto, N. Harada, R. Ohgaito, and Y. Okazaki (2012), Removing the North Pacific halocline: Effects on global climate, ocean circulation and the carbon cycle, Deep Sea Research Part II: Topical Studies in Oceanography, 61–64(0), 106-113.

Meyers, P. A., and J. L. Teranes (2001), Sediment Organic Matter, in Tracking Environmental Change Using Lake Sediments, edited by W. M. Last and J. P. Smol, pp. 239-269, Netherlands, Springer.

Mix, A. C., N. G. Pisias, W. Rugh, J. Wilson, A. Morey, and T. K. Hagelberg (1995), Benthic foraminifer stable isotope record from Site 849 (0-5 Ma): Local and global climate changes in N.G. Pisias, L.A. Mayer,T.R. Janecek,A. Palmer-Julson, and T.H. van Andel, eds., Proceedings of the Ocean Drilling Program, Scientific Results, 371-412.

Ohkushi, K., T. Itaki, and N. Nemoto (2003), Last Glacial-Holocene change in intermediate-water ventilation in the Northwestern Pacific, Quaternary Science Reviews, 22(14), 1477-1484.

Okazaki, Y., K. Takahashi, H. Asahi, K. Katsuki, J. Hori, H. Yasuda, Y. Sagawa, and H. Tokuyama (2005), Productivity changes in the Bering Sea during the late Quaternary, Deep-Sea Research Part II-Topical Studies in Oceanography, 52(16-18), 2150-2162.

Okazaki, Y., A. Timmermann, L. Menviel, N. Harada, A. Abe-Ouchi, M. O. Chikamoto, A. Mouchet, and H. Asahi (2010), Deepwater Formation in the North Pacific During the Last Glacial Termination, Science, 329(5988), 200-204.

Okumura, Y. M., C. Deser, A. Hu, A. Timmermann, and S. P. Xie (2009), North Pacific Climate Response to Freshwater Forcing in the Subarctic North Atlantic: Oceanic and Atmospheric Pathways, Journal of Climate, 22(6), 1424-1445.

Overland, J. E., and C. H. Pease (1982), Cyclone climatology of the Bering Sea and its relation to sea ice extent, Monthly Weather Review, 110(1), 5-13.

Paillard, D. L., L. Labeyrie, and P. Yiou (1996), Machintosh program performs time-series analysis, in Eos Trans AGU, edited.

Ravelo, A. C., and C. Hillaire-Marcel (2007), The use of oxygen and carbon isotopes of foraminifera in studies of paleoceanography, in C. Hillaire-Marcel, and A. de Vernal, eds., Proxies in late Cenozoice Paleoceanography, Developments in Marine Geology, Elsevier, Amsterdam.

Rella, S. F., R. Tada, K. Nagashima, M. Ikehara, T. Itaki, K. Ohkushi, T. Sakamoto, N. Harada, and M. Uchida (2012), Abrupt changes of intermediate water properties on the northeastern slope of the Bering Sea during the last glacial and deglacial period, Paleoceanography, 27.

Riethdorf, J. R., D. Nurnberg, L. Max, R. Tiedemann, S. A. Gorbarenko, and M. I. Malakhov (2013), Millennial-scale variability of marine productivity and terrigenous matter supply in the western Bering Sea over the past 180 kyr, Climate of the Past, 9(3), 1345-1373.

Rodionov, S. N., N. A. Bond, and J. E. Overland (2007), The Aleutian Low, storm tracks, and winter climate variability in the Bering Sea, Deep-Sea Research Part II-Topical Studies in Oceanography, 54(23-26), 2560-2577.

Rohling, E. J., K. Grant, M. Bolshaw, A. P. Roberts, M. Siddall, C. Hemleben, and M. Kucera (2009), Antarctic temperature and global sea level closely coupled over the past five glacial cycles, Nature Geoscience, 2(7), 500-504.

Ruddiman, W. F., M. E. Raymo, D. G. Martinson, B. M. Clement, and J. Backman (1989), Pleistocene Evolution: Northern Hemisphere ice sheets and North Atlantic Ocean, Paleoceanography, 4(4), 353-412.

Saenko, O. A., A. Schmittner, and A. J. Weaver (2004), The Atlantic-Pacific seesaw, Journal of Climate, 17(11), 2033-2038.

Sarnthein, M., B. Schneider, and P. M. Grootes (2013), Peak glacial ^{14}C ventilation ages suggest major draw-down of carbon into the abyssal ocean, Climate of the Past, 9(6), 2595-2614.

Schlung, S. A., et al. (2013), Millennial-scale climate change and intermediate water circulation in the Bering Sea from 90 ka: A high-resolution record from IODP Site U1340, Paleoceanography, 28(1).

Schumacher, J. D., K. Aagaard, C. H. Pease, and R. B. Tripp (1983), Effects of a shelf polynya on flow and water propoerties in the northern Bering Sea, Journal of Geophysical Research-Oceans and Atmospheres, 88(NC5), 2723-2732.

Shackleton, N. J. (1974), Attainment of isotopic equilibrium between ocean water and benthonic foraminifera genus Uvigerina: isotopic changes in the ocean during the last glacial, Colloques int Cent natn Res Scient, 219, 203-209.

Shackleton, N. J. (2000), The 100,000-year ice-age cycle identified and found to lag temperature, carbon dioxide, and orbital eccentricity, Science, 289(5486), 1897-1902.

Shaffer, G., and J. Bendtsen (1994), Role of the Bering Strait in controlling North Atlantic ocean circulation and climate, Nature, 367(6461), 354-357.

Shcherbina, A. Y., L. D. Talley, and D. L. Rudnick (2003), Direct observations of North Pacific ventilation: Brine rejection in the Okhotsk Sea, Science, 302(5652), 1952-1955.

Sosdian, S., and Y. Rosenthal (2009), Deep-Sea temperature and ice volume changes across the Pliocene-Pleistocene climate transitions, Science, 325(5938), 306-310.

Talley, L. D. (2003), Shallow, intermediate, and deep overturning components of the global heat budget, Journal of Physical Oceanography, 33(3), 530-560.

Tan, F. C., and W. D. Fraser (1976), Oxygen isotope studies on sea ice in Gulf of St. Lawrence, Journal of the Fisheries Research Board of Canada, 33(6), 1397-1401.

Tan, F. C., and P. M. Strain (1996), Sea ice and oxygen isotopes in Foxe Basin, Hudson Bay, and Hudson Strait, Canada, Journal of Geophysical Research-Oceans, 101(C9), 20869-20876.

Tanaka, S., and K. Takahashi (2005), Late Quaternary paleoceanographic changes in the Bering Sea and the western subarctic Pacific based on radiolarian assemblages, Deep-Sea Research Part II-Topical Studies in Oceanography, 52(16-18), 2131-2149.

Venz, K. A., D. A. Hodell, C. Stanton, and D. A. Warnke (1999), A 1.0 Myr record of glacial North Atlantic intermediate water variability from ODP site 982 in the northeast Atlantic, Paleoceanography, 14(1), 42-52.

Warner, M. J., and G. I. Roden (1995), Chlorofluorocarbon evidence for recent ventilation of the deep Bering Sea, Nature, 373(6513), 409-412.

Warren, B. A. (1983), Why is no deep water formed in the North Pacific?, Journal of Marine Research, 41(2), 327-347.

Woodgate, R. A., T. J. Weingartner, and R. Lindsay (2012), Observed increases in Bering Strait oceanic fluxes from the Pacific to the Arctic from 2001 to 2011 and their impacts on the Arctic Ocean water column, Geophysical Research Letters, 39.

Yasuda, I. (1997), The origin of the North Pacific Intermediate Water, Journal of Geophysical Research-Oceans, 102(C1), 893-909.

Zahn, R., K. Winn, and M. Samthein (1986), Benthic foraminiferal $\delta^{13}C$ and accumulation rates of organic carbon: *Uvigerina peregrina* group and *cibicidoides wuellerstorfi*, Paleoceanography, 1(1), 27-42.

Chapter 2

Enhanced subarctic Pacific stratification and nutrient utilization during glacials over the last 1.2 Myr

---

Abstract

The relationship between climate, biological productivity, and nutrient flux is of considerable interest in the subarctic Pacific, which represents an important high-nitrate, low-chlorophyll region. While previous studies suggest that changes in iron supply and/or physical ocean stratification could hypothetically explain orbital-scale fluctuations in subarctic Pacific nutrient utilization and productivity, previous records of nutrient utilization are too short to evaluate these relationships over many glacial-interglacial cycles. We present new, high-resolution records of sedimentary $\delta^{15}N$, which offer the first opportunity to evaluate systematic, orbital-scale variations in subarctic Pacific nitrate utilization from 1.2 Ma. Nitrate utilization was enhanced during all glacials, varied with orbital-scale periodicity since the Mid-Pleistocene Transition, was strongly correlated with enhanced aeolian dust and low atmospheric CO_2, but was not correlated with productivity. These results suggest that glacial stratification, rather than iron fertilization,

systematically exerted an important regional control on nutrient utilization and air-sea carbon flux.

1. Introduction

Today, the Southern Ocean and the subarctic Pacific represent the world's most prominent high-nitrate, low-chlorophyll (HNLC) regions. Since biological productivity in these regions is currently iron-limited [Boyd et al., 2007] and has been shown to undergo large fluctuations associated with changes in climate [e.g. Francois et al., 1997; Jaccard et al., 2010; Jaccard et al., 2005], these HNLC areas are of particular interest in regard to understanding changes in the biological pump and carbon sequestration [Francois et al., 1997; Galbraith et al., 2007; Haug et al., 1999; Jaccard et al., 2010; Sigman et al., 2010] and predicting how biogeochemical processes will influence, or be influenced by, future climate change [e.g. Ardyna et al., 2014].

Two primary mechanisms have been considered as possible explanations for variations in the utilization of major nutrients (i.e. nitrate and phosphorus) in the polar oceans: changes in iron flux and changes in water column stratification. Iron represents an important micronutrient that limits primary productivity at high latitudes [Boyd et al., 2007]; however, Lam et al. [2013] provide evidence that North Pacific productivity spiked during the last deglaciation (ca. 10-18 ka) without an increased iron flux. Additionally, Antarctic and subarctic Pacific nitrogen isotope ($\delta^{15}N$) records show that nitrate utilization was enhanced during previous glacials [Brunelle et al., 2007; Brunelle et al., 2010; Francois et al., 1992; Francois et al., 1997; Galbraith et al., 2008; Kim et al., 2015; Riethdorf et al., 2015; Robinson et al., 2005; Sigman et al., 2004; Sigman et al., 1999b; Studer et al., 2015], even while several records of Antarctic and subarctic Pacific export production demonstrate low glacial productivity [Brunelle et al., 2007; Brunelle et al., 2010; Francois et al., 1997; Gebhardt et al., 2008; Jaccard et al., 2013; Jaccard et al., 2010; Jaccard et al., 2005; Kienast et al., 2004; Kim et al., 2015; Kim et al., 2011]. The authors of these studies suggest that changes in stratification may reconcile their findings. Strong stratification limits nutrient availability at the surface, making complete nutrient consumption feasible, while weak stratification enables upwelling of nutrient-rich deep water and a renewed supply of nutrients, promoting enhanced productivity. Thus, these authors suggest that stronger stratification during cold climates may have made it possible for nitrate utilization to increase without increasing total primary productivity, and weaker stratification during warm climates may have relieved nitrate limitation and enabled high productivity (which would then be iron-limited, as in the modern ocean) without increasing the degree of nutrient utilization.

$\delta^{15}N$ recorded in ocean sediments can be used to reconstruct spatial and temporal changes in nitrate utilization in order to investigate the possible mechanisms that control primary productivity. However, previous records of $\delta^{15}N$ have been almost entirely limited to the last glacial/interglacial (G/IG) cycle in both the subarctic Pacific [Brunelle et al., 2007; Kim et al., 2011; Schlung et al., 2013] and the Antarctic [Francois et al., 1992; Francois et al., 1997; Robinson et al., 2005;

Sigman et al., 1999b], making it difficult to determine whether there is a consistent, recurring orbital-scale relationship between nutrient utilization, climate, and productivity. Galbraith et al. [2008] previously provided the longest records of nitrate utilization from the subarctic Pacific, which show that nitrate utilization was enhanced during glacials over the past 450 kyr; however, this study could not determine whether stratification or iron flux was responsible for changes in nutrient utilization. Furthermore, these records may not be long enough to confidently determine orbital-scale trends at 100-kyr periodicity, and they cannot determine potential changes over the Mid-Pleistocene Transition (MPT; 1200-700 ka), an important climate regime shift from dominant low-amplitude, 40-kyr cycles to high-amplitude, 100-kyr G/IG cycles. The longest HNLC records of nitrate utilization are 1.1 and 2.6 Myr Antarctic records of diatom-bound $\delta^{15}N$ from Giuliani et al. [2011], but these records do not have sufficient resolution or age control to enable statistical characterization of orbital-scale variability. Here we present new, long, continuous records of sedimentary $\delta^{15}N$ from Integrated Ocean Drilling Program (IODP) Expedition 323 Site U1342 from the Bering Sea (Figure 1), which resolve high-resolution changes in subarctic Pacific nutrient utilization over the last 1.2 Myr. These records provide an unprecedented opportunity to evaluate variability and trends in nutrient utilization over many G/IG cycles within an important HNLC region.

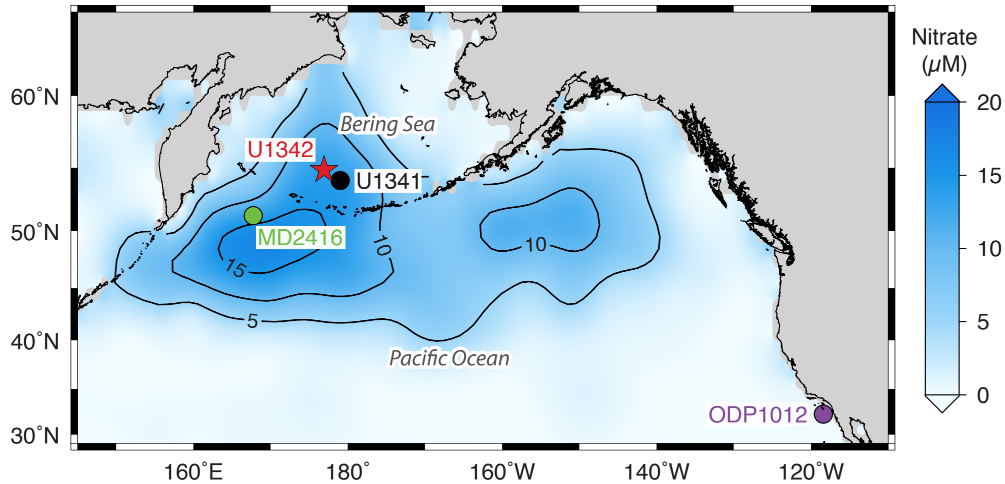

Figure 1. (a) Subarctic Pacific map of summer surface nitrate concentrations (July-September) [Garcia, 2010], with locations of IODP Site U1342 (54.83°N, 176.92°E, 818 m; this study) and U1341 (54.03°N, 179.01°E, 2140 m) located in the Bering Sea on Bowers Ridge. Also shown are ODP 1012 (32.28°N, 118.40°W, 1772 m) and MD2416 (51.27°N, 167.73°E, 2317 m).

2. Material and Methods

Cores from IODP Site U1342 (54.83°N, 176.92°E, 818 m) were sampled at ~3-cm intervals within massive sediments and 1-cm intervals within laminated sediments, yielding an average sampling frequency of ~1 sample/kyr, based on the age model applied from Knudson and Ravelo [2015]. Unwashed sediment samples were freeze-dried and crushed using a mortar and pestle. Bulk sediments (unacidified) were analyzed for $\delta^{15}N$ ($\delta^{15}N_{bulk}$) and weight percent total nitrogen (wt% N). Nitrogen mass accumulation rate (NMAR) was calculated as (dry bulk density) × (sedimentation rate) × (wt% N). A subset of carbonate-free samples from the last 250 kyr were additionally analyzed for organic $\delta^{13}C$ ($\delta^{13}C_{org}$) and C/N ratios; prior to analysis, these samples were acidified using a buffered solution of glacial acetic acid (pH=5) and repeatedly rinsed with deionized water and centrifuged to remove acid.

Sediment samples were run on a Carlo Erba 1108 elemental analyzer, interfaced to a Thermo Finnigan Delta Plus XP IRMS, at the University of California-Santa Cruz. $\delta^{15}N_{bulk}$ and $\delta^{13}C_{org}$ are expressed as per mil (‰) in conventional delta notation, relative to Vienna Pee Dee Belemnite (VPDB) for carbon isotopes, and relative to atmospheric nitrogen for nitrogen isotopes. Precision for $\delta^{15}N$ and $\delta^{13}C_{org}$ is 0.2‰, based on replicates and in-house sediment standards.

Cross-spectral analyses were conducted with AnalySeries2.0 [Paillard et al., 1996]. $\Delta\delta^{15}N$ (U1342 $\delta^{15}N_{bulk}$ – ODP1012 $\delta^{15}N_{bulk}$) was calculated following the methods of Galbraith et al. [2008]: prior to subtracting the records, both $\delta^{15}N_{bulk}$ records were linearly interpolated to 1-kyr intervals, normalized by removing the mean, and smoothed using a 9-kyr running average. Average $\Delta\delta^{15}N$ during glacials and interglacials were calculated from 0-1.2 Ma, using the LR04 benthic $\delta^{18}O$ stack from Lisiecki and Raymo [2005] to define glacial and interglacial intervals as those 1 sigma above or below a 100-kyr moving window of $\delta^{18}O$.

3. Subarctic Pacific nitrate utilization recorded by nitrogen isotopes

$\delta^{15}N_{bulk}$ provides a useful indicator of nitrate utilization—the fraction of the surface nitrate pool consumed by phytoplankton. Phytoplankton preferentially utilize ^{14}N nitrate over ^{15}N nitrate and carry this low-$\delta^{15}N$ signature to the sediments as organic matter is exported, leaving the surface nitrate pool relatively ^{15}N-enriched [Altabet and Francois, 1994]. Thus, under low-nutrient utilization conditions $\delta^{15}N_{bulk}$ is low, and under high-nutrient utilization conditions the $\delta^{15}N_{bulk}$ value approaches the $\delta^{15}N$ value of the source nitrate ($\delta^{15}N_{nitrate}$) [Altabet and Francois, 1994; Sigman et al., 1999a], which is 5-6‰ in the Bering Sea today [Lehmann et al., 2005]. $\delta^{15}N_{bulk}$ can also be affected by changes in the $\delta^{15}N_{nitrate}$, which may be influenced by changes in source waters (with different $\delta^{15}N_{nitrate}$ values) and/or water column denitrification, which raises the $\delta^{15}N_{nitrate}$ [Sigman et al., 2009]. The $\delta^{15}N_{bulk}$ values at U1342 range from approximately 0.2 to 7.0‰ (Figure 2). Since there are peaks in the record that are close to or exceed the present day source water, and considering the fact that nitrate is not fully utilized within the Bering Sea [Riethdorf et al., 2015], it appears that changes in $\delta^{15}N_{nitrate}$ of the source water must affect the U1342 record to some extent. $\delta^{15}N$ values exceeding modern $\delta^{15}N_{nitrate}$ have also been demonstrated in other, shorter Bering Sea records from Bowers Ridge, including a $\delta^{15}N_{bulk}$ record from Site U1340, which showed peaks exceeding 8‰ [Schlung et al., 2013], and a record of diatom-bound $\delta^{15}N$ from Site JPC-17, which had peaks of up to 9‰, although possible fractionation due to diatom uptake is poorly understood [Brunelle et al., 2007].

Since $\delta^{15}N_{nitrate}$ values can change over time, the recorded $\delta^{15}N_{bulk}$ signature reflects both the $\delta^{15}N_{nitrate}$ of its source and the degree of nitrate utilization in the proximal surface waters. Therefore, it is necessary to subtract the source water $\delta^{15}N_{nitrate}$ signal from the $\delta^{15}N_{bulk}$ signal in order to determine changes in nitrate utilization. No North Pacific $\delta^{15}N_{bulk}$ stack is available to represent regional background conditions, as very few North Pacific $\delta^{15}N_{bulk}$ records extend before the last glacial cycle. Therefore, we follow the methodology of Galbraith et al. [2008] by using the long $\delta^{15}N_{bulk}$ record from ODP Site 1012 [Liu et al., 2005] in the Eastern North Pacific (32.28°N, 118.40°W, 1772 m) to represent changes in the North Pacific $\delta^{15}N_{nitrate}$ (i.e. the background $\delta^{15}N_{nitrate}$), which we subtract from our $\delta^{15}N_{bulk}$ record, to yield a record of nitrate utilization. A similar method of calculating nitrate utilization in the equatorial Pacific has also been employed by Rafter and Charles [2012]. Because Site 1012 has nearly complete nitrate utilization (Figure 1), its $\delta^{15}N_{bulk}$ record is thought to be representative of $\delta^{15}N_{nitrate}$ [Galbraith et al., 2008; Liu et al., 2005]. Thus, we use $\Delta\delta^{15}N$ (calculated as U1342 $\delta^{15}N_{bulk}$ – Site 1012 $\delta^{15}N_{bulk}$) to represent the signal at U1342 that is predominantly due to changes in nitrate utilization, with relatively high $\Delta\delta^{15}N$ values indicating high nitrate utilization, and vice versa.

To verify that changes in the amount of terrestrial organic matter do not strongly bias the U1342 $\delta^{15}N_{bulk}$ signal, we measured $\delta^{13}C_{org}$ and C/N ratios from Site U1342 (Figure B1a in Appendix B) and used their respective marine and terrestrial end-member values (Table B1 in Appendix B) in the context of a linear mixing model to estimate the relative contribution of terrestrial and marine organic matter (Figure B1b in Appendix B), then calculated a record of the marine-component $\delta^{15}N$. A detailed account of these methods is discussed in Appendix B text B1. The values and variability of the calculated marine $\delta^{15}N$ record are very similar to the measured $\delta^{15}N_{bulk}$ record (Figure B1c in Appendix B), indicating that the $\delta^{15}N_{bulk}$ signal at U1342 strongly reflects the isotopic variability of marine nitrogen sources.

Additionally, Site U1342 is optimally located to avoid the effects of $\delta^{15}N_{bulk}$ diagenetic alteration for two reasons: (1) sediments deposited in high-productivity regions reflect the $\delta^{15}N$ of the falling particles [Altabet, 2006; Robinson et al., 2012], and (2) shallow/intermediate depth sites are less likely to undergo diagenesis compared to open ocean sites [Altabet et al., 1999]. As further evidence, the $\delta^{15}N_{bulk}$ record from Site U1342 is consistent with a short (40 kyr) record of diatom-bound $\delta^{15}N$ from nearby Site JPC-17 [Brunelle et al., 2007], which shows a 2‰ change between Marine Isotope Stages (MIS) 1 and 2. The $\Delta\delta^{15}N$ record at Site U1342 also matches western subarctic Pacific site MD2416 (51.27°N, 167.73°E, 2317 m) from Galbraith et al. [2008] (Figure 2c), which diatom-bound $\delta^{15}N$ values confirmed was unaffected by diagenesis.

4. $\Delta\delta^{15}N$ results compared to records of climate, primary productivity, and iron

The unprecedented length and resolution of this new nitrogen isotope record enables us, for the first time, to resolve orbital-scale variability and conduct statistically robust tests to evaluate the potential mechanisms that may have systematically influenced subarctic Pacific nutrient utilization. Changes in nitrate utilization ($\Delta\delta^{15}N$) at Site U1342 (Figure 2c) are strongly correlated ($R=0.71$) with changes in global climate (i.e. global ice sheet volume and ocean temperature) represented by the LR04 benthic $\delta^{18}O$ stack from Lisiecki and Raymo [2005], and a cross-plot of the two variables (Figure B2 in Appendix B) shows that all glacials from 1.2 Ma had high nitrate utilization. This consistent relationship can also be seen in Figure 2c. Over the span of the whole 1.2 Myr record, average $\Delta\delta^{15}N$ during glacials (0.82‰) and interglacials (-1.34‰) showed a statistically significant difference ($p<0.0001$). Spectral analyses reveal that the $\Delta\delta^{15}N$ record varied on Milankovitch orbital timescales, with dominant periodicity at 100 kyr (i.e. eccentricity timescales), while 41 and 23-kyr periodicities (i.e. obliquity and precession timescales) were less pronounced and represent much less of the total variability (Figure B3 in Appendix B). While nitrate utilization was consistently higher during all glacials throughout the 1.2 Myr record, these cyclical trends on Milankovitch periodicities came into prominence only after the MPT (~700 ka; Figure B4 in Appendix B).

To test if increased nitrate utilization was related to iron fertilization or another mechanism, such as stratification, we use cross-spectral analyses to assess coherency and phase between the $\Delta\delta^{15}N$ record from U1342 and available records of iron variability and primary productivity. Here, we focus our attention on cross-spectral analyses conducted on just the portion of the record after the MPT (700-0 ka) in order to isolate patterns of variability occurring in this recent time interval and to avoid possible complications related to changes in variability during the MPT itself. A strong, positive correlation between $\Delta\delta^{15}N$, iron, and primary productivity would support the hypothesis that iron flux controlled biological productivity and nitrate utilization, whereas a negative or low correlation between $\Delta\delta^{15}N$ and primary productivity would support an inferred interpretation that stratification, rather than iron flux, was responsible for enhanced nitrate utilization. We also compare these records of $\Delta\delta^{15}N$, iron, and primary productivity to climate records in order to determine potential patterns related to G/IG cycles.

Figure 2 shows our new record of U1342 $\Delta\delta^{15}N$, compared with regional and global records representing windblown dust and iron: EPICA ice core dust mass [Lambert et al., 2008], Pacific Southern Ocean sediment iron (wt.%) [Lamy et al., 2014], and Chinese loess magnetic susceptibility [Clemens et al., 2008]. Enhanced dust (iron) flux is marked by high values of EPICA ice core dust mass and Pacific Southern Ocean sediment iron (wt.%) and low values of Chinese loess magnetic susceptibility. While local dust (iron) flux records would be ideal for this comparison, none are currently available. Of the three records used here, Chinese loess may be the most representative of Bering Sea iron deposition, as Asia is believed to be a dominant source of dust to the North Pacific and Bering Sea [Mahowald et al., 2011; Mahowald et al., 2009; Rea, 1994].

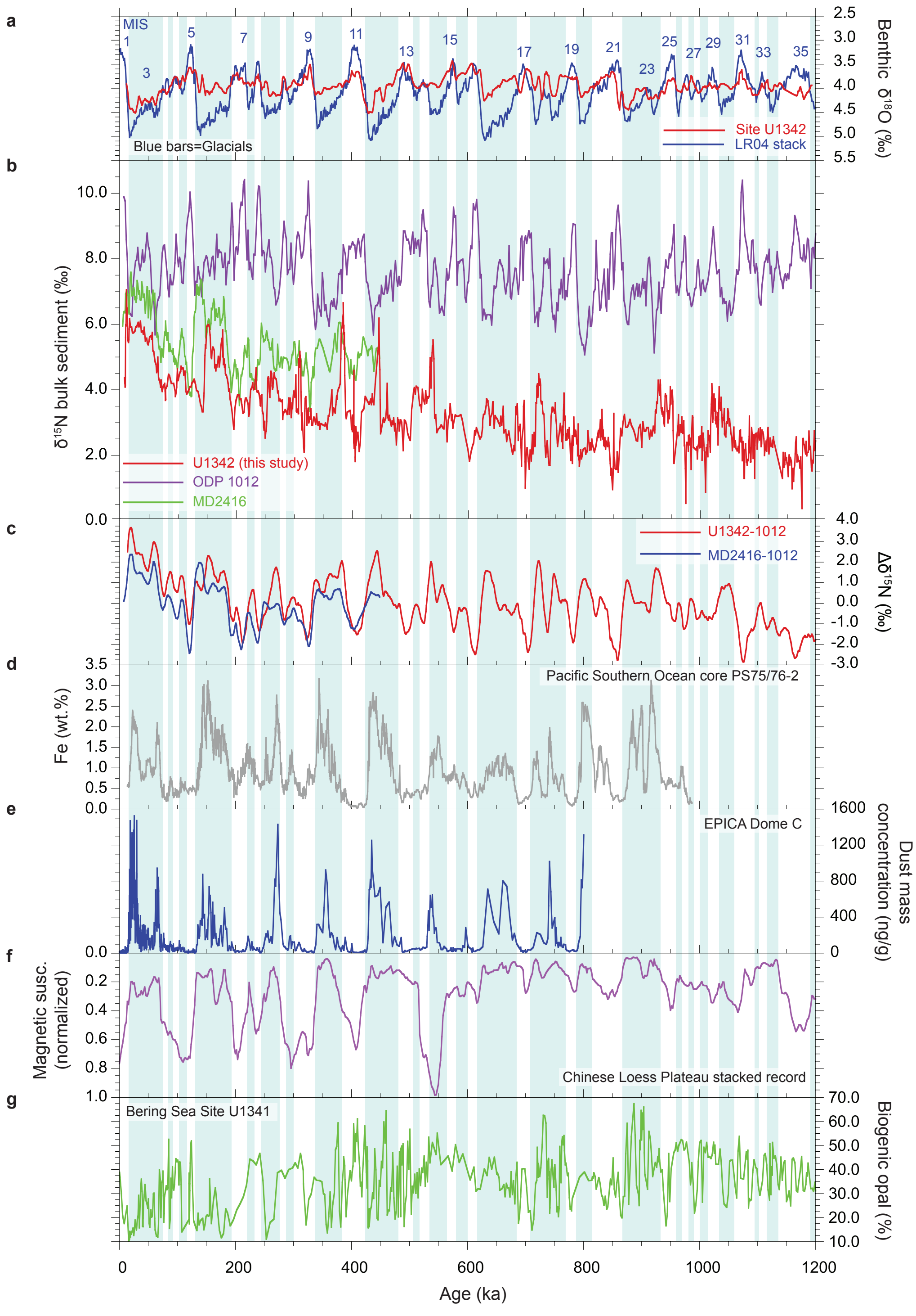

Figure 2. (a) The LR04 benthic δ^{18}O stack (blue) [Lisiecki and Raymo, 2005], reflecting global ice volume and ocean temperature. Glacial intervals, where LR04 δ^{18}O $\geq$ 4.0‰, are highlighted with blue vertical bars. Smoothed benthic

foraminiferal $\delta^{18}O$ from Site U1342 (red) [Knudson and Ravelo, 2015] shows that the U1342 record is continuous to Marine Isotope Stage (MIS) 35. **(b)** $\delta^{15}N_{bulk}$ of Site U1342 (red) compared to IODP Site 1012 [Liu et al., 2005] (violet) and MD2416 [Galbraith et al., 2008] (green). **(c)** Nitrate utilization ($\Delta\delta^{15}N$) records at Site U1342 (this study; red) and MD2416 [Galbraith et al., 2008] (blue). **(d)** Iron (wt.%) in Southern Ocean sediment core PS75/076 [Lamy et al., 2014]. **(e)** Coulter Counter dust mass concentration from EPICA Dome C [Lambert et al., 2008]. **(f)** Chinese loess magnetic susceptibility, in which lower values represent greater iron flux [Clemens et al., 2008]. **(g)** U1341 biogenic opal representing primary productivity [Iwasaki et al., 2012].

Table 1. Cross-spectral analysis results after the MPT (0-700 ka). Phase (kyr) relative to $\Delta\delta^{15}N$, for coherency ≥0.70. See Table B2 in Appendix B for exact coherency values. Positive phase indicates lag behind $\Delta\delta^{15}N$; negative phase indicates lead ahead of $\Delta\delta^{15}N$.

Record used in cross-spectral analysis with $\Delta\delta^{15}N$	100 kyr periodicity	41 kyr periodicity	23 kyr periodicity
Solar insolation (min.) at 65°N[1]	-	-5.7±1.1	-3.8±0.9
U1341 biogenic opal (%) (min.)[2]	-	-	-1.4±1.4
China loess magnetic susceptibility (min.)[3]	-	-0.9±2.4	-0.7±1.3
EPICA pCO_2 (min.)[4]	-1.0±2.1	2.2±1.6	-2.4±1.4
LR04 $\delta^{18}O$ (max. glacial)[5]	2.1±1.6	1.6±0.8	-2.4±0.6
EPICA dust mass[6]	2.2±2.2	-2.9±2.1	-2.5±1.2
Pacific Southern Ocean iron (wt.%)[7]	2.5±2.9	-1.2±1.6	-

The datasets used in the cross-spectral analyses are from [1]Laskar et al. [2004]; [2]Iwasaki et al. [2012]; [3]Clemens et al. [2008]; [4]Luthi et al. [2008]; [5]Lisiecki and Raymo [2005]; [6]Lambert et al. [2008]; [7]Lamy et al. [2014]. There was no significant coherency between $\Delta\delta^{15}N$ and wt %N or nitrogen mass accumulation rate (NMAR), two proxies of productivity from Site U1342.

A summary of the cross-spectral analyses is provided in Table 1. We first consider the results at 100-kyr periodicity, the dominant variability for $\Delta\delta^{15}N$ records, in order to assess the mechanisms potentially most responsible for changes in nitrate utilization. At 100-kyr periodicity, $\Delta\delta^{15}N$ is coherent and in phase (within error) with EPICA ice core dust, Pacific Southern Ocean sediment iron, and pCO_2 minima from EPICA Dome C [Luthi et al., 2008], and $\Delta\delta^{15}N$ is approximately in phase with glacial maxima (maximum $\delta^{18}O$ in the LR04 benthic stack). These results suggest that there is a general, recurring relationship in which Bering Sea nitrate utilization is highest when global aeolian iron availability is at a maximum, which occurs near peak glacials with low pCO_2.

At 41-kyr periodicity, $\Delta\delta^{15}N$ is in phase (within error) with Pacific Southern Ocean sediment iron and Chinese loess magnetic susceptibility (minima) and slightly lags EPICA ice core dust (by 2.9±2.1 kyr). At 23-kyr periodicity, $\Delta\delta^{15}N$ occurs in phase with Chinese loess (magnetic susceptibility minima) and slightly lags EPICA dust (by 2.5±1.2 kyr), but has no strong coherency (≥0.70) with Pacific Southern Ocean iron. Together, results at all three dominant Milankovitch periodicities, which represent the strongest $\Delta\delta^{15}N$ variability, show a consistent pattern in which nitrate utilization is highest when iron/dust availability is also at (or near) a maximum. However, while the timing between nitrate utilization and aeolian iron availability is approximately in phase, the correlation alone cannot be used to demonstrate a causal link between the two variables. We must also look at productivity changes in order to assess whether increased nitrate utilization can be attributed to iron fertilization.

Therefore, as a next step, we compare our record of $\Delta\delta^{15}N$ to several orbital-scale records representing local primary productivity (Figure 2; Figure B5 in Appendix B): biogenic opal (%) at nearby Site U1341 from Iwasaki et al. [2012], U1342 NMAR, U1342 wt% N, and U1342 density measured by gamma ray attenuation (GRA) from Expedition 323 Scientists, [2011]. (Low GRA values have been shown to indicate high biogenic opal content [Knudson and Ravelo, 2015]). Cross-spectral results (Table 1) show that U1341 biogenic opal (%) is not coherent with $\Delta\delta^{15}N$ at 100-kyr and 41-kyr periodicities, and is approximately antiphase with $\Delta\delta^{15}N$ at 23-kyr periodicities. These results suggest that enhanced nitrate utilization is not coincident with enhanced productivity and therefore is not likely attributed to variations in aeolian iron availability.

Additionally, the other proxies of productivity we considered are not coherent at the major Milankovitch periodicities and thus cannot explain the most dominant variability in $\Delta\delta^{15}N$. U1342 NMAR and wt% N show no significant coherency to $\Delta\delta^{15}N$ on any orbital timescale (also see Figure B6 in Appendix B), and U1342 density (GRA) is only coherent with $\Delta\delta^{15}N$ at 29-kyr periodicities (density minima leads $\Delta\delta^{15}N$ by 3.3±1.7 kyr). Thus, while productivity may be potentially influential on Bering Sea nitrate utilization at non-Milankovitch timescales (due to the correlation between high nitrate utilization and high productivity indicated by low GRA at 29-kyr periodicity), the prevailing variability in nitrate utilization (at Milankovitch periodicities) must be explained by some other factor. These results, which show there is likely not a strong, consistent relationship between primary productivity and nitrate utilization in the Bering Sea at the dominant orbital timescales, challenge the argument that iron fertilization and associated productivity was the mechanism that led to more complete nitrate utilization during past glacials.

Besides G/IG trends, both the U1342 and MD2416 $\Delta\delta^{15}N$ records exhibit long-term trends of increasing glacial values starting at approximately 400 ka (Figure 2c), indicating regionally enhanced nitrate utilization during glacial periods in the youngest part of the record. As this increase in nitrate utilization is not accompanied by an increase in local productivity (Figure 2d-2f), we infer that stratification must have been particularly strong in these most recent glacials. It has been suggested that the subarctic Pacific steep vertical salinity gradient, a dominant control on upper-ocean stratification, could have been intensified during extensive glaciations in the past [Haug et al., 1999]. The increased presence of Arctic sea ice since ~400 ka [Polyak et al., 2013; Polyak et al., 2010] is consistent with a regional cooling trend and may support the idea that glacial stratification intensified during this time.

5. Discussion and Conclusions

Collectively, our $\Delta\delta^{15}N$ records and statistical tests show that glacial climates have been consistently associated with enhanced nitrate utilization over the past 1.2 Myr. Cross-spectral analyses of records since the MPT reveal a general association in which glacial climates had relatively high subarctic Pacific nitrate utilization and enhanced deposition of aeolian iron, while productivity on orbital scales was unrelated. In order to achieve enhanced nitrate utilization without increasing the overall primary productivity, the nitrate pool available for phytoplankton consumption must be reduced. While other studies have suggested this mechanism over the most recent glacial cycle [e.g. Brunelle et al., 2007], our data indicate that for all glacials of the last 35 MIS, strong physical stratification of subarctic Pacific surface waters provided a necessary mechanism for isolating nitrate at the surface (by preventing upwelling of additional nitrate from underlying water), such that the surface nitrate could be used to near completion.

Although there is synchronous timing of dust/iron availability and nitrate utilization, the lack of a consistent relationship between nitrate utilization and primary productivity demonstrates that iron fertilization is not a major factor in controlling primary productivity or nitrate utilization in the Bering Sea. However, the generation of more long, high-resolution productivity records for comparison would strengthen this interpretation. Given the available data, we suggest that the coherency between dust and nitrate utilization is coincidental, rather than causal, and can be attributed to changes in climate, as Northern Hemisphere glacial climate may have coincidentally enhanced dust flux as well as stratification. Ruling out iron fertilization as the main mechanism, we propose that stratification was the dominant control on nitrate utilization during past glacials, similar to what occurs in the nitrate-limited subtropical Pacific today.

Our interpretation of recurring, enhanced glacial stratification is supported by several other subarctic Pacific studies based on much shorter records, which find evidence for high nitrate utilization (using $\delta^{15}N$), but low primary productivity, and infer this to be indicative of enhanced stratification during very recent glacials [Brunelle et al., 2007; Brunelle et al., 2010; Riethdorf et al., 2015; Schlung et al., 2013]. A short (2.6-2.8 Ma) subarctic Pacific $\delta^{15}N$ record from Sigman et al. [2004] also shows enhanced glacial nitrate utilization during times of low productivity, leading these authors to suggest glacial stratification. Records of nitrate utilization over the last 450 kyr from Galbraith et al. [2008] also demonstrate enhanced glacial nutrient utilization (Figure 2), but these authors were unable to determine if this trend was due to changes in stratification or iron flux. Additionally, records of subarctic Pacific productivity from Jaccard et al. [2010] over the past 800 kyr indicate that productivity was relatively low in glacials compared to interglacials. Although they do not measure nitrate utilization, these authors infer that physical stratification could be a primary factor in controlling nutrient supply and productivity. Our 1.2 Myr records of nitrate utilization enable us to conduct the first statistical tests capable of determining consistent, orbital-scale trends in HNLC polar region nitrate utilization and its relationship to climate and productivity. Results from this study indicate that stratification has been an important, recurring mechanism for nitrate utilization over many glacial cycles, and that this behavior has occurred at orbital-scale (Milankovitch) cycles since the end of the MPT.

Our results have implications for understanding the interactions between the biological pump and atmospheric CO_2 on G/IG timescales. In the subarctic Pacific and Southern Ocean, dense waters rich in nutrients and dissolved CO_2 outcrop at the surface, providing the opportunity for enhanced phytoplankton growth (and associated carbon fixation) but also the ability for CO_2 previously sequestered in the deep ocean to be released to the atmosphere [Jaccard et al., 2010]. Therefore, either increased productivity and/or stronger stratification should enhance CO_2 sequestration during glacials. Thus, some important studies [e.g. Francois et al., 1997; Jaccard et al., 2010; Sigman et al., 2010] have proposed that atmospheric pCO_2 was lower in past glacials due in part to polar stratification and not iron-induced productivity, as previously suggested [Blain et al., 2007; Martin, 1990; Pollard et al., 2009]. However, the longest available records of North Pacific paleoproductivity, Jaccard et al. [2010], are limited by poor age control and thus cannot help resolve orbital-scale coherency between productivity and CO_2. Our findings show that subarctic Pacific nitrate utilization ($\Delta\delta^{15}N$) and pCO_2 are nearly in phase at the timescale of dominant $\Delta\delta^{15}N$ variability (100-kyr periodicity). These results agree with the idea that stratification is an important factor in controlling CO_2 sequestration, because pCO_2 minima occurred when nitrate utilization maxima indicates that stratification was strongest. It therefore appears that polar ocean stratification could have reduced oceanic CO_2 "leakage" to the atmosphere, acting as a climate feedback that enhanced cooling.

In proposing that stratification is the principal driver of nitrate utilization, the question that follows is whether stratification itself can lead to complete nitrate utilization in biologically iron-limited areas, or whether increased iron flux is also needed. While nitrate-limited areas, such as sub-tropical gyres, exhibit complete nitrate utilization, productivity in the Bering Sea—even during glacials—was much higher than in modern sub-tropical gyres. Therefore, additional iron may have been required to sustain enhanced nitrate utilization, even if stratification was the primary control on nitrate availability. Our results, which show that high dust flux was correlated to glacial climates and enhanced nitrate utilization, may support this idea. If so, this would suggest the possibility that the enhanced availability of iron during glacials helped to change the region into one in which productivity was nitrate-limited rather than iron-limited, as it is today. Future work focused on directly determining past stratification (with long, high-resolution records of sea surface temperature or salinity) within the HNLC polar regions will be instrumental in conclusively distinguishing the relative contributions of stratification and iron fertilization to nitrate utilization and primary productivity. While many previous studies have suggested high-latitude stratification as an explanation for enhanced nitrate consumption [e.g. Brunelle et al., 2010; Francois et al., 1997; Sigman et al., 2004], stratification itself has never been measured. Long, high resolution records of productivity are also needed for statistical analyses to confirm the relationship between nutrient utilization and productivity, and to confirm the suggestions made here that stratification is primarily responsible for enhanced nutrient utilization.

Additionally, records of local iron flux would allow for more direct evaluation of the link between iron availability and productivity.

These records from U1342 represent well-dated orbital-scale records of Bering Sea nitrate utilization over the last 1.2 Myr, and there is a clear need for other long, high-resolution records of nutrient utilization within HNLC polar regions. Having a broad database of long, detailed $\delta^{15}N$ records with excellent age control would allow us to determine if the nitrate utilization changes in the polar oceans were synchronous—which would be a strong argument for stratification as a large-scale, straightforward mechanism for changing nutrient utilization. Overall, knowing more about nitrate utilization will increase our ability to understand large-scale processes, including nutrient cycling, productivity, CO_2 sequestration, and other physical and biogeochemical relationships within the ocean and atmosphere.

Acknowledgments

Samples were provided by the Integrated Ocean Drilling Program (IODP). Funding was provided by a Schlanger Ocean Drilling Fellowship from the Consortium for Ocean Leadership and NSF Grant OCE0963144. We would like to thank the IODP Expedition 323 Shipboard Party for core collection and many members of the Ravelo Lab for help with sampling. We are also grateful to Dyke Andreasen, Chih-Ting Hsieh, Timothy Lambert, and Colin Carney for support with instrumentation, as well as several members of the Ravelo lab for laboratory assistance, including Elektra Robinson, Joey Hermosillo, Max Aung, and others. We would also like to thank Ivano Aiello, Phoebe Lam, and James Zachos for their helpful discussions, and two anonymous reviewers for their constructive comments on this manuscript.

References

Altabet, M. A. (2006), Isotopic Tracers of the Marine Nitrogen Cycle: Present and Past, in Marine Organic Matter: Biomarkers, Isotopes and DNA, edited by J. K. Volkman, pp. 251-293, Springer Berlin Heidelberg.

Altabet, M. A., and R. Francois (1994), Sedimentary nitrogen isotopic ratio as a recorder for surface ocean nitrate utilization, Global Biogeochemical Cycles, 8(1), 103-116, doi:10.1029/93gb03396.

Altabet, M. A., C. Pilskaln, R. Thunell, C. Pride, D. Sigman, F. Chavez, and R. Francois (1999), The nitrogen isotope biogeochemistry of sinking particles from the margin of the Eastern North Pacific, Deep-Sea Research Part I-Oceanographic Research Papers, 46(4), 655-679, doi:10.1016/s0967-0637(98)00084-3.

Ardyna, M., M. Babin, M. Gosselin, E. Devred, L. Rainville, and J. E. Tremblay (2014), Recent Arctic Ocean sea ice loss triggers novel fall phytoplankton blooms, Geophysical Research Letters, 41(17), 6207-6212, doi:10.1002/2014gl061047.

Blain, S., et al. (2007), Effect of natural iron fertilization on carbon sequestration in the Southern Ocean, Nature, 446(7139), 1070-U1071, doi:10.1038/nature05700.

Boyd, P. W., et al. (2007), Mesoscale iron enrichment experiments 1993-2005: Synthesis and future directions, Science, 315(5812), 612-617, doi:10.1126/science.1131669.

Brunelle, B. G., D. M. Sigman, M. S. Cook, L. D. Keigwin, G. H. Haug, B. Plessen, G. Schettler, and S. L. Jaccard (2007), Evidence from diatom-bound nitrogen isotopes for subarctic Pacific stratification during the last ice age and a link to North Pacific denitrification changes, Paleoceanography, 22(1), doi:10.1029/2005pa001205.

Brunelle, B. G., D. M. Sigman, S. L. Jaccard, L. D. Keigwin, B. Plessen, G. Schettler, M. S. Cook, and G. H. Haug (2010), Glacial/interglacial changes in nutrient supply and stratification in the western subarctic North Pacific since the penultimate glacial maximum, Quaternary Science Reviews, 29(19-20), 2579-2590, doi:10.1016/j.quascirev.2010.03.010.

Clemens, S. C., W. L. Prell, Y. B. Sun, Z. Y. Liu, and G. S. Chen (2008), Southern Hemisphere forcing of Pliocene $\delta^{18}O$ and the evolution of Indo-Asian monsoons, Paleoceanography, 23(4), doi:10.1029/2008pa001638.

Expedition 323 Scientists (2011), Site U1342. In Takahashi, K., Ravelo, A.C., Alvarez Zarikian, C.A., and the Expedition 323 Scientists. Proceedings of the Integrated Ocean Drilling Program, 323: Tokyo (Integrated Ocean Drilling Program Management International, Inc.)

Francois, R., M. A. Altabet, and L. H. Burckle (1992), Glacial to interglacial changes in surface nitrate utilization in the Indian sector of the Southern Ocean as recorded by sediment $\delta^{15}N$, Paleoceanography, 7(5), 589-606, doi:10.1029/92pa01573.

Francois, R., M. A. Altabet, E. F. Yu, D. M. Sigman, M. P. Bacon, M. Frank, G. Bohrmann, G. Bareille, and L. D. Labeyrie (1997), Contribution of Southern Ocean surface-water stratification to low atmospheric CO_2 concentrations during the last glacial period, Nature, 389(6654), 929-935, doi:10.1038/40073.

Galbraith, E. D., M. Kienast, S. L. Jaccard, T. F. Pedersen, B. G. Brunelle, D. M. Sigman, and T. Kiefer (2008), Consistent relationship between global climate and surface nitrate utilization in the western subarctic Pacific throughout the last 500 ka, Paleoceanography, 23(2), doi:10.1029/2007pa001518.

Galbraith, E. D., S. L. Jaccard, T. F. Pedersen, D. M. Sigman, G. H. Haug, M. Cook, J. R. Southon, and R. Francois (2007), Carbon dioxide release from the North Pacific abyss during the last deglaciation, Nature, 449(7164), 890-U899, doi:10.1038/nature06227.

Garcia, H. E., R. A. Locarnini, T. P. Boyer, and J. I. Antonov (2010), World Ocean Atlas 2009, Volume 4: Nutrients (phosphate, nitrate, silicate). S. Levitus, Ed. NOAA Atlas NESDIS 71, U.S. Government Printing Office, Washington, D.C., 398 pp.

Gebhardt, H., M. Sarnthein, P. M. Grootes, T. Kiefer, H. Kuehn, F. Schmieder, and U. Rohl (2008), Paleonutrient and productivity records from the subarctic North Pacific for Pleistocene glacial terminations I to V, Paleoceanography, 23(4), doi:10.1029/2007pa001513.

Giuliani, S., L. Capotondi, P. Maffioli, L. Langone, F. Giglio, R. Yam, M. Frignani, and M. Ravaioli (2011), Paleoenvironmental changes in the Pacific sector of the Southern Ocean (Antarctica) during the past 2.6 Ma, Global and Planetary Change, 77(1-2), 34-48, doi:10.1016/j.gloplacha.2011.02.008.

Haug, G. H., D. M. Sigman, R. Tiedemann, T. F. Pedersen, and M. Sarnthein (1999), Onset of permanent stratification in the subarctic Pacific Ocean, Nature, 401(6755), 779-782, doi:10.1038/44550.

Iwasaki, S., K. Takahashi, T. Maesawa, T. Sakamoto, S. Sakai, and K. Iijima (2012), Paleoceanography of the last 500 kyrs in the central Okhotsk Sea based on geochemistry, Deep-Sea Research Part II-Topical Studies in Oceanography, 61-64, 50-62, doi:10.1016/j.dsr2.2011.03.003.

Jaccard, S. L., C. T. Hayes, A. Martinez-Garcia, D. A. Hodell, R. F. Anderson, D. M. Sigman, and G. H. Haug (2013), Two modes of change in Southern Ocean productivity over the past million years, Science, (339)6126, 1419-1423, doi: 10.1126/science.1227545.

Jaccard, S. L., E. D. Galbraith, D. M. Sigman, and G. H. Haug (2010), A pervasive link between Antarctic ice core and subarctic Pacific sediment records over the past 800 kyrs, Quaternary Science Reviews, 29(1-2), 206-212, doi:10.1016/j.quascirev.2009.10.007.

Jaccard, S. L., G. H. Haug, D. M. Sigman, T. F. Pedersen, H. R. Thierstein, and U. Rohl (2005), Glacial/interglacial changes in subarctic North Pacific stratification, Science, 308(5724), 1003-1006, doi:10.1126/science.1108696.

Kienast, S. S., I. L. Hendy, J. Crusius, T. F. Pedersen, and S. E. Calvert (2004), Export production in the subarctic North Pacific over the last 800 kyrs: No evidence for iron fertilization?, Journal of Oceanography, 60(1), 189-203, doi:10.1023/B:JOCE.0000038326.73943.aa.

Kim, S., B. K. Khim, and K. Takahashi (2015), Late Pliocene to early Pleistocene (2.4-1.25 Ma) paleoproductivity changes in the Bering Sea: IODP Expedition 323 Hole U1343E, Deep-Sea Research II, in press.

Kim, S., B. K. Khim, M. Uchida, T. Itaki, and R. Tada (2011), Millennial-scale paleoceanographic events and implication for the intermediate-water ventilation in the northern slope area of the Bering Sea duriing the last 71 kyrs, Global and Planetary Change, 79(1-2), 89-98, doi:10.1016/j.gloplacha.2011.08.004.

Knudson, K. P., and A. C. Ravelo (2015), North Pacific Intermediate Water circulation enhanced by the closure of the Bering Strait, Paleoceanography, in press, doi:10.1002/2015PA002840.

Lam, P. J., L. F. Robinson, J. Blusztajn, C. Li, M. S. Cook, J. F. McManus, and L. D. Keigwin (2013), Transient stratification as the cause of the North Pacific productivity spike during deglaciation, Nature Geoscience, 6(8), 622-626, doi:10.1038/ngeo1873.

Lambert, F., B. Delmonte, J. R. Petit, M. Bigler, P. R. Kaufmann, M. A. Hutterli, T. F. Stocker, U. Ruth, J. P. Steffensen, and V. Maggi (2008), Dust-climate couplings over the past 800,000 years from the EPICA Dome C ice core, Nature, 452(7187), 616-619, doi:10.1038/nature06763.

Lamy, F., R. Gersonde, G. Winckler, O. Esper, A. Jaeschke, G. Kuhn, J. Ullermann, A. Martinez-Garcia, F. Lambert, and R. Kilian (2014), Increased Dust Deposition in the Pacific Southern Ocean During Glacial Periods, Science, 343(6169), 403-407, doi:10.1126/science.1245424.

Laskar, J., P. Robutel, F. Joutel, M. Gastineau, A. C. M. Correia, and B. Levrard (2004), A long-term numerical solution for the insolation quantities of the Earth, Astron. Astrophys., 428(1), 261–285, doi:10.1051/0004-6361:20041335.

Lehmann, M. F., D. M. Sigman, D. C. McCorkle, B. G. Brunelle, S. Hoffmann, M. Kienast, G. Cane, and J. Clement (2005), Origin of the deep Bering Sea nitrate deficit: Constraints from the nitrogen and oxygen isotopic composition of water column nitrate and benthic nitrate fluxes, Global Biogeochemical Cycles, 19(4), doi:10.1029/2005gb002508.

Lisiecki, L. E., and M. E. Raymo (2005), A Pliocene-Pleistocene stack of 57 globally distributed benthic $\delta^{18}O$ records, Paleoceanography, 20(1), doi:10.1029/2004pa001071.

Liu, Z. H., M. A. Altabet, and T. D. Herbert (2005), Glacial-interglacial modulation of eastern tropical North Pacific denitrification over the last 1.8-Myr, Geophysical Research Letters, 32(23), doi:10.1029/2005gl024439.

Luthi, D., et al. (2008), High-resolution carbon dioxide concentration record 650,000-800,000 years before present, Nature, 453(7193), 379-382, doi:10.1038/nature06949.

Mahowald, N. M., S. Albani, S. Engelstaedter, G. Winckler, and M. Goman (2011), Model insight into glacial-interglacial paleodust records, Quaternary Science Reviews, 30(7-8), 832-854, doi:10.1016/j.quascirev.2010.09.007.

Mahowald, N. M., et al. (2009), Atmospheric Iron Deposition: Global Distribution, Variability, and Human Perturbations, Annual Review of Marine Science, 1, 245-278, doi:10.1146/annurev.marine.010908.163727.

Martin, J. H. (1990), Glacial-interglacial CO_2 change: The iron hypothesis, Paleoceanography, 5(1), 1-13, doi:10.1029/PA005i001p00001.

Paillard, D. L., L. Labeyrie, and P. Yiou (1996), Machintosh program performs time-series analysis, in Eos Trans AGU, edited.

Pollard, R. T., et al. (2009), Southern Ocean deep-water carbon export enhanced by natural iron fertilization, Nature, 457(7229), 577-U581, doi:10.1038/nature07716.

Polyak, L., et al. (2010), History of sea ice in the Arctic, Quat. Sci. Rev., 29 (15 16), 1757–1778, doi:10.1016/j.quascirev.2010.02.010.

Polyak, L., K. M. Best, K. A. Crawford, E. A. Council, and G. St-Onge (2013), Quaternary history of sea ice in the western Arctic Ocean based on foraminifera, Quat. Sci. Rev., 79, 145–156, doi:10.1016/j.quascirev.2012.12.018.

Rafter, P. A., and C. D. Charles (2012), Pleistocene equatorial Pacific dynamics inferred from the zonal asymmetry in sedimentary nitrogen isotopes, Paleoceanography, 27, doi:10.1029/2012pa002367.

Rea, D. K. (1994), The paleoclimatic record provided by eolian deposition in the deep sea: The geological history of wind, Reviews of Geophysics, 32(2), 159-195, doi:10.1029/93rg03257.

Riethdorf, J. R., B. Thibodeau, M. Ikehara, D. Nurnberg, L. Max, R. Tiedemann, and Y. Yokoyama (2015), Surface nitrate utilization in the Bering Sea since 180 ka BP: Insight from sedimentary nitrogen isotopes, Deep Sea Research II, in press.

Robinson, R. S., D. M. Sigman, P. J. DiFiore, M. M. Rohde, T. A. Mashiotta, and D. W. Lea (2005), Diatom-bound $^{15}N/^{14}N$: New support for enhanced nutrient consumption in the ice age subantarctic, Paleoceanography, 20(3), doi:10.1029/2004pa001114.

Robinson, R. S., et al. (2012), A review of nitrogen isotopic alteration in marine sediments, Paleoceanography, 27, doi:10.1029/2012pa002321.

Schlung, S. A., et al. (2013), Millennial-scale climate change and intermediate water circulation in the Bering Sea from 90 ka: A high-resolution record from IODP Site U1340, Paleoceanography, 28(1), doi:10.1029/2012pa002365.

Sigman, D. M., S. L. Jaccard, and G. H. Haug (2004), Polar ocean stratification in a cold climate, Nature, 428(6978), 59-63, doi:10.1038/nature02357.

Sigman, D. M., K. L. Karsh, and K. L. Casciotti (2009), Nitrogen isotopes in the ocean, in Encyclopedia of Ocean Sciences, edited by J. H. Steele, K. K. Turekian and S. A. Thorpe, Academic Press, London.

Sigman, D. M., M. P. Hain, and G. H. Haug (2010), The polar ocean and glacial cycles in atmospheric CO_2 concentration, Nature, 466(7302), 47-55, doi:10.1038/nature09149.

Sigman, D. M., M. A. Altabet, D. C. McCorkle, R. Francois, and G. Fischer (1999a), The $\delta^{15}N$ of nitrate in the Southern Ocean: Consumption of nitrate in surface waters, Global Biogeochemical Cycles, 13(4), 1149-1166, doi:10.1029/1999gb900038.

Sigman, D. M., M. A. Altabet, R. Francois, D. C. McCorkle, and J. F. Gaillard (1999b), The isotopic composition of diatom-bound nitrogen in Southern Ocean sediments, Paleoceanography, 14(2), 118-134, doi:10.1029/1998pa900018.

Studer, A. S., et al. (2015), Antarctic Zone nutrient conditions during the last two glacial cycles, Paleoceanography, 30(7), 845-862, doi: 10.1002/2014pa002745.

Chapter 3

Abrupt anoxic events in the Bering Sea caused by enhanced primary productivity

---

Abstract

Several North Pacific records from the last glacial cycle show that the deglaciation was marked by a pronounced, widespread expansion of oxygen minimum zones, but the cause of these synchronous, abrupt anoxic events is still unresolved, and it is unclear whether deoxygenation was a consistent, recurring trend of past deglaciations. Long paleoceanographic records containing abrupt deoxygenation events are needed to better understand the mechanisms and climatic conditions that control oceanic oxygen concentrations on long and short timescales. Here, we present new long, high-resolution, continuous records of primary productivity, bulk sediment nitrogen isotopes ($\delta^{15}N_{bulk}$) indicative of nitrate utilization, and non-disruptive x-ray fluorescence over the last 1.2 Myr from Integrated Ocean Drilling Program Site U1342 (818 m water depth), a site in the

Bering Sea near the depth of the modern oxygen minimum zone. Punctuated laminated intervals, representing anoxic conditions, occurred primarily within interglacial climates and were correlated with high productivity and high $\delta^{15}N_{bulk}$. These results indicate that abrupt anoxia at intermediate depths within the Bering Sea was related to high productivity events in the surface waters and suggest that iron fertilization likely played an important role in stimulating primary productivity, as no other mechanism could explain the correlation between high productivity and high $\delta^{15}N_{bulk}$ values. We posit that iron fertilization was typically promoted by relatively high interglacial sea levels, which covered the continental shelves and promoted lateral iron transport to the open ocean. However, some anoxic events recorded by laminated intervals at Site U1342 were not confined to interglacial climates, demonstrating that the mechanisms that contributed to Bering Sea anoxic events were not consistent over the last 1.2 Myr.

1. Introduction

Understanding how climate variability is related to oceanic oxygen concentrations and biological primary productivity is of great interest and importance as we face anthropogenic climate change. The distribution and concentration of oxygen in the world's oceans is regulated by the combined effects of air-sea gas exchange, ocean circulation, and productivity from photosynthetic organisms. With warmer climate, dissolved oxygen content in the oceans is expected to diminish due to decreased gas solubility and a possible reduction in ocean circulation and convection [Shaffer et al., 2009]. Recent observations have already demonstrated a reduction in oxygen concentrations in the subarctic North Pacific and the tropics over the last few decades [Nakanowatari et al., 2007; Ono et al., 2001; Stramma et al., 2008; Whitney et al., 2007], and model estimates predict a 1-7% decline in global ocean oxygen by the year 2100, with a trajectory of diminishing oxygen concentrations reaching at least a thousand years into the future [Keeling et al., 2010]. A loss of dissolved oceanic O_2, or "deoxygenation," of this magnitude will likely have substantial effects on the biogeochemical cycling of many important elements (e.g. C, N, P, Fe, etc.) [Deutsch et al., 2014; Ingall and Jahnke, 1994; Lohan and Bruland, 2008], marine ecosystem health and species distributions [Bijma et al., 2013; Diaz and Rosenberg, 2008; Moffitt et al., 2015], and the economic viability of coastal communities [Koslow et al., 2011].

Looking at paleoceanographic records from places that record abrupt changes in oxygen can help us better understand processes that cause deoxygenation. Oxygen minimum zones (OMZs) represent important regions that have unusually low oxygen levels ($[O_2]<0.5$ ml/L) and are particularly sensitive to rapid deoxygenation changes, making them ideal locations for these types of investigations. The North Pacific contains the largest OMZ area due to the relatively weak Pacific overturning circulation, O_2-poor source waters, and high rates of primary productivity that lead to respiration and oxygen consumption at depth [Keeling et al., 2010]. Several marine sediment records from the last glacial cycle demonstrate that OMZs across the entire Pacific Basin intensified during past warming events. Punctuated laminated intervals from the last deglaciation (ca. 10-

18 ka) signifying an abrupt change to nearly anoxic conditions ([O_2]<0.1 ml/L) are recorded at several Pacific margin locations, including the western California margin and Santa Barbara Basin [Behl and Kennett, 1996; Kennett and Ingram, 1995; vanGeen et al., 1996; Zheng et al., 2000] the Gulf of California [Keigwin and Jones, 1990], the Bering Sea [Cook et al., 2005; Kuehn et al., 2014; Schlung et al., 2013], the Gulf of Alaska [Davies et al., 2011], and the Japan margin [Ikehara et al., 2006; Shibahara et al., 2007].

A close connection between global climate and North Pacific anoxia during the last deglaciation has been established by studies correlating Dansgaard-Oeschger events recorded in Greenland ice core records to laminations from the California margin [Behl and Kennett, 1996; Cannariato and Kennett, 1999], the Santa Barbara Basin [Hendy et al., 2002; Kennett and Ingram, 1995], and the Bering Sea [Kuehn et al., 2014]. However, the cause of abrupt North Pacific anoxic events is still debated, with some studies suggesting changes in the pathway and composition of North Pacific Intermediate Water (NPIW) [Behl and Kennett, 1996; Keigwin, 1998; Kennett and Ingram, 1995; vanGeen et al., 1996; Zheng et al., 2000], others proposing increased phytoplankton productivity and associated oxygen consumption from decomposition at depth [Crusius et al., 2004; Davies et al., 2011; Kuehn et al., 2014; Ortiz et al., 2004; Schlung et al., 2013], and some suggesting a possible combination of both mechanisms [Cook et al., 2005; Hendy and Pedersen, 2005].

One major limiting factor that all previous North Pacific OMZ studies have in common is that they focus only on the last glacial cycle. These short records cannot determine recurring trends relating climate, abrupt anoxic events, and the potential causes of anoxia (i.e. productivity and NPIW fluctuations). In this study, we examine millennial-scale variability in nitrogen and productivity records from Site U1342 in the Bering Sea (Figure 1a), a site which contains several abrupt intervals of laminated sediments representing episodic anoxic events occuring since 1.2 Ma. Knudson and Ravelo [2015a] focused on orbital scale glacial-interglacial (G/IG) variations and provided strong evidence that nitrate utilization at Site U1342 was consistently enhanced during glacials due to stratification. However, higher-frequency variability in nitrate utilization and productivity in long Bering Sea records has not yet been examined in detail. Thus, this study provides the first high-resolution analysis of abrupt North Pacific anoxic events over multiple G/IG cycles, in order to determine whether changes in productivity and/or ventilation consistently affected North Pacific anoxia.

2. Study area and oceanographic setting

The Bering Sea is the third largest marginal sea in the world and consists of a broad, shallow continental shelf in the north and three deep basins (i.e. Komandorsky, Bowers, and Aleutian basins) up to 3500 m deep in the south. The surface circulation in the Bering Sea is a gyre that is primarily influenced by the relatively warm Alaskan Stream, which enters the basin though the Aleutian Islands [Stabeno et al., 1999]. Some fresh water flow exits the Bering Sea through the

Bering Strait (50 m depth) and enters the Arctic Ocean. Deep and intermediate waters flow between the North Pacific and the Bering Sea through deep channels, allowing the Bering Sea to continuously communicate with the North Pacific.

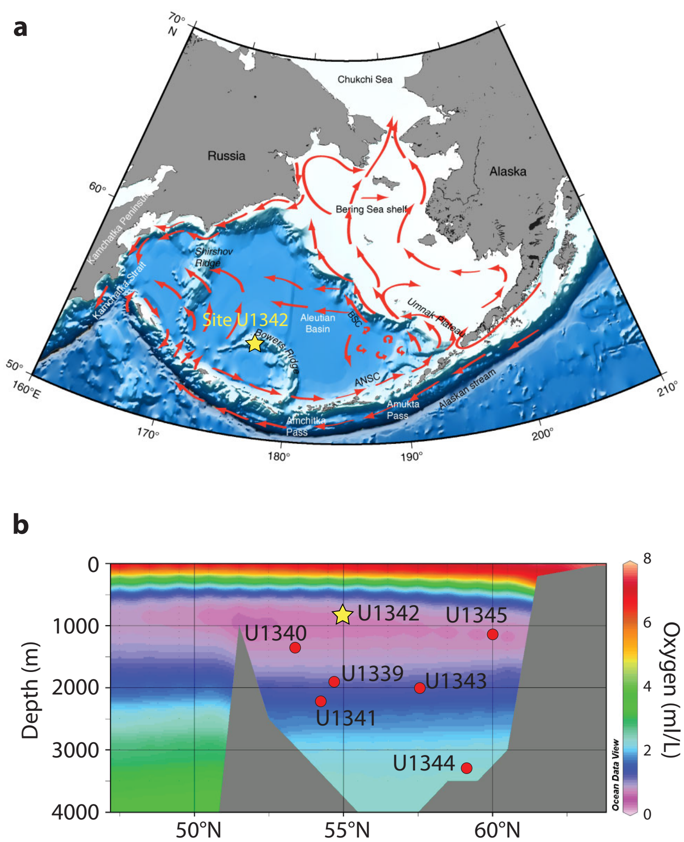

Figure 1. Bering Sea maps of (a) surface circulation (red arrows) and location of Site U1342 on Bowers Ridge (starred) and (b) a profile of dissolved oxygen [O_2] along the 180° transect. Site U1342 (818 m) is the shallowest of all of the Expedition 323 Sites and is located near the modern oxygen minimum zone. (Modified from Expedition 323 Scientists, 2011).

The OMZ in the Bering Sea has the potential to undergo large fluctuations over time. The Bering Sea, like the rest of the high-latitude Pacific, presently experiences sluggish circulation and weak ventilation, which promote low-oxygen conditions at intermediate depths (Figure 1b). Additionally, strong oxygen utilization within the water column due to high primary productivity further contributes to OMZ conditions. However, ventilation strength likely increased during past glacials when the Bering Strait was closed [Knudson and Ravelo, 2015b]. The Bering Sea is one of the world's most productive regions [Walsh et al., 1989], particularly along the continental shelf (i.e. the "Green Belt"), where nutrient-rich waters are advected into the photic zone [Springer et al., 1996]. Today, productivity in the Bering Sea is iron-limited [Boyd et al., 2007], and there is evidence that this was also the case in previous interglacial periods [Knudson and Ravelo, 2015a]. In contrast, glacial periods had enhanced stratification that changed the region into one that was nitrate-limited [Knudson and Ravelo, 2015a].

Site U1342 on Bowers Ridge is the shallowest of the IODP Expedition 323 sites and is ideally located to detect changes in the prominence of Bering Sea dissolved oxygen, because it is located just above the modern OMZ (~1000 m; Figure 1b) and near the depth of NPIW ventilation during past glacials [Horikawa et al., 2010; Knudson and Ravelo, 2015b]. Furthermore, excellent foraminiferal preservation at Site U1342 enabled the strongest age model of all of the Expedition 323 Sites [Knudson and Ravelo, 2015b]. This shallow, highly productive site is also optimally located to avoid the effects of bulk sediment nitrogen isotope diagenetic alteration, as sediments deposited in high-productivity regions reflect the $\delta^{15}N$ of the falling particles [Altabet, 2006; Robinson et al., 2012], and shallow/intermediate depth sites are less likely to undergo diagenesis compared to open ocean sites [Altabet et al., 1999].

3. Materials and Methods

Cores from IODP Site U1342 (54.83°N, 176.92°E, 818 m) were sampled at ~3-cm intervals within massive sediments and 1-cm intervals within laminated sediments, yielding an average sampling frequency of ~1 sample/kyr, based on the age model applied from Knudson and Ravelo [2015b]. Intervals of laminated sediments were identified based on visual inspection of core sediments and photos. Grain counts were conducted on a subset of laminated and massive samples using the >150 μm size fraction. Samples were split if necessary to obtain 300 to 500 clasts per sample, and clasts were classified as one of the following types: (1) lithic: quartz, feldspars, and phaneritic clasts; (2) pyroclastic material: ash and pumice; or (3) volcaniclastic: aphanitic and porpheritic iron-rich clasts (black-grey, dark green, red). The total number of clasts per gram of sediment (c_g) was calculated as: $c_g = (c/0.5^n)/m$, where: c = the number of clasts counted in a given number of sample split; n = number of sample splits; m = prewash mass (grams). Subsequently, lithic grains (%), pyroclastic grains (%), and volcaniclastic grains (%) were calculated relative to the total number of grains.

Major element compositions were measured on all the U1342 cores using non-disruptive x-ray fluorescence (XRF) at 0.50 cm resolution with the TATSCAN-F2 at the Japan Agency for Marine-Earth Technology. This instrument, analytical methods, precision, and accuracy are described in detail in Sakamoto et al. [2006]. Si/Ti, Fe/Ti, and Fe/S ratios were calculated based on the mass measurements of each of these elements.

4. Results

Intervals of laminated sediments occur as short, punctuated events several times throughout the 1.2 Myr record at Site U1342, and their occurrence is not cyclical (Figure 2). Although some laminated intervals occur during glacials, they predominantly occur during interglacial climates, as indicated by relatively low benthic foraminiferal $\delta^{18}O$ from the LR04 stack from Lisiecki and Raymo [2005] (Figure 2a). The average value of LR04 $\delta^{18}O$ during laminated intervals is 3.88‰, significantly lower than the average value during non-laminated intervals, 3.97‰ ($p<0.0001$; Table 1).

Several established proxies of primary productivity display abrupt, peak values during laminated intervals (Figure 2). Density, measured by gamma ray attenuation (GRA), is significantly lower during laminated intervals compared to non-laminated intervals (1.26 versus 1.54, $p<0.0001$), as laminations are characterized by low-density biogenic opal [Expedition 323 Scientists, 2011]. Additionally Si/Ti ratios, another Bering Sea biogenic opal proxy, which is not affected by post-depositional alteration [Kuehn et al., 2014], and sedimentary wt.%N, a proxy for preserved organic matter, increase significantly in laminated intervals compared to non-laminated intervals (Table 1; Figure 2c-d). Average Si/Ti ratios increase from a background value of 31.64 to an average laminated value of 98.48 ($p<0.0001$), with peaks greater than 587, and wt.%N values increase from a background of 0.08% to an average laminated value of 0.10% ($p<0.0001$), with peaks exceeding 0.20%. Nitrogen mass accumulation rate, another conventional proxy for primary productivity, is not presented here, as this calculation is strongly dependent on sedimentation rate, and we were unable to precisely constrain sedimentation rates across the brief laminated events. A high-resolution record of U1342 bulk sediment $\delta^{15}N$ ($\delta^{15}N_{bulk}$) from Knudson and Ravelo [2015a], which reflects both nitrate utilization and source nitrate values, varies from approximately 0.2 to 7.0‰, with several high, abrupt peaks occurring within laminated sediments (Figure 2b). The average $\delta^{15}N_{bulk}$ value within laminations is statistically higher than average background values (3.46‰ versus 3.15‰, $p<0.0001$).

Average values of Fe/Ti ratios were significantly higher in laminated intervals compared to non-laminated intervals (12.42 versus 9.35, $p<0.0001$), and displayed several peaks above 30 in laminated intervals (Figure 2f). Yet, grain count data to quantify potential aeolian iron sources showed no consistent trends throughout the three massive and three laminated intervals analyzed (Figure 3). Pyroclastic grains spiked to 95% in one laminated interval, but did not show elevated values throughout either of the other two laminated intervals analyzed for grain counts (Figure 3c). Average Fe/S ratios (Figure 2g) were significantly lower during laminated intervals compared to non-laminated intervals (8.76 versus 17.25, $p<0.0001$).

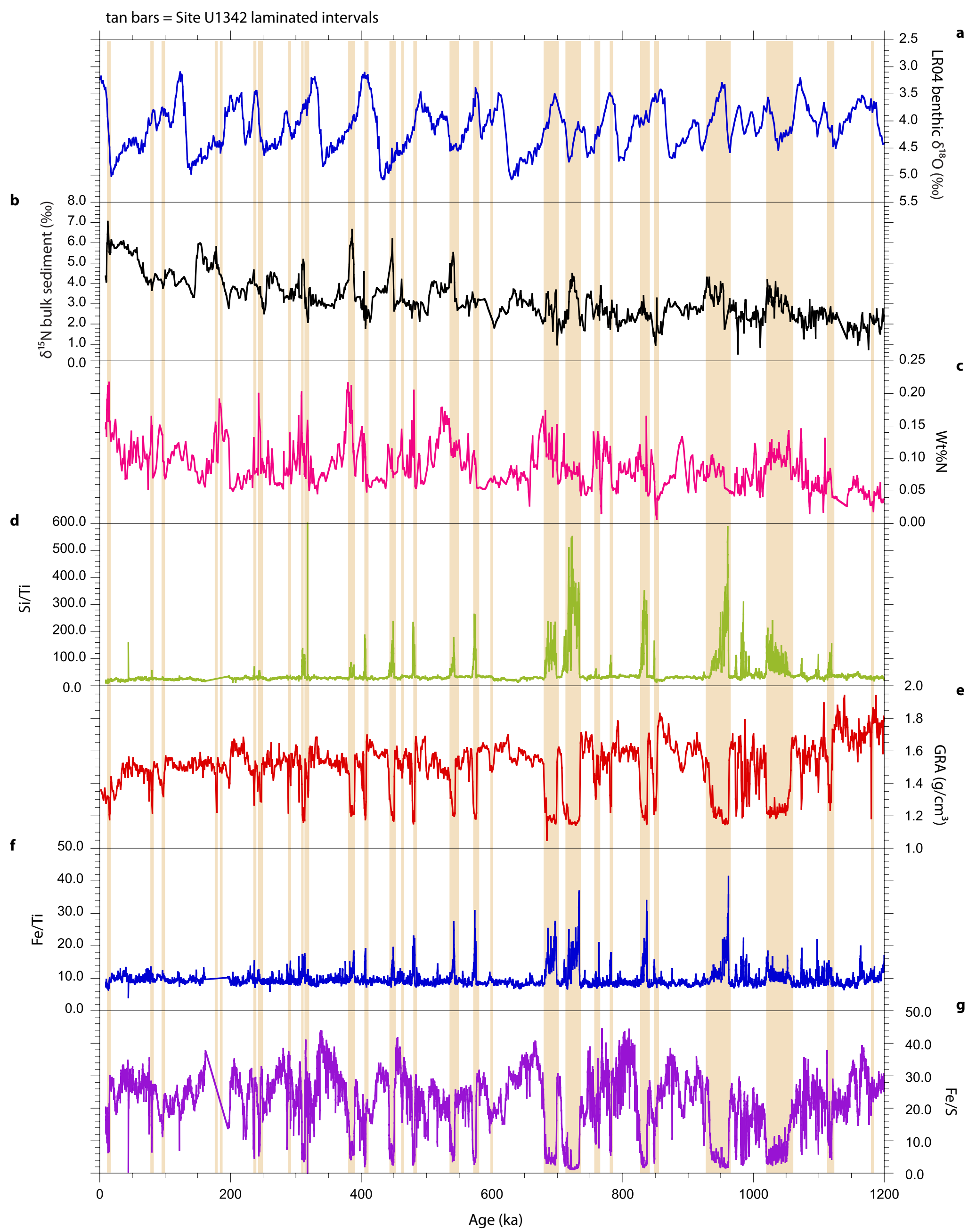

Figure 2. Compilation graph comparing the occurrences of laminated sediments at Site U1342 (shown by vertical tan bars) over the last 1.2 Myr and (a) LR04 benthic foraminiferal stack from Lisiecki and Raymo [2005], which is indicative of global glacial/interglacial climate changes, (b) bulk sedimentary $\delta^{15}N$ from Site U1342 from Knudson and Ravelo [2015a], which reflects changes in nitrate utilization, as well as changes in the source nitrate and possible denitrification, (c) weight percent

nitrogen at Site U1342, in which high values indicate enhanced primary productivity, (d) Si/Ti ratios calculated from XRD analyses at Site U1342, in which high values indicate enhanced biogenic opal deposition, (e) density measured by gamma ray attenuation (GRA) at Site U1342 from Expedition 323 Scientists [2011], in which relatively low values reflect high percentages of biogenic opal, (f) Fe/Ti ratios from XRD analyses at Site U1342, and (g) Fe/S ratios from XRD analyses at Site U1342, in which low values may indicate post-depositional pyrite precipitation.

Table 1. Average and standard deviation values within intervals of laminated and massive sediments from U1342.

	Laminated		**Non-laminated**		**Two-tailed P value**
	Avg.	**S.D.**	**Avg.**	**S.D.**	
Bulk sedimentary $\delta^{15}N$ (‰)	3.46	1.15	3.15	1.05	<0.0001
Benthic foram. $\delta^{18}O$ (‰)	3.88	0.22	3.97	0.25	<0.0001
Wt %N	0.10	0.03	0.08	0.03	<0.0001
GRA	1.26	0.10	1.54	0.09	<0.0001
Si/Ti	98.48	86.78	31.64	11.01	<0.0001
Fe/Ti	12.42	4.20	9.35	1.37	<0.0001
Fe/S	8.76	6.86	17.25	3.92	<0.0001

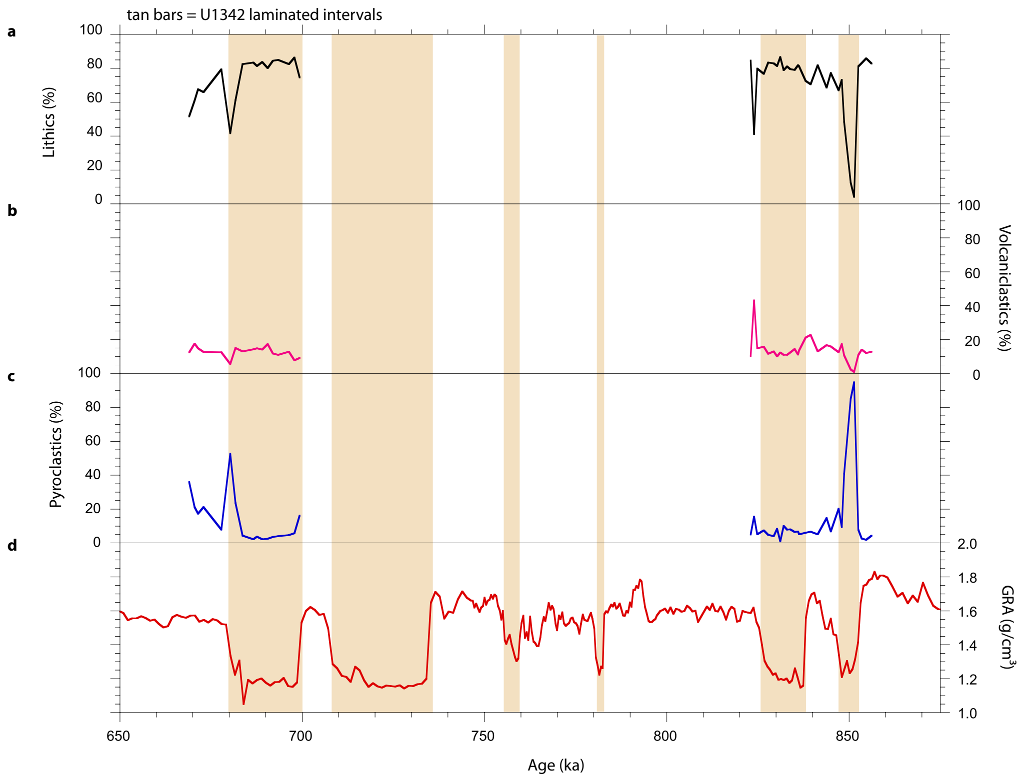

Figure 3. Site U1342 grain count records of (a) lithic grains (%), (b) volcaniclastic grains (%), and (c) pyroclastic grains (%), compared to laminated intervals (marked by tan bars) and (d) density measured by gamma ray attenuation (GRA).

5. Discussion

The unique, high-resolution, continuous datasets for Site U1342 allow us to evaluate the possible cause(s) of brief, recurring episodes anoxia, which are recorded as preserved intervals of laminated sediments. Here we first evaluate the two leading mechanisms proposed for local anoxia: reductions in NPIW ventilation and/or increased oxygen utilization due to high local productivity. The laminated intervals have durations that are shorter than the major Milankovitch climate cycles indicating that the relationship between climate and anoxia is not straightforward, although the majority of the laminations do occur within interglacials (Figure 2a; Table 1). One possible explanation for the tendency of laminations to occur during interglacials is the fact that interglacials were less well ventilated [Knudson and Ravelo, 2015b]. Changes in ventilation of the Bering Sea due to fluctuations in the relative strength of oxygen-rich NPIW may have preconditioned the Bering Sea such that it was more susceptible to anoxia, and therefore prone to preservation of laminations, during the interglacials compared to the glacials. A detailed study of Bering Sea sediments throughout the last deglaciation, which finds no significant variations in benthic-planktonic foraminifera ventilation ages between laminated and non-laminated intervals, supports the interpretation that ventilation changes cannot explain all Bering Sea anoxic events [Kuehn et al., 2014]. Therefore, the evidence suggests while weak interglacial ventilation may have helped to precondition the region for anoxic events, another, higher-frequency mechanism was more influential in the development of anoxia in the Bering Sea.

The comparison of the occurrence of laminated intervals to several primary productivity records from U1342 strongly indicates that local anoxic events can be attributed to the effects of enhanced productivity. Records of Si/Ti, GRA density, and wt.%N all demonstrate abrupt, statistically significant peaks in primary productivity coincident with laminated intervals (Figure 2). Additionally, a detailed examination from 0-275 ka of two other U1342 productivity records, wt.%C and carbon mass accumulation rate, also indicate that productivity was high during laminated intervals [Knudson and Ravelo, 2015b]. These findings at Site U1342 agree with other studies on shorter records within the Bering Sea, which found evidence for high productivity recorded in laminated sediments from the Bølling-Allerød (B/A; ca. 13-15 ka) [Katsuki et al., 2014; Khim et al., 2010; Kuehn et al., 2014; Schlung et al., 2013] and Pre-boreal (ca. 11-12 ka) [Khim et al., 2010; Kuehn et al., 2014]. Yet, the long records at Site U1342 over the last 1.2 Myr demonstrate that these high-productivity, OMZ expansion events are not limited to deglacial climates, as laminations occur mostly during interglacials and occasionally during glacials (Figure 2a).

5.2 Elevated $\delta^{15}N_{bulk}$ in laminated intervals

The $\delta^{15}N_{bulk}$ record at Site U1342 reflects biological processes but cannot be considered a productivity proxy, because it is influenced by several factors [Knudson and Ravelo, 2015a], and therefore we are discussing it here separately. In general, the $\delta^{15}N_{bulk}$ record can reflect changes in nitrate utilization (i.e. the fraction of the surface nitrate pool consumed by phytoplankton), because phytoplankton preferentially utilize ^{14}N nitrate over ^{15}N nitrate and carry this low-$\delta^{15}N$ signature to the sediments as organic matter is exported. Thus under low-nutrient utilization conditions $\delta^{15}N_{bulk}$ is low, and under high-nutrient utilization conditions the $\delta^{15}N_{bulk}$ value approaches the $\delta^{15}N$ value of the source nitrate ($\delta^{15}N_{nitrate}$) [Altabet and Francois, 1994; Sigman et al., 2009], which is 5-6‰ in the Bering Sea today [Lehmann et al., 2005]. $\delta^{15}N_{bulk}$ is also affected by changes in the $\delta^{15}N$ values of $\delta^{15}N_{nitrate}$, which can be altered by changing water masses with different $\delta^{15}N_{nitrate}$ values and/or water column denitrification, which raises the $\delta^{15}N_{nitrate}$.

Knudson and Ravelo [2015a] calculated an orbital-scale record of nitrate utilization ($\Delta\delta^{15}N$) by subtracting a $\delta^{15}N_{bulk}$ record representing background nitrate (ODP Site 1012 from Liu et al. [2005]) from the U1342 $\delta^{15}N_{bulk}$ record. However, the resolution of the Site 1012 $\delta^{15}N_{bulk}$ record is not as high the Site U1342 record (which has an average resolution of ~1 kyr). Due to this discrepancy in resolution, the nitrate utilization ($\Delta\delta^{15}N$) record from Knudson and Ravelo cannot resolve millennial-scale changes, such as those characterizing laminated events. Therefore, in this study we focus on the high-resolution changes in $\delta^{15}N_{bulk}$ in order to characterize laminated intervals, even though this measurement reflects processes besides nitrate utilization.

These high-resolution changes in $\delta^{15}N_{bulk}$ demonstrate high values during laminated intervals, when productivity is also high. The fact that $\delta^{15}N_{bulk}$ values are strongly correlated to proxies of productivity shows that changes in the source nitrate and/or dentrification cannot account for all the variability in this record, because changes in these parameters would not alter total primary productivity. Thus, the peaks in $\delta^{15}N_{bulk}$ during laminated intervals can likely be at least partially explained by abrupt events of enhanced nitrate utilization by phytoplankton.

5.3 Evidence for iron fertilization during laminated intervals

Some studies from the Bering Sea over the last glacial cycle that found evidence for higher productivity during the last deglaciation have suggested that this increase may have been attributed to the effects of melting Northern Hemisphere ice sheets, which would have increased fluvial runoff, providing additional nutrients that fostered enhanced primary productivity [Itaki et al., 2009; Sancetta et al., 1984]. Another, related suggestion is that a deglacial meltwater event may have enhanced upper-ocean stratification, relieving light limitation and allowing more complete consumption of available nutrients in the photic zone [Katsuki et al., 2014; Kuehn et al., 2014; Lam et al., 2013]. However, our results over the last 1.2 Myr show that laminated events are not limited to deglacial climates (Figure 2a). Thus, although mechanisms associated with a meltwater event may have been important for the last deglacial, and possibly some other past deglaciations, these effects cannot explain most of the Bering Sea anoxic events of the last 1.2 Myr.

Therefore, there must be some other, high-frequency mechanism capable of inducing enhanced primary productivity within the Bering Sea. Considering the available evidence, we suggest that iron fertilization may offer an explanation. In an environment where productivity is limited by available iron, phytoplankton completely exhaust the iron supply before they can consume all of the surface nitrate; the only way to achieve more complete nitrate utilization is with an additional influx of iron, which would thereby also increase total (net) productivity. For this reason, during an iron fertilization event, there is no way to get enhanced productivity without also simultaneously fractionating the surface nitrate pool though increased nitrate utilization. Thus, an iron fertilization event should be marked by both high $\delta^{15}N_{bulk}$ values and high productivity, and the fact that primary productivity is high during laminated intervals at U1342, when $\delta^{15}N_{bulk}$ values are also high, indicates that iron fertilization must have occurred during laminated intervals.

Enhanced stratification alone could not explain the observed results, because this mechanism would result in high nitrate utilization but not high net productivity, unless iron fertilization also occurred. Looking at orbital scale variability, Knudson and Ravelo [2015a] demonstrated that glacials were regularly associated with high nitrate utilization ($\Delta\delta^{15}N$) and low productivity at Site U1342, which together provide support for strong glacial stratification. However, the $\delta^{15}N_{bulk}$ is clearly different than $\Delta\delta^{15}N$ record, in that the $\delta^{15}N_{bulk}$ record has peak values that correlate to high (not low) productivity values during the laminated intervals (and most of the peak values occur during interglacials). Iron fertilization events, which would stimulate high productivity and increase $\delta^{15}N_{bulk}$, is the best way to explain why the $\delta^{15}N_{bulk}$ record .

High Fe/Ti ratios during laminated intervals (Figure 2f) potentially support the idea of iron fertilization, but overall these results are inconclusive. Dividing Fe by Ti normalizes for changing biogenic sediment flux, because Ti is related to siliciclastic sediments and is unaffected by weathering and post-depositional alteration. Thus, high Fe/Ti ratios should indicate high rates of Fe accumulation. If taken at face value, these results would then support the idea that an increased flux of iron stimulated high rates of productivity that led to anoxia at each of the laminated intervals. However, we cannot rule out the possibility that these high Fe/Ti ratios during laminated intervals could reflect post-depositional overprinting due to early diagenesis. Fe-oxides in oxygen-poor, organic-rich sediments are easily reduced to Fe^{2+}, which can dissolve in porewater and migrate upwards into overlying sediments [Passier et al., 1996]. At Site U1342, Fe^{2+} from massive sediments could migrate upwards until reaching a layer of laminated sediments. Due to the low oxygen conditions present in the laminations, sulfate is easily reduced to H_2S and HS^-, and the interaction of these species with dissolved Fe^{2+} would enable the formation and precipitation of pyrite (FeS_2) [Passier et al., 1996], resulting in high Fe/Ti and low Fe/S ratios. Therefore, as Site U1342 has low Fe/S ratios during laminated intervals (Figure 2g; Table 1), it is possible that the high Fe/Ti ratios, observed during laminations, may not reflect original Fe deposition. Due to this, overall the Fe/Ti ratios by themselves cannot be used as conclusive evidence for the idea that laminated intervals represent iron fertilization events, and unfortunately there are no other records of local iron deposition that can be used for comparison. In the absence of a straightforward record of local iron flux, the idea that laminations are marked by both high $\delta^{15}N_{bulk}$ values and high productivity provides the best available information supporting the idea that iron fertilization was responsible for events of high productivity and anoxia at Site U1342.

5.4 Mechanisms for iron fertilization at Site U1342

Potential sources of iron to Site U1342 include iron advected from the continental shelf, aeolian dust deposits, and volcanic ash from the nearby Aleutian

Arc. Given the available data, we suggest that lateral transport of iron from continental shelves to the open ocean could provide a feasible mechanism for iron fertilization events at Site U1342 that is consistent with our findings of laminations occurring primarily within interglacial intervals. Today, lateral transport of iron from the continental shelves is an important process that contributes to the highly productive modern “Green Belt” in the Bering Sea [Springer et al., 1996]. During interglacials, this flux of iron from the shelves may have been enhanced when relatively weak Bering Sea ventilation created low oxygen conditions within the basin [Knudson and Ravelo, 2015b], because low-oxygen conditions are conducive to the chemical remobilization of iron from continental shelf sediments [Lohan and Bruland, 2008]. Iron from the shelf was also likely more prone to physical transport during interglacials, when sea level was higher and the shelves were inundated with water. Thus, interglacial conditions would be prime for intensified advection and lateral transport of iron from the continental shelves to the open ocean. Once iron reached the upper water column near Site U1342, subsequent upwelling due to wind mixing would enable iron to enter the photic zone, thereby fostering high rates of biological productivity. Upwelling would be particularly active during interglacials, when the Bering Sea is less strongly stratified [Knudson and Ravelo, 2015a], another supporting reason for why laminated sediments may be mostly observed during these climatic intervals.

Lam et al. [2006] demonstrated the feasibility of particulate iron transport from the continental shelf to the open subarctic Pacific Ocean using measurements of iron in suspended particles and an ocean general circulation model. Results from this modeling experiment indicate that micron-sized Fe particles in the upper 200 m could be laterally transported more than 800 km from shore, possibly due to facilitated transport along a strong year-round horizontal pycnocline that exists at approximately the depth (150 m) of the nearby continental shelves. As a marginal sea, the Bering Sea is surrounded with continental shelves, which, based on the results from Lam et al. [2013], are close enough to have feasibly provided particulate iron to the upper water column near Site U1342.

While aeolian dust is also typically considered to be an important source of iron that relieves iron limitation at high latitudes [Boyd et al., 2007], it is unlikely that a dust source could explain the occurrences of most of the high productivity events at Site U1342. Asian dust sources, which represent the largest dust sources to the subarctic North Pacific [Mahowald et al., 2011; Mahowald et al., 2009; Rea, 1994], display highest fluxes during glacials rather than interglacials [Clemens et al., 2008] and thus could not have contributed to the pattern of predominantly interglacial high productivity events. However, the possibility that high fluxes of Asian dust may have contributed to some of the productivity events at Site U1342 is still feasible and may help to explain why a few of the laminated intervals are found during glacial climates. Additionally, while volcanic ash from the active Aleutian Arc is another source of iron to the open ocean Bering Sea, the grain count results from Site U1342 do not indicate that productivity events observed in these records are consistently related to volcanic input, as only one of the three laminated intervals studied with grain counts showed enhanced percentages of pyroclastic grains. So while this iron source may also have contributed to some of the laminated events, it is likely that most of the productivity events represented by the laminated intervals were stimulated by iron from the continental shelves.

The idea that the observed anoxic events are stimulated by iron from the continental shelves during intervals of high sea level is relevant in the context of long-term climate evolution and may provide insights into why there is a general transition from thicker to thinner laminated intervals over time. The older portion of the U1342 record includes the Mid-Pleistocene Transition (MPT), a fundamental change that occurred between ~1200 to 700 ka, in which dominant glacial-interglacial climate variability changed from low-amplitude 40 kyr cycles to high-amplitude 100 kyr cycles. Thus, the glacial sea levels before and during the MPT were higher than they were after the MPT concluded (~700 ka). If the continental shelves were a needed source of iron for anoxic events, it is feasible that the low glacial sea levels after the MPT reduced the capacity for iron remobilization, making large glacial anoxic events more difficult. In addition, it may also be possible that the larger glaciations after the MPT removed organic matter from the shelves, such that less organic matter was available during the interglacials after the MPT compared to interglacials before the MPT. The U1342 record shows relatively long laminated intervals during both glacials and interglacials during the MPT, but not after, which may imply that a combination of these influences was important for controlling strong anoxic events.

6. Conclusions

Long continuous paleoceanographic reconstructions from episodically laminated sediments from Bering Sea Site U1342 provide an unprecedented opportunity to observe the past relationship between climate, oxygen fluctuations, and primary productivity near one of the prominent North Pacific oxygen minimum zones. Laminated intervals, indicative of anoxic conditions at Site U1342, occur throughout the 1.2 Myr record and are found primarily within interglacial intervals but a few are also found during glacials and deglaciations. These long records of laminated intervals add significantly to our understanding of when and how past oceanic anoxia was formed, because until now, North Pacific studies of laminated sediments have been limited to the last glacial cycle and have focused on explaining why laminated sediments were found during the deglaciation [Behl and Kennett, 1996; Cook et al., 2005; Davies et al., 2011; Ikehara et al., 2006; Keigwin and Jones, 1990; Kennett and Ingram, 1995; Kuehn et al., 2014; Schlung et al., 2013; Shibahara et al., 2007; vanGeen et al., 1996; Zheng et al., 2000]. Our new records, which show that laminations were not just limited to deglaciations, demonstrate that the trends over the last glacial cycle are not representative of other glacial cycles in the past, and highlight the need for a new mechanism to explain how Bering Sea anoxia is typically created.

Long, high-resolution records of $\delta^{15}N_{bulk}$ and productivity (density indicative of biogenic opal, Si/Ti ratios, and wt %N) at Site U1342 display peak values during laminated intervals. Together, these results indicate that anoxia at

Site U1342 was typically caused by events of enhanced productivity, and we can infer that most of these events were likely due to high fluxes of iron to this region, which is iron limited today. Because laminated intervals primarily occur within interglacials, we suggest that most of these high productivity events can be explained by a flux of iron from continental shelves delivered to the open ocean during these times of relatively high sea level. Some iron contributions from Asian dust and volcanic ash may also explain some, but not most, of the laminated intervals. These results emphasize the importance of iron recycling in simulating future changes of oxygenation conditions and suggest the need to incorporate this process into models, which so far focus on changes in gas solubility, ocean circulation and convection [Shaffer et al., 2009].

This study provides the first high-resolution look at changes in North Pacific oxygenation and productivity over multiple G/IG cycles, but much work is still needed to understand the timing, extent, and causes of North Pacific deoxygenations events. Firstly, more long, high resolution records of laminated sediments from other geographic regions and depths would help to constrain the extent, magnitude, and timing of North Pacific OMZ expansion. Future work to reconstruct long, high-resolution records of local iron flux from various sources, including dust, volcanic ash, and continental shelf particles would be extremely helpful to quantify the oxygenation response to iron in this region and to illuminate the precise mechanisms responsible for high productivity events. Furthermore, additional long, high-resolution records of productivity and $\delta^{15}N_{bulk}$ from laminated sediments in other North Pacific regions would be instrumental in determining whether high productivity is a characteristic feature associated with basin-wide anoxic events over long timescales. Synchronous changes in productivity and anoxia over a Pacific-wide scale would be strong support for a simple mechanism of iron delivery such as the one we propose here, whereas separate regional trends would imply individualized mechanisms to promote anoxia.

Acknowledgements

This research used samples and data from the Integrated Ocean Drilling Program (IODP). Funding for this research was provided by a Schlanger Ocean Drilling Fellowship from the Consortium for Ocean Leadership and NSF grant OCE0963144. Tatsuhiko Sakamoto contributed the XRF scan data and Michelle Drake conducted the grain count analysis. We also thank Ivano Aiello, Phoebe Lam, Mitch Lyle, and Laura Wehrmann for helpful discussions that contributed to the interpretations presented here.

References

Altabet, M. A. (2006), Isotopic Tracers of the Marine Nitrogen Cycle: Present and Past, in Marine Organic Matter: Biomarkers, Isotopes and DNA, edited by J. K. Volkman, pp. 251-293, Springer Berlin Heidelberg.

Altabet, M. A., and R. Francois (1994), Sedimentary nitrogen isotopic ratio as a recorder for surface ocean nitrate utilization, Global Biogeochemical Cycles, 8(1), 103-116, doi:10.1029/93gb03396.

Altabet, M. A., C. Pilskaln, R. Thunell, C. Pride, D. Sigman, F. Chavez, and R. Francois (1999), The nitrogen isotope biogeochemistry of sinking particles from the margin of the Eastern North Pacific, Deep-Sea Research Part I-Oceanographic Research Papers, 46(4), 655-679, doi:10.1016/s0967-0637(98)00084-3.

Behl, R. J., and J. P. Kennett (1996), Brief interstadial events in the Santa Barbara basin, NE Pacific, during the past 60 kyr, Nature, 379(6562), 243-246, doi:10.1038/379243a0.

Bijma, J., H.-O. Poertner, C. Yesson, and A. D. Rogers (2013), Climate change and the oceans - What does the future hold?, Marine Pollution Bulletin, 74(2), 495-505, doi:10.1016/j.marpolbul.2013.07.022.

Boyd, P. W., et al. (2007), Mesoscale iron enrichment experiments 1993-2005: Synthesis and future directions, Science, 315(5812), 612-617, doi:10.1126/science.1131669.

Cannariato, K. G., and J. P. Kennett (1999), Climatically related millennial-scale fluctuations in strength of California margin oxygen-minimum zone during the past 60 k.y, Geology, 27(11), 975-978, doi:10.1130/0091-7613(1999)027<0975:crmsfi>2.3.co;2.

Clemens, S. C., W. L. Prell, Y. B. Sun, Z. Y. Liu, and G. S. Chen (2008), Southern Hemisphere forcing of Pliocene delta(18)O and the evolution of Indo-Asian monsoons, Paleoceanography, 23(4), doi:10.1029/2008pa001638.

Cook, M. S., L. D. Keigwin, and C. A. Sancetta (2005), The deglacial history of surface and intermediate water of the Bering Sea, Deep-Sea Research Part II-Topical Studies in Oceanography, 52(16-18), 2163-2173, doi:10.1016/j.dsr2.2005.07.004.

Crusius, J., T. F. Pedersen, S. Kienast, L. Keigwin, and L. Labeyrie (2004), Influence of northwest Pacific productivity on North Pacific Intermediate Water oxygen concentrations during the Boiling-Allerod interval (14.7-12.9 ka), Geology, 32(7), 633-636, doi:10.1130/g20508.1.

Davies, M. H., A. C. Mix, J. S. Stoner, J. A. Addison, J. Jaeger, B. Finney, and J. Wiest (2011), The deglacial transition on the southeastern Alaska Margin: Meltwater input, sea level rise, marine productivity, and sedimentary anoxia, Paleoceanography, 26, doi:10.1029/2010pa002051.

Deutsch, C., et al. (2014), Centennial changes in North Pacific anoxia linked to tropical trade winds, Science, 345(6197), 665-668, doi:10.1126/science.1252332.

Diaz, R. J., and R. Rosenberg (2008), Spreading dead zones and consequences for marine ecosystems, Science, 321(5891), 926-929, doi:10.1126/science.1156401.

Expedition 323 Scientists (2011), in Proceedings of the Integrated Ocean Drilling Program, vol. 323, edited by K. Takahashi et al.,pp. 1–71, Integrated Ocean Drill. Program Manage. Int., Inc., Tokyo, doi:10.2204/iodp.proc.323.106.2011.

Hendy, I. L., and T. F. Pedersen (2005), Is pore water oxygen content decoupled from productivity on the California Margin? Trace element results from Ocean Drilling Program Hole 1017E, San Lucia slope, California, Paleoceanography, 20(4), doi:10.1029/2004pa001123.

Hendy, I. L., J. P. Kennett, E. B. Roark, and B. L. Ingram (2002), Apparent synchroneity of submillennial scale climate events between Greenland and Santa Barbara Basin, California from 30-10 ka, Quaternary Science Reviews, 21(10), 1167-1184, doi:10.1016/s0277-3791(01)00138-x.

Horikawa, K., Y. Asahara, K. Yamamoto, and Y. Okazaki (2010), Intermediate water formation in the Bering Sea during glacial periods: Evidence from neodymium isotope ratios, Geology, 38(5), 435-438, doi:10.1130/g30225.1.

Ikehara, K., K. Ohkushi, A. Shibahara, and M. Hoshiba (2006), Change of bottom water conditions at intermediate depths of the Oyashio region, NW Pacific over the past 20,000 yrs, Global and Planetary Change, 53(1-2), 78-91, doi:10.1016/j.gloplacha.2006.01.011.

Ingall, E., and R. Jahnke (1994), Evidence for enhanced phosphorus regeneration from marine sediments overlain by oxygen depleted waters, Geochimica Et Cosmochimica Acta, 58(11), 2571-2575, doi:10.1016/0016-7037(94)90033-7.

Itaki, T., M. Uchida, S. Kim, H. S. Shin, R. Tada, and B. K. Khim (2009), Late Pleistocene stratigraphy and palaeoceanographic implications in northern Bering Sea slope sediments: evidence from the radiolarian species Cycladophora davisiana, Journal of Quaternary Science, 24(8), 856-865, doi:10.1002/jqs.1356.

Katsuki, K., T. Itaki, B. K. Khim, M. Uchida, and R. Tada (2014), Response of the Bering Sea to 11-year solar irradiance cycles during the Bolling-Allerod, Geophysical Research Letters, 41(8), 2892-2898, doi:10.1002/2014gl059509.

Keeling, R. F., A. Kortzinger, and N. Gruber (2010), Ocean Deoxygenation in a Warming World, Annual Review of Marine Science, 2, 199-229, doi:10.1146/annurev.marine.010908.163855.

Keigwin, L. D. (1998), Glacial-age hydrography of the far northwest Pacific Ocean, Paleoceanography, 13(4), 323-339, doi:10.1029/98pa00874.

Keigwin, L. D., and G. A. Jones (1990), Deglacial climatic oscillations in the Gulf of California, Paleoceanography, 5(6), 1009-1023, doi:10.1029/PA005i006p01009.

Kennett, J. P., and B. L. Ingram (1995), A 20,000 year record of ocean circulation and climate change from the Santa Barbara Basin, Nature, 377(6549), 510-514, doi:10.1038/377510a0.

Khim, B.-K., S. Kim, M. Uchida, and T. Itaki (2010), High organic carbon deposition in the northern margin of the Aleutian Basin (Bering Sea) before the last deglaciation, Ocean Science Journal, 45(4), 203-211.

Knudson, K. P., and A. C. Ravelo (2015a), Enhanced subarctic Pacific stratification and nutrient utilization during glacials over the last 1.2 Myr Geophysical Research Letters, doi:10.1002/2015GL066317.

Knudson, K. P., and A. C. Ravelo (2015b), North Pacific Intermediate Water circulation enhanced by the closure of the Bering Strait, Paleoceanography, doi:10.1002/2015PA002840.

Koslow, J. A., R. Goericke, A. Lara-Lopez, and W. Watson (2011), Impact of declining intermediate-water oxygen on deepwater fishes in the California Current, Marine Ecology Progress Series, 436, 207-218, doi:10.3354/meps09270.

Kuehn, H., L. Lembke-Jene, R. Gersonde, O. Esper, F. Lamy, H. Arz, G. Kuhn, and R. Tiedemann (2014), Laminated sediments in the Bering Sea reveal atmospheric teleconnections to Greenland climate on millennial to decadal timescales during the last deglaciation, Climate of the Past, 10(6), 2215-2236.

Lam, P. J., J. K. B. Bishop, C. C. Henning, M. A. Marcus, G. A. Waychunas, and I. Y. Fung (2006), Wintertime phytoplankton bloom in the subarctic Pacific supported by continental margin iron, Global Biogeochemical Cycles, 20(1), doi:10.1029/2005gb002557.

Lam, P. J., L. F. Robinson, J. Blusztajn, C. Li, M. S. Cook, J. F. McManus, and L. D. Keigwin (2013), Transient stratification as the cause of the North Pacific productivity spike during deglaciation, Nature Geoscience, 6(8), 622-626, doi:10.1038/ngeo1873.

Lehmann, M. F., D. M. Sigman, D. C. McCorkle, B. G. Brunelle, S. Hoffmann, M. Kienast, G. Cane, and J. Clement (2005), Origin of the deep Bering Sea nitrate deficit: Constraints from the nitrogen and oxygen isotopic composition of water column nitrate and benthic nitrate fluxes, Global Biogeochemical Cycles, 19(4), doi:10.1029/2005gb002508.

Lisiecki, L. E., and M. E. Raymo (2005), A Pliocene-Pleistocene stack of 57 globally distributed benthic delta O-18 records, Paleoceanography, 20(1), doi:10.1029/2004pa001071.

Liu, Z. H., M. A. Altabet, and T. D. Herbert (2005), Glacial-interglacial modulation of eastern tropical North Pacific denitrification over the last 1.8-Myr, Geophysical Research Letters, 32(23), doi:10.1029/2005gl024439.

Lohan, M. C., and K. W. Bruland (2008), Elevated Fe(II) and dissolved Fe in hypoxic shelf waters off Oregon and Washington: An enhanced source of iron to coastal upwelling regimes, Environmental Science & Technology, 42(17), 6462-6468, doi:10.1021/es800144j.

Mahowald, N. M., S. Albani, S. Engelstaedter, G. Winckler, and M. Goman (2011), Model insight into glacial-interglacial paleodust records, Quaternary Science Reviews, 30(7-8), 832-854, doi:10.1016/j.quascirev.2010.09.007.

Mahowald, N. M., et al. (2009), Atmospheric Iron Deposition: Global Distribution, Variability, and Human Perturbations, Annual Review of Marine Science, 1, 245-278, doi:10.1146/annurev.marine.010908.163727.

Moffitt, S. E., R. A. Moffitt, W. Sauthoff, C. V. Davis, K. Hewett, and T. M. Hill (2015), Paleoceanographic Insights on Recent Oxygen Minimum Zone Expansion: Lessons for Modern Oceanography, Plos One, 10(1), doi:10.1371/journal.pone.0115246.

Nakanowatari, T., K. I. Ohshima, and M. Wakatsuchi (2007), Warming and oxygen decrease of intermediate water in the northwestern North Pacific, originating from the Sea of Okhotsk, 1955-2004, Geophysical Research Letters, 34(4), doi:10.1029/2006gl028243.

Ono, T., T. Midorikawa, Y. W. Watanabe, K. Tadokoro, and T. Saino (2001), Temporal increases of phosphate and apparent oxygen utilization in the subsurface waters of western subarctic Pacific from 1968 to 1998, Geophysical Research Letters, 28(17), 3285-3288, doi:10.1029/2001gl012948.

Ortiz, J. D., S. B. O'Connell, J. DelViscio, W. Dean, J. D. Carriquiry, T. Marchitto, Y. Zheng, and A. van Geen (2004), Enhanced marine productivity off western North America during warm climate intervals of the past 52 ky, Geology, 32(6), 521-524, doi:10.1130/g20234.1.

Passier, H. F., J. J. Middelburg, B. J. H. VanOs, and G. J. DeLange (1996), Diagenetic pyritisation under eastern Mediterranean sapropels caused by downward sulphide diffusion, Geochimica Et Cosmochimica Acta, 60(5), 751-763, doi:10.1016/0016-7037(95)00419-x.

Rea, D. K. (1994), The paleoclimatic record provided by eolian deposition in the deep sea: The geological history of wind, Reviews of Geophysics, 32(2), 159-195, doi:10.1029/93rg03257.

Robinson, R. S., et al. (2012), A review of nitrogen isotopic alteration in marine sediments, Paleoceanography, 27, doi:10.1029/2012pa002321.

Sakamoto, T., K. Kuroki, T. Sugawara, K. Aoike, K. Iijima, and S. Sugisaki (2006), Non-destructive X-ray fluorescence (XRF) core-imaging scanner, TATSCAN-F2, Sci. Drill, 2, 37-39.

Sancetta, C., L. Heusser, L. Labeyrie, A. S. Naidu, and S. W. Robinson (1984), Wisconsin—Holocene paleoenvironment of the Bering Sea: Evidence from diatoms, pollen, oxygen isotopes and clay minerals, Marine Geology, 62(1), 55-68.

Schlung, S. A., et al. (2013), Millennial-scale climate change and intermediate water circulation in the Bering Sea from 90 ka: A high-resolution record from IODP Site U1340, Paleoceanography, 28(1), doi:10.1029/2012pa002365.

Shaffer, G., S. M. Olsen, and J. O. P. Pedersen (2009), Long-term ocean oxygen depletion in response to carbon dioxide emissions from fossil fuels, Nature Geoscience, 2(2), 105-109, doi:10.1038/ngeo420.

Shibahara, A., K. Ohkushi, J. P. Kennett, and K. Ikehara (2007), Late Quaternary changes in intermediate water oxygenation and oxygen minimum zone, northern Japan: A benthic foraminiferal perspective, Paleoceanography, 22(3), doi:10.1029/2005pa001234.

Sigman, D. M., K. L. Karsh, and K. L. Casciotti (2009), Nitrogen isotopes in the ocean, in Encyclopedia of Ocean Sciences, edited by J. H. Steele, K. K. Turekian and S. A. Thorpe, Academic Press, London.

Springer, A. M., C. P. McRoy, and M. V. Flint (1996), The Bering Sea Green Belt: Shelf-edge processes and ecosystem production, Fisheries Oceanography, 5(3-4), 205-223, doi:10.1111/j.1365-2419.1996.tb00118.x.

Stabeno, P. J., J. D. Schumacher, and K. Ohtani (1999), The physical oceanography of the Bering Sea. In Loughlin, T.R., Ohtani, K. (Eds.), Dynamics of the Bering Sea, University of Alaska Sea Grant, Fairbanks.

Stramma, L., G. C. Johnson, J. Sprintall, and V. Mohrholz (2008), Expanding oxygen-minimum zones in the tropical oceans, Science, 320(5876), 655-658, doi:10.1126/science.1153847.

vanGeen, A., R. G. Fairbanks, P. Dartnell, M. McGann, J. V. Gardner, and M. Kashgarian (1996), Ventilation changes in the northeast Pacific during the last deglaciation, Paleoceanography, 11(5), 519-528, doi:10.1029/96pa01860.

Walsh, J. J., et al. (1989), Carbon and nitrogen cycling within the Bering Chukchi Seas- Source regions for organic matter effecting AOU demands of the Arctic Ocean, Progress in Oceanography, 22(4), 277-359, doi:10.1016/0079-6611(89)90006-2.

Whitney, F. A., H. J. Freeland, and M. Robert (2007), Persistently declining oxygen levels in the interior waters of the eastern subarctic Pacific, Progress in Oceanography, 75(2), 179-199, doi:10.1016/j.pocean.2007.08.007.

Zheng, Y., A. van Geen, R. F. Anderson, J. V. Gardner, and W. E. Dean (2000), Intensification of the northeast Pacific oxygen minimum zone during the Bolling-Allerod warm period, Paleoceanography, 15(5), 528-536, doi:10.1029/1999pa000473.

Appendix A

Supporting information for

Chapter 1: North Pacific Intermediate Water circulation enhanced by the closure of the Bering Strait

Contents of this file

Introduction

This file contains tables, text, and figures supporting the Chapter 1:

Table A1. U1342 age model based on tie point correlation to LR04 stack.

Text A1. Information regarding the application of the U1342 age model.

Table A2. Revised Site 849 age model points.

Table A3. Site U1342 single foraminifer measurements from peak glacials, which were used to show that the 3-foraminifera averaged measurements were robust.

Table A4. U1342 benthic foraminiferal Mg/Ca measurements from three G/IG pairs, as evidence of negative $\delta^{18}O$ seawater during glacials, indicative of local brine formation.

Table A5. Bering Sea benthic foraminiferal stable isotope values at the Holocene and Last Glacial Maximum (LGM), which show enhanced LGM ventilation on a regional scale.

Figure A1. Benthic $\delta^{18}O_c$ from Site U1343 compared to Site U1342, as evidence for ventilation influence at intermediate depths within the Bering Sea during extreme glacials.

Figure A2. Cross-plot of NPIW proxies ($\Delta\delta^{13}C$ vs. $\Delta\delta^{18}O$).

Table A6. The t-test results for average $\Delta\delta^{13}C$ and $\Delta\delta^{18}O$ during open and closed Bering Strait conditions over the last 1.2 Myrs.

Figure A3. Records of benthic $\delta^{18}O_c$ and $\delta^{13}C_c$ from the North Atlantic used to determine changes in UNADW and LNADW.

Table A1. U1342 age model based on tie point correlation to LR04 stack.

U1342 depth (CCSF-A)	Age (ka)	Sedimentation rate (m/kyr)
0.32	14.70	0.06
0.51	18.00	0.04
1.16	36.11	0.04
2.23	61.64	0.05
3.28	82.00	0.02
3.55	95.18	0.03
3.55	95.18	0.03
4.50	122.29	0.03
4.96	139.94	0.04
6.56	185.11	0.03
7.97	239.00	0.04
9.63	284.81	0.06
12.41	328.83	0.03
14.83	401.72	0.07
15.39	410.00	0.01
15.72	433.20	0.04
18.01	491.29	0.03
19.61	552.00	0.03
20.29	578.19	0.02
21.26	630.70	0.02
23.63	746.32	0.05
26.45	798.59	0.03
28.47	859.48	0.02
30.19	955.99	0.04
35.34	1071.90	0.04

Text A1. U1342 age model and assessing phase between independent records

The LR04 benthic $\delta^{18}O_c$ stack from Lisiecki and Raymo [2005], which was used as a basis for our age model, averages out regional $\delta^{18}O$ differences in phase (i.e. timing) and thus assumes globally synchronous glacial-interglacial (G/IG) changes. While $\delta^{18}O$ variability primarily reflects global ice volume, there is some evidence that regional, temperature-related $\delta^{18}O$ variability can cause North Pacific benthic $\delta^{18}O_c$ records to lag those from the North Atlantic by up to ~4 kyr [Lisiecki and Raymo, 2009; Skinner and Shackleton, 2005]. However, these lags have been debated (see Venti et al. [2013]), given the Pacific's large contribution to global oceanic volume (70%) and the relatively fast mixing time of the ocean (~1 kyr [Duplessy et al., 1991]). Therefore, given that the potential lag is relatively short compared to the timescales considered in this study, we have applied the LR04 stack correlation with no further age correction. The relatively small uncertainties in our age model do not inhibit our objective, which is to broadly assess whether the changes in North Pacific Intermediate Water (NPIW) are antiphase relative to lower North Atlantic Deep Water (LNADW) and upper North Atlantic Deep Water (UNADW). Additionally, correlation to the LR04 stack does not affect the relationship between internal records using same age model [Bintanja and van de Wal, 2008] (e.g. U1342 $\delta^{13}C$ and $\delta^{18}O$), because these records represent unique measurements with trends that are independent from one another regardless of the assigned ages. As such, while the LR04 and U1342 $\delta^{18}O$ records are expected to be in phase, temporal relationships (i.e. lead and lag relationships) between the records of LR04 $\delta^{18}O$ and U1342 $\delta^{13}C$ (and $\Delta\delta^{13}C_{849\text{-}U1342}$) can be assessed without implicating circular reasoning.

Table A2. Revised Site 849 age model points.

Published age (ka)	Revised age (ka)	Benthic $\delta^{18}O$ (‰)	Benthic $\delta^{13}C$ (‰)
412.5	430	4.83	-0.39
427.5	432	4.86	-0.34
430.5	434	5.05	-0.42
433.0	436	4.82	-0.31

All Site 849 ages were assigned as published by Mix et al. [1995] except for the ages displayed in this table, which were adjusted for stronger correlation to the LR04 benthic stack from Lisiecki and Raymo [2005].

Table A3. Site U1342 single foraminifer measurements from peak glacials.

Single foraminifer sample ID	Age (ka)	Single foraminifer $\delta^{18}O_c$ (‰)	Avg. of foraminifer shells $\delta^{18}O_c$ (‰)	Original measurement[1] $\delta^{18}O_c$ (‰)
U1342D 1H-1 84-88a	27	4.64	4.43±0.07	4.57
U1342D 1H-1 84-88b		4.58		
U1342D 1H-1 84-88c		4.48		
U1342D 1H-1 84-88d		4.47		
U1342D 1H-1 84-88e		4.49		
U1342C 2H-4 102-106a	338	4.48	4.34±0.09	4.28
U1342C 2H-4 102-106b		4.31		
U1342C 2H-4 102-106c		4.32		
U1342C 2H-4 102-106d		4.37		
U1342C 2H-4 102-106e		4.42		
U1342C 2H-6 98-100a	431	4.52	4.56±0.12	4.65
U1342C 2H-6 98-100b		4.73		
U1342C 2H-6 98-100c		4.54		
U1342C 2H-6 98-100d		4.45		
U1342C 3H-3 62-63a	640	4.54	4.32±0.24	4.4
U1342C 3H-3 62-63b		4.62		
U1342C 3H-3 62-63c		4.20		
U1342C 3H-3 62-63d		4.08		
U1342C 3H-3 62-63e		4.14		
U1342C 3H-4 128-130a	746	4.35	4.43±0.08	4.25
U1342C 3H-4 128-130b		4.53		
U1342C 3H-4 128-130c		4.39		
U1342C 3H-4 128-130d		4.46		
U1342D 4H-2 65-68a	876	4.17	4.31±0.16	4.57
U1342D 4H-2 65-68b		4.51		
U1342D 4H-2 65-68c		4.16		
U1342D 4H-2 65-68d		4.44		
U1342D 4H-2 65-68e		4.27		

[1] Original measurements to construct the U1342 stratigraphy used 1-3 (typically 3) combined Uvigernia peregrina shells.

Table A4. U1342 benthic foraminiferal Mg/Ca from three G/IG pairs.

Marine Isotope Stage (MIS)	**Sample ID**	**Age (ka)**	**Benthic $\delta^{18}O_c$ (‰)**	**Benthic Mg/Ca**
MIS 1	U1342D 1H-1 0-2	9.2	3.70	0.80
	U1342D 1H-1 3-5	9.7	4.08	0.90
	U1342D 1H-1 9-7	10.3	3.93	1.01
Deglaciation	U1342D 1H-1 11-13	11.0	3.75	0.75
	U1342D 1H-1 15-17	11.7	4.07	0.85
	U1342D 1H-1 19-21	12.4	3.88	0.83
	U1342D 1H-1 26-28	13.6	4.00	1.06
	U1342D 1H-1 30-32	14.3	4.15	0.86
	U1342D 1H-1 34-36	14.9	4.02	0.85
	U1342D 1H-1 44-46	16.6	4.32	0.71
	U1342D 1H-1 49-51	17.5	4.48	0.77
MIS 2	U1342D 1H-1 52-56	18.0	4.57	0.86
	U1342D 1H-1 64-68	21.4	4.40	0.77
	U1342D 1H-1 75-79	24.5	4.46	0.75
	U1342D 1H-1 84-88	27.0	4.57	0.78
MIS 5	U1342D 1H-3 125-128	115.0	3.67	0.78
	U1342D 1H-3 145-148	120.7	3.69	0.87
MIS 6	U1342D 1H-4 44-47	138.8	4.27	0.94
	U1342D 1H-4 48-52	140.2	4.02	0.85
	U1342D 1H-4 69-73	146.2	4.28	0.97
	U1342D 1H-4 74-76	147.6	4.20	0.87
	U1342D 1H-4 77-79	148.4	4.22	0.91
	U1342D 1H-4 85-87	150.7	4.17	0.85
MIS 9	U1342C 2H-4 64-67	327.8	3.44	0.74
	U1342C 2H-4 68-71	328.1	2.81	0.74
	U1342C 2H-4 72-75	329.3	3.39	0.88
	U1342C 2H-4 76-79	330.5	3.56	0.74
MIS 10	U1342C 2H-4 85-88	333.2	4.00	0.71
	U1342C 2H-4 97-101	336.9	4.08	0.71
	U1342C 2H-4 102-106	338.4	4.27	0.73
	U1342C 2H-4 112-116	341.4	4.00	0.76

Table A5. Bering Sea benthic foraminiferal stable isotope values at the Holocene and Last Glacial Maximum (LGM).

Core name	Water depth (m)	$\delta^{13}C_c$ (‰ VPDB)			$\delta^{18}O_c$ (‰ VPDB)		
		Holocene	LGM	$\Delta\delta^{13}C$ (LGM-Holocene)	Holocene	LGM	$\Delta\delta^{18}O$ (LGM-Holocene)
HLY-02-02-57JPC*	700	-0.80	-1.10	-0.30	3.25	4.70	1.45
U1342	818	-1.25	-1.08	0.17	3.70	4.57	0.87
U1345	1008	-1.02	-1.20	-0.18	3.38	4.92	1.54
U1340	1295	-0.95	-1.12	-0.17	3.75	5.03	1.28
HLY02-02-51JPC*	1467	-0.68	-1.25	-0.57	3.34	5.29	1.95
U1339*	1868	-1.28	-1.55	-0.27	3.74	5.24	1.50
U1343	1953	-	-	-	2.80	4.32	1.51
U1341	2140	-1.10	-0.87	0.23	3.35	5.20	1.85
HLY02-02-17JPC	2209	-0.73	-0.73	0.00	3.39	5.35	1.96
U1344	3173	-0.58	-1.01	-0.43	3.38	5.27	1.89

Data is from this study (U1342), Asahi et al. [2014] (U1343), and several records compiled by Cook et al. [in review] Records are from U. peregrina except for U1341, 17JPC, and U1344, which used U. senticosa, and U1343, which used E. batialis. Sites marked with asterisk (*) are on the Umnak Plateau, which may have received limited circulation due to its remote location.

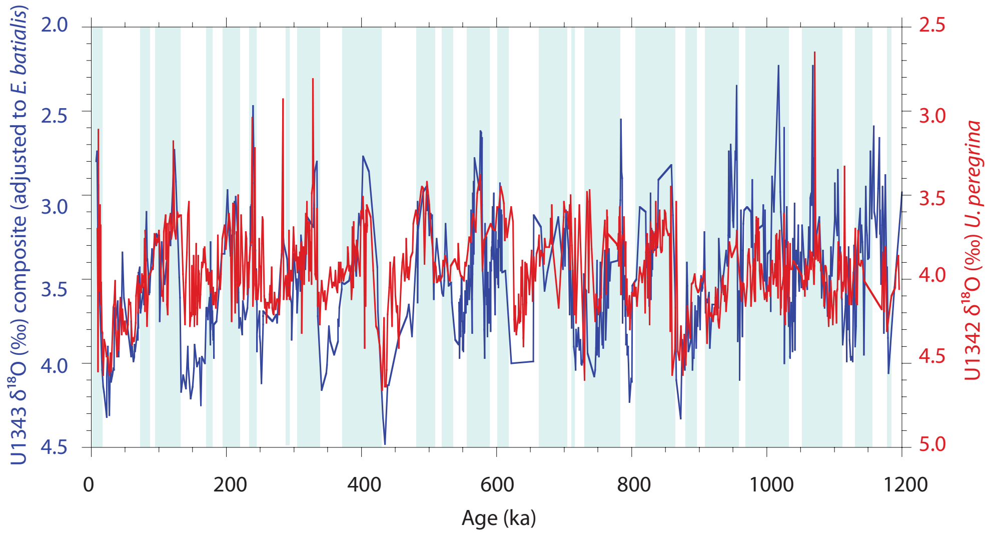

Figure A1. Evidence for ventilation influence at intermediate depths within the Bering Sea during extreme glacials. Benthic $\delta^{18}O_c$ composite (adjusted to E. batialis) from Bering Sea Site U1343 (blue lines) from Asahi et al. [2014] compared to U1342 U. peregrina $\delta^{18}O_c$ (red lines). Blue vertical bars represent intervals in which the Bering Strait was open (interglacials and weak glacials), and white vertical bars indicate extreme glacials in which the Bering Strait was closed. Site U1343 (1,953 m water depth) exhibits a larger $\delta^{18}O_c$ amplitude than Site U1342 (818 m water depth) during extreme glacials, providing evidence that intermediate depths within the Bering Sea were ventilated by enhanced local brine production when the Bering Strait was closed.

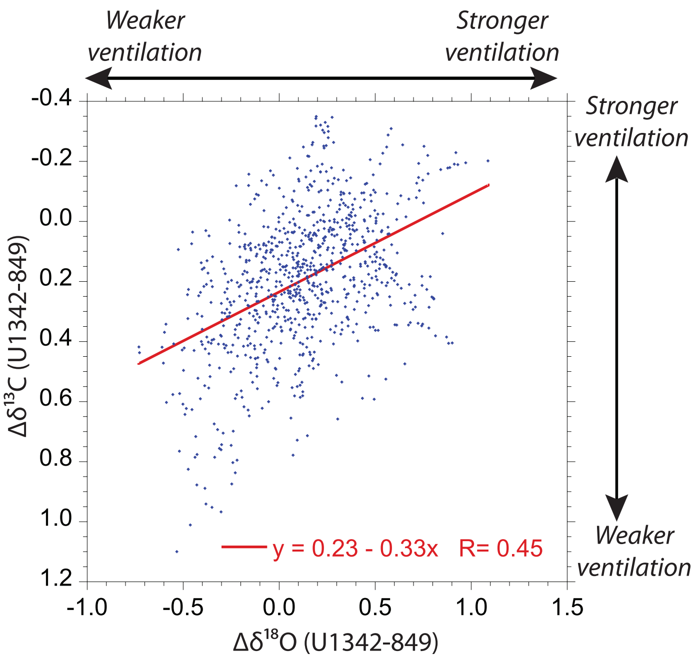

Figure A2. Cross-plot of NPIW proxies ($\Delta\delta^{13}C$ vs. $\Delta\delta^{18}O$). Strong statistical significance ($p<0.0001$) between $\Delta\delta^{13}C$(849-U1342) and $\Delta\delta^{18}O$(849-U1342) supports the idea that NPIW ventilation could explain variability in both of these variables, while some scatter in the cross-plot reveals that these variables are also affected by independent processes other than NPIW. While cross-spectral analyses show that there is coherency between these two variables at orbital timescales (see Main Text Figures 7 and 8), the two variables are likely controlled by a variety of other mechanisms on non-orbital timescales.

Table A6. The t-test results for average $\Delta\delta^{13}C$ and $\Delta\delta^{18}O$ during open and closed Bering Strait conditions over the last 1.2 Myr.

	t-test population	p-value	95% confidence interval (lower bound)	95% confidence interval (upper bound)
$\Delta\delta^{13}C$ (849-U1342)	**G vs. IG**	0.002	-0.130	-0.031
	G-CBS vs. IG	4.65×10^{-7}	-0.191	-0.086
	G-CBS vs. G-OBS	6.21×10^{-5}	-0.204	-0.072
	G-OBS vs. IG	0.987	-0.068	0.067
$\Delta\delta^{18}O$ (849-U1342)	**G vs. IG**	0.003	0.042	0.203
	G-CBS vs. IG	9.76×10^{-11}	0.215	0.391
	G-CBS vs. G-OBS	7.02×10^{-19}	0.347	0.513
	G-OBS vs. IG	0.014	-0.227	-0.026

Glacials (G) and interglacials (IG) are defined by points that are 1 sigma above (or below) a 100 kyr moving window of the U1342 smoothed $\delta^{18}O$. Open and closed Bering Strait (OBS and CBS) are defined as occurring when relative sea level was above or below -50 m, as determined by Rohling et al. [2009] and Sosdian and Rosenthal [2009]. Site 849 benthic stable isotope data from Mix et al. [1995].

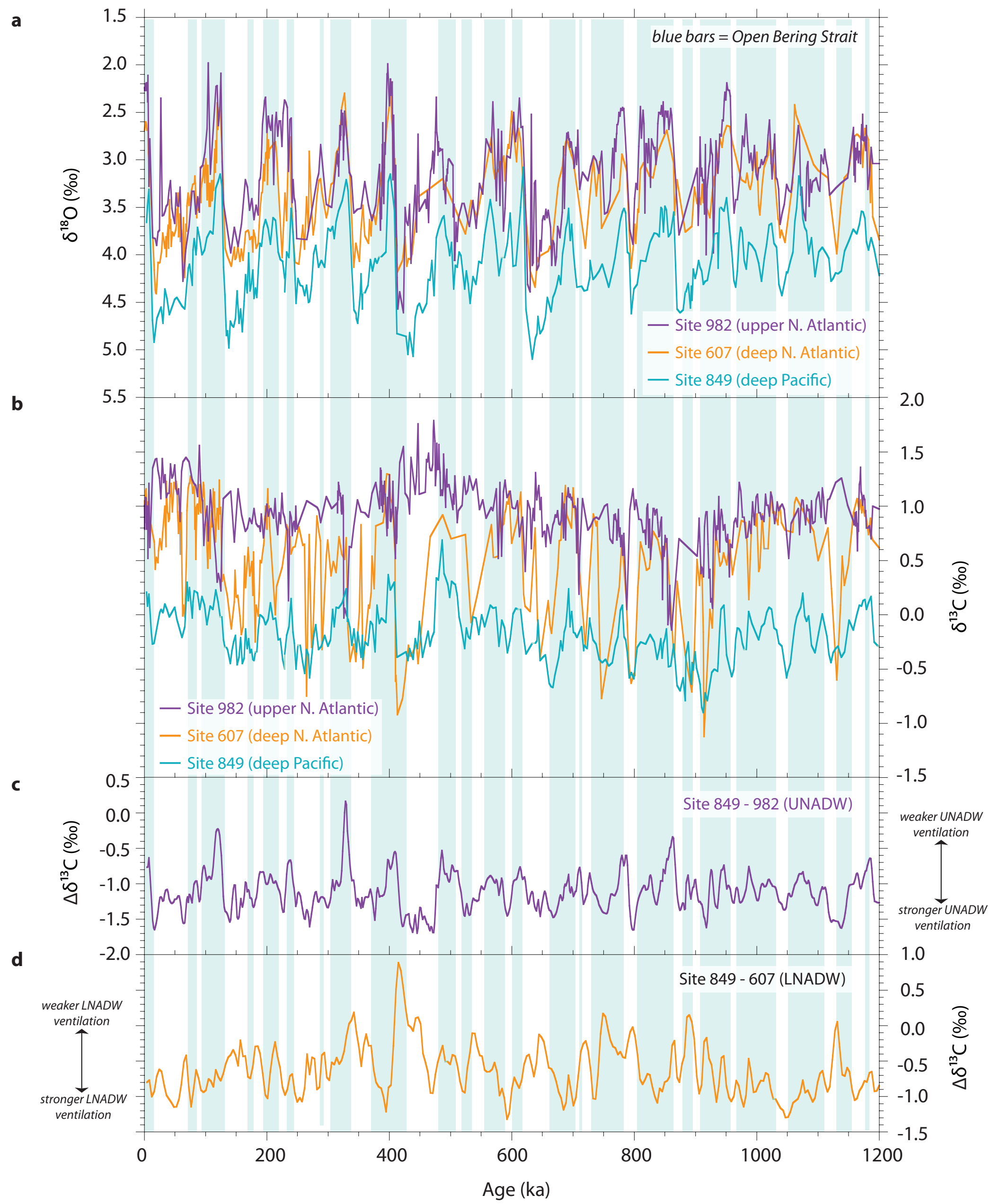

Figure A3. Records of benthic $\delta^{18}O_c$ and $\delta^{13}C_c$ from the North Atlantic used to determine changes in UNADW and LNADW. (a) Comparison of $\delta^{18}O_c$ records from deep equatorial Pacific Site 849 (3,851 m) from Mix et al. [1995] shown in teal, intermediate depth North Atlantic site ODP 982 (1,135 m) from Venz et al. [1999] shown in purple, and deep North Atlantic site DSDP 607 (3,427 m) from Ruddiman et al. [1989] shown in orange. **(b)** Same as in (a) but for $\delta^{13}C_c$. **(c)** $\Delta\delta^{13}C$ record of upper North Atlantic Deep Water (UNADW) calculated as $\delta^{13}C_c$ (Site

849-982), which shows UNADW is enhanced during intervals of Bering Strait closure. **(d)** $\Delta\delta^{13}C$ record of lower North Atlantic Deep Water (LNADW) calculated as $\delta^{13}C_c$ (Site 849-607), which appears to behave independently of Bering Strait closure. These records in (b) and (c), which are not antiphase to the NPIW records from Site U1342, support the idea that there is no seesaw relationship between NPIW and NADW on orbital timescales.

References

Asahi, H., S. Kender, M. Ikehara, T. Sakamoto, K. Takahashi, A. C. Ravelo, C. A. Alvarez Zarikian, B. K. Khim, and M. J. Leng (2014), Orbital-scale benthic foraminiferal oxygen isotope stratigraphy at the northern Bering Sea Slope Site U1343 (IODP Expedition 323) and its Pleistocene paleoceanographic significance, Deep Sea Research II.

Bintanja, R., and R. S. W. van de Wal (2008), North American ice-sheet dynamics and the onset of 100,000-year glacial cycles, Nature, 454(7206), 869-872.

Cook, M. S., A. C. Ravelo, A. Mix, I. M. Nesbitt, N. V. Miller, and D. C. McCorkle (in review), Tracing Bering Sea circulation with benthic foraminiferal stable isotopes during the Pleistocene, Deep Sea Research.

Duplessy, J. C., E. Bard, M. Arnold, N. J. Shackleton, J. Duprat, and L. Labeyrie (1991), How fast did the ocean-atmosphere system run during the last deglaciation?, Earth and Planetary Science Letters, 103(1-4), 27-40.

Lisiecki, L. E., and M. E. Raymo (2005), A Pliocene-Pleistocene stack of 57 globally distributed benthic $\delta^{18}O$ records, Paleoceanography, 20(1).

Lisiecki, L. E., and M. E. Raymo (2009), Diachronous benthic $\delta^{18}O$ responses during late Pleistocene terminations, Paleoceanography, 24.

Mix, A. C., N. G. Pisias, W. Rugh, J. Wilson, A. Morey, and T. K. Hagelberg (1995), Benthic foraminifer stable isotope record from Site 849 (0-5 Ma): Local and global climate changes in N.G. Pisias, L.A. Mayer,T.R. Janecek,A. Palmer-

Julson, and T.H. van Andel, eds., Proceedings of the Ocean Drilling Program, Scientific Results, 371-412.

Rohling, E. J., K. Grant, M. Bolshaw, A. P. Roberts, M. Siddall, C. Hemleben, and M. Kucera (2009), Antarctic temperature and global sea level closely coupled over the past five glacial cycles, Nature Geoscience, 2(7), 500-504.

Ruddiman, W. F., M. E. Raymo, D. G. Martinson, B. M. Clement, and J. Backman (1989), Pleistocene Evolution: Northern Hemisphere ice sheets and North Atlantic Ocean, Paleoceanography, 4(4), 353-412.

Skinner, L. C., and N. J. Shackleton (2005), An Atlantic lead over Pacific deep-water change across Termination I: implications for the application of the marine isotope stage stratigraphy, Quaternary Science Reviews, 24(5-6), 571-580.

Sosdian, S., and Y. Rosenthal (2009), Deep-Sea temperature and ice volume changes across the Pliocene-Pleistocene climate transitions, Science, 325(5938), 306-310.

Venti, N. L., K. Billups, and T. D. Herbert (2013), Increased sensitivity of the Plio-Pleistocene northwest Pacific to obliquity forcing, Earth and Planetary Science Letters, 384, 121-131.

Venz, K. A., D. A. Hodell, C. Stanton, and D. A. Warnke (1999), A 1.0 Myr record of glacial North Atlantic intermediate water variability from ODP site 982 in the northeast Atlantic, Paleoceanography, 14(1), 42-52.

Appendix B

Supporting information for

Chapter 2: Enhanced subarctic Pacific stratification and nutrient utilization during glacials over the last 1.2 Myr

Contents of this file

Text B1
Figures B1 to B5
Table B1

Introduction

This supporting information contains the following:

- **Text B1** and **Table B1** provide the methods used for determining the percentage of terrigenous organic matter and the calculated record of marine $\delta^{15}N$ at Site U1342.
- **Figure B1** shows records of measured organic $\delta^{13}C$ and C/N, records of calculated percentage of terrigenous organic matter, and records of calculated marine $\delta^{15}N$ compared to bulk sediment $\delta^{15}N$. These results are used to justify the use of bulk sediment $\delta^{15}N$, in the main article, as a good representation of the isotopic signature of marine organic matter.
- **Figure B2** presents a cross-plot between Site U1342 $\Delta\delta^{15}N$ (nitrate utilization proxy) and the LR04 benthic $\delta^{18}O$ stack from Lisiecki and Raymo [2005], which shows consistent enhancement of nitrate utilization during glacial climates.
- **Figure B3** shows the Blackman-Tukey spectra for $\Delta\delta^{15}N$, demonstrating the periodicities of dominant frequency occurring at Milankovitch orbital cycles.
- **Table B2** provides coherency values for spectral analysis results corresponding to Table 1 in the main text.
- **Figure B4** presents the evolutionary spectra for $\Delta\delta^{15}N$ at Site U1342.
- **Figure B5** compares the U1342 $\Delta\delta^{15}N$ record with records of benthic $\delta^{18}O$ from Site U1342 and the LR04 stack, Pacific bulk sediment $\delta^{15}N$ records, and records of local primary productivity.
- **Figure B6** presents cross plots of $\Delta\delta^{15}N$ versus NMAR and wt%N, two proxies of local primary productivity, showing nitrate utilization was not well correlated to changes in productivity over the last 1.2 Myrs.

Text B1. Marine $\delta^{15}N$ signature at Site U1342

One underlying assumption in our study is that the record of bulk sediment $\delta^{15}N$ ($\delta^{15}N_{bulk}$) at Site U1342 reflects mainly nitrogen from marine organic matter. To evaluate the potential impact that terrestrial nitrogen sources might have on the U1342 $\delta^{15}N_{bulk}$ signal, we used measurements of organic sedimentary $\delta^{13}C$ ($\delta^{13}C_{org}$) from Site U1342, and a linear mixing model between the end-member values of marine organic matter $\delta^{13}C$ ($\delta^{13}C_{marine}$) and terrigenous organic matter $\delta^{13}C$ ($\delta^{13}C_{terr}$) shown in Table S1, to estimate the fraction of terrigenous organic matter ($TOM_{fraction}$) in each bulk sample. We then used the calculated $TOM_{fraction}$, an end-member terrigenous organic matter $\delta^{15}N$ ($\delta^{15}N_{terr}$) value (Table S1), and the measured $\delta^{15}N_{bulk,}$ to calculate a $\delta^{15}N$ record of the marine organic matter ($\delta^{15}N_{marine}$). To double-check this result, we repeated this calculation using the measured C/N ratio and the end-member C/N values (Table S1) to obtain estimates of $TOM_{fraction}$, before calculating $\delta^{15}N_{marine}$. The records of measured $\delta^{13}C_{org}$ and C/N, as well as the calculated records of $TOM_{fraction}$ and $\delta^{15}N_{marine}$, are shown in Appendix Figure B1.

$TOM_{fraction}$, the fraction of organic matter of terrigenous origin, was calculated as follows:

$$\mathbf{TOM_{fraction} = (\delta^{13}C_{sample} - \delta^{13}C_{marine}) / (\delta^{13}C_{terr} - \delta^{13}C_{marine})}$$

$$\mathbf{TOM_{fraction} = (C/N_{sample} - C/N_{marine}) / (C/N_{terr} - C/N_{marine})}$$

In the equations above, $\delta^{13}C_{sample}$ and C/N_{sample} are measured values of bulk sediment from U1342. Values of $\delta^{13}C_{marine}$, $\delta^{13}C_{terr}$, C/N_{marine}, C/N_{terr} are end-member published values, shown in Table S1.

The $\delta^{15}N$ of marine sediment origin ($\delta^{15}N_{marine}$) was then calculated as:

$\mathbf{\delta^{15}N_{marine} = (\delta^{15}N_{bulk} - (TOM_{fraction} \times \delta^{15}N_{terr}))/(1- TOM_{fraction})}$, in which $\delta^{15}N_{terr}$ is the assumed terrigenous organic matter end-member shown in Table S1.

Table B1. Organic matter end-member values used to calculate $TOM_{fraction}$ and $\delta^{15}N_{marine}$.

	Marine	Terrigenous
$\delta^{13}C$	-21‰ [Cooper et al., 2009; Meyers, 1994]	-26.2‰ [Guo and Macdonald, 2006]
C/N	6.5 [Cooper et al., 2009]	15 [Guo and Macdonald, 2006]
$\delta^{15}N$	-----	3.0‰ [McClelland et al., 2014]

In these calculations, we assume that the marine organic matter at our site reflects the chemical signature of marine phytoplankton, while the terrigenous organic matter at our site reflects the chemical signature of particulate organic matter from a Yukon source [Guo and Macdonald, 2006; Guo et al., 2004]. Similar end-member values and sources were assumed by Riethdorf et al. [2015] in calculating $TOM_{\mathbf{fraction}}$ at a different Bering Sea site. Our results (Figure S1) show that values and variability of the estimated $\delta^{15}N_{\mathbf{marine}}$ record are very similar to the measured $\delta^{15}N_{bulk}$ record, indicating that the $\delta^{15}N_{bulk}$ signal at U1342 strongly reflects the isotopic variability of marine nitrogen sources.

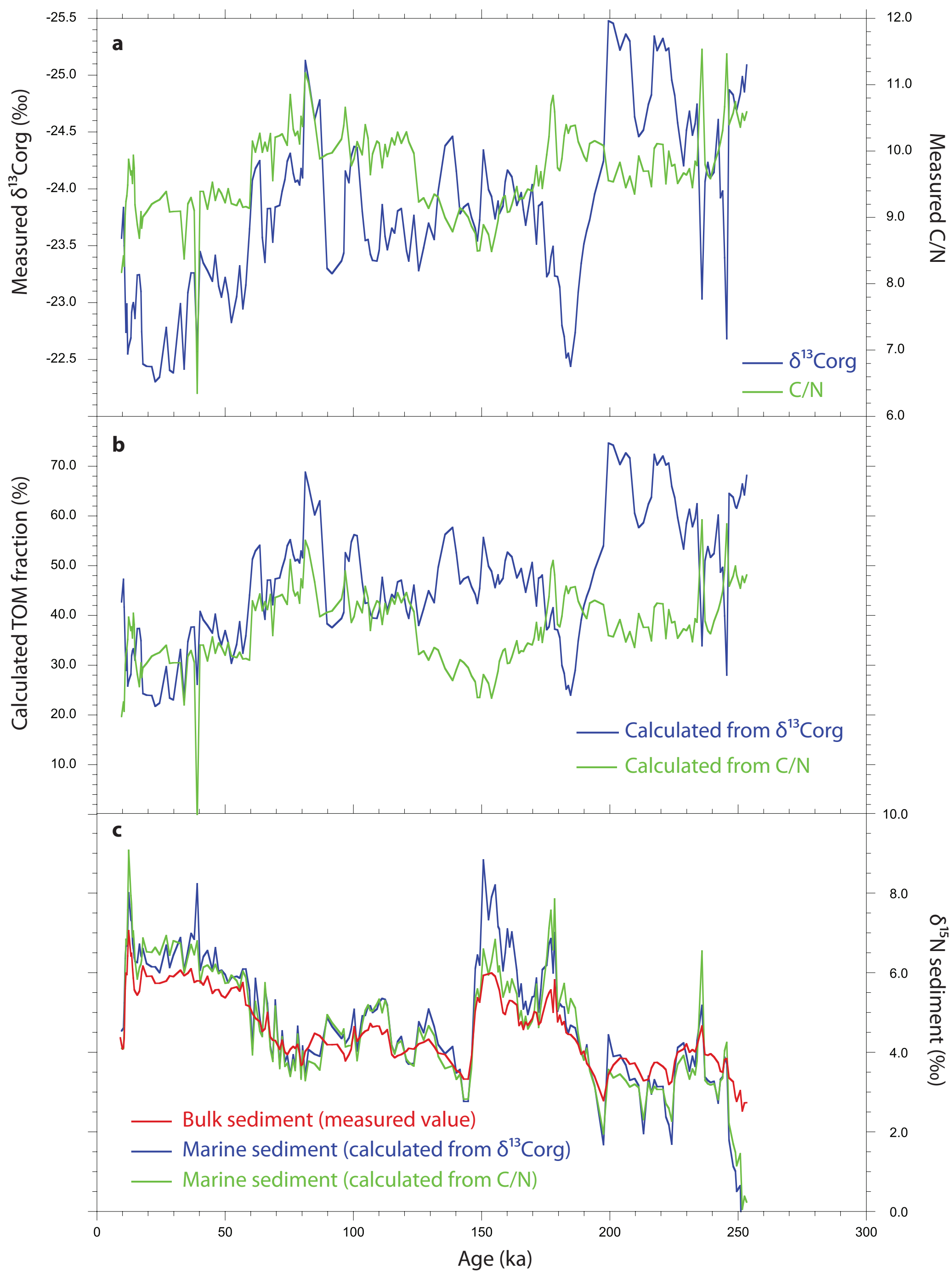

Figure B1. U1342 stable isotope measurements and calculations. **(a)** Measured organic $\delta^{13}C$ (blue) and C/N ratios (green), **(b)** percent terrigenous content calculated from organic $\delta^{13}C$ (blue) and C/N ratios (green), and **(c)** measured values of $\delta^{15}N_{bulk}$ (red), compared to $\delta^{15}N_{marine}$ calculated from organic $\delta^{13}C$ (blue), and $\delta^{15}N_{marine}$ calculated from C/N ratios (green).

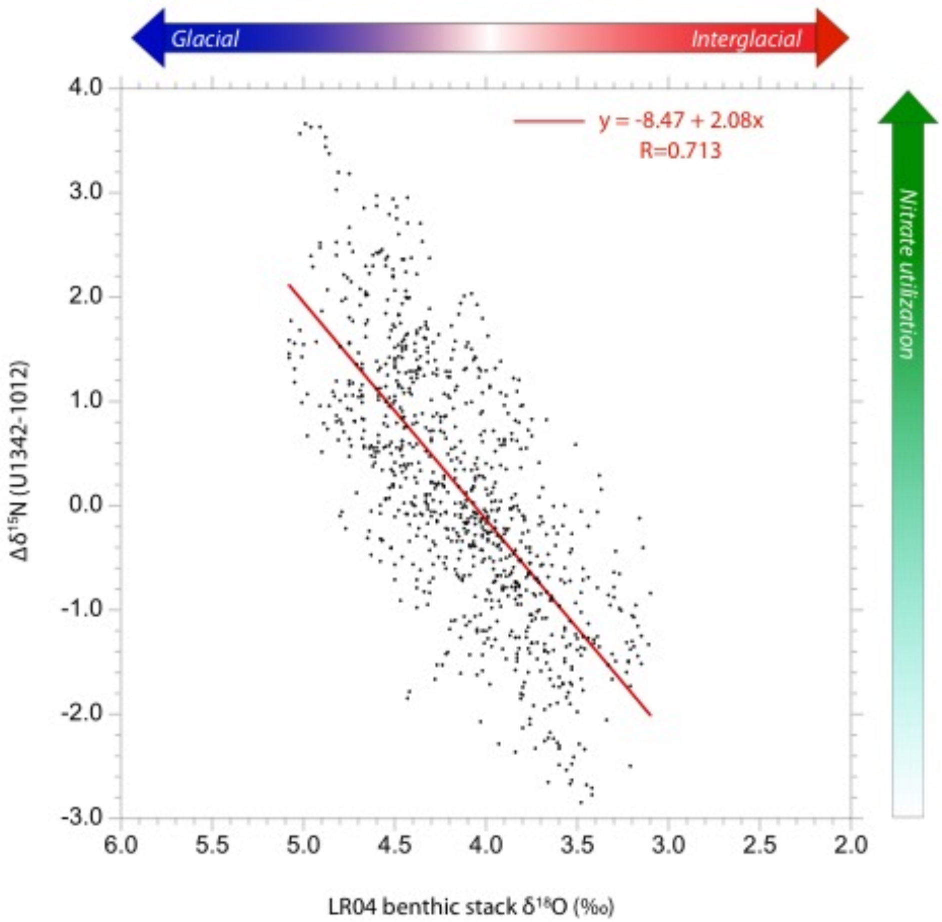

Figure B2. Cross-plot of $\Delta\delta^{15}N$ (U1342 $\delta^{15}N_{bulk}$ – Site 1012 $\delta^{15}N_{bulk}$) versus benthic $\delta^{18}O$ values from the LR04 stack from Lisiecki and Raymo [2005], including all data from 0-1.2 Ma. This plot illustrates a high correlation (R=0.713) between $\Delta\delta^{15}N$, a proxy for nitrate utilization at Site U1342, and LR04 $\delta^{18}O$, global climate characterization representing global ice sheet volume and oceanic temperature. Relatively high nitrate utilization (high $\Delta\delta^{15}N$) is consistently found during glacial climates (marked by high values of $\delta^{18}O$). These data, along with statistical results presented in the main article and spectral analysis results shown in Table 1 (Main Text) and Appendix Figures B3 and B4, indicate that subarctic Pacific nitrate utilization was consistently enhanced during glacials over the last 1.2 Myr.

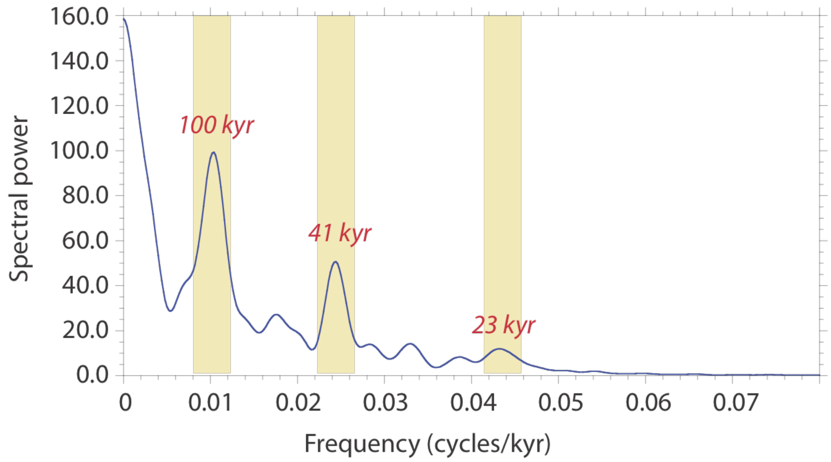

Figure B3. Blackman-Tukey spectral analysis of $\Delta\delta^{15}N$ (U1342-1012), indicating prominent frequencies for U1342 nitrate utilization (blue line) correspond with Milankovitch orbital cycles (highlighted with yellow bars), primarily at 100-kyr periodicity.

Table B2. Coherency values (≥0.70) of cross-spectral analysis results corresponding to phase values in Table 1 in the main text.

	100 kyr periodicity	41 kyr periodicity	23 kyr periodicity
Solar insolation (min.) at 65°N[1]	-	0.90	0.83
U1341 biogenic opal (%) (min.)[2]	-	-	0.70
China loess magnetic susceptibility (min.)[3]	-	0.70	0.72
EPICA pCO_2 (min.)[4]	0.94	0.82	0.70
LR04 $\delta^{18}O$ (max. glacial)[5]	0.96	0.94	0.90
EPICA dust mass[6]	0.93	0.74	0.73
Pacific Southern Ocean iron (wt.%)[7]	0.89	0.82	-

The datasets used in the cross spectral analyses are from [1]Laskar et al., 2004; [2]Iwasaki et al., 2012; [3]Clemens et al., 2008; [4]Luthi et al., 2008; [5]Lisiecki and Raymo, 2005; [6]Lambert et al., 2008; [7]Lamy et al., 2014.

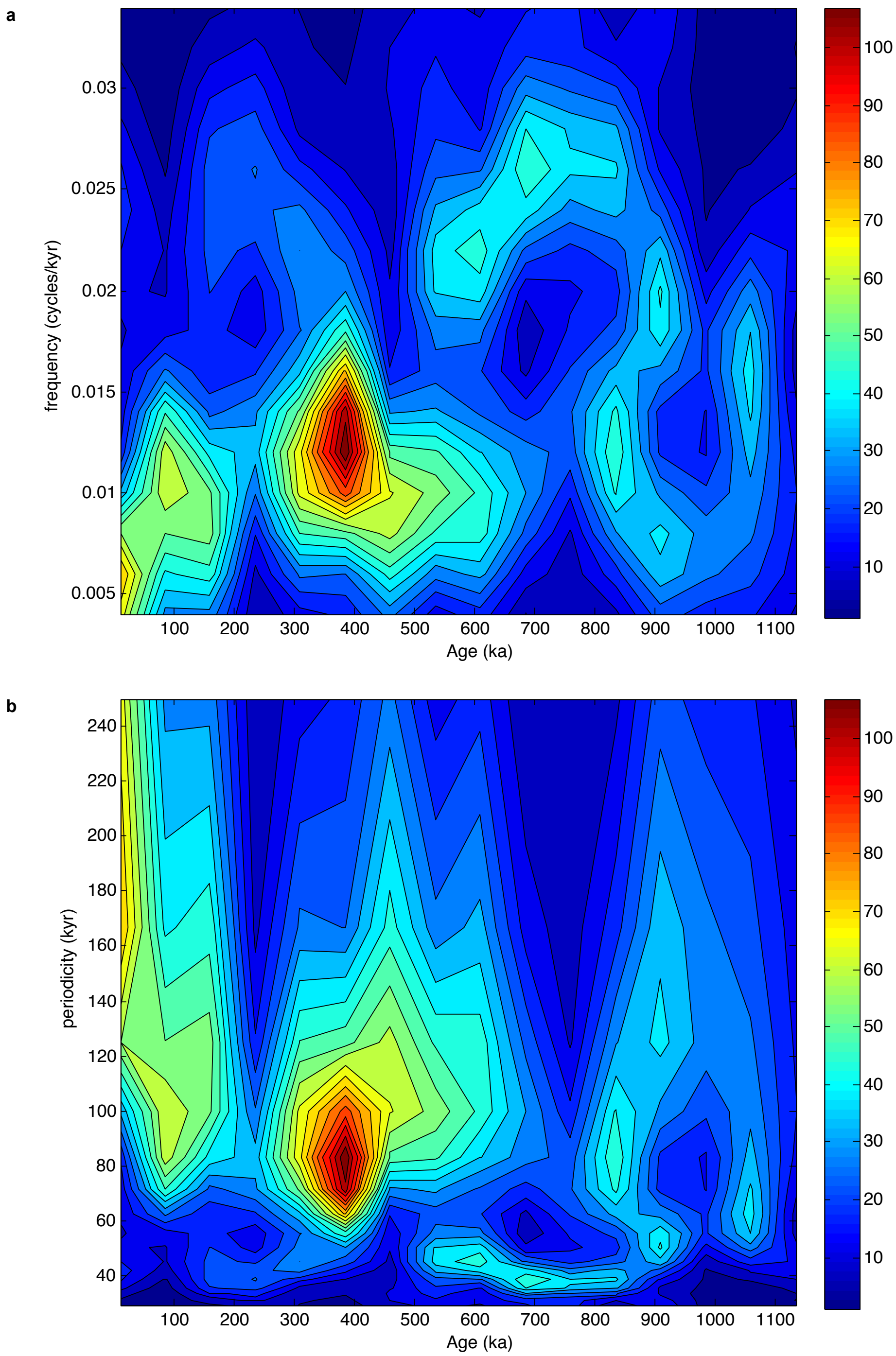

Figure B4. Evolutionary power spectra of $\Delta\delta^{15}N$ (U1342 $\delta^{15}N_{bulk}$ – Site 1012 $\delta^{15}N_{bulk}$) showing **(a)** frequency and **(b)** periodicity, over the last 1.2 Myr. Analyses were conducted in AnalySeries2.0 [Paillard et al., 1996] using the Blackman-Tukey method.

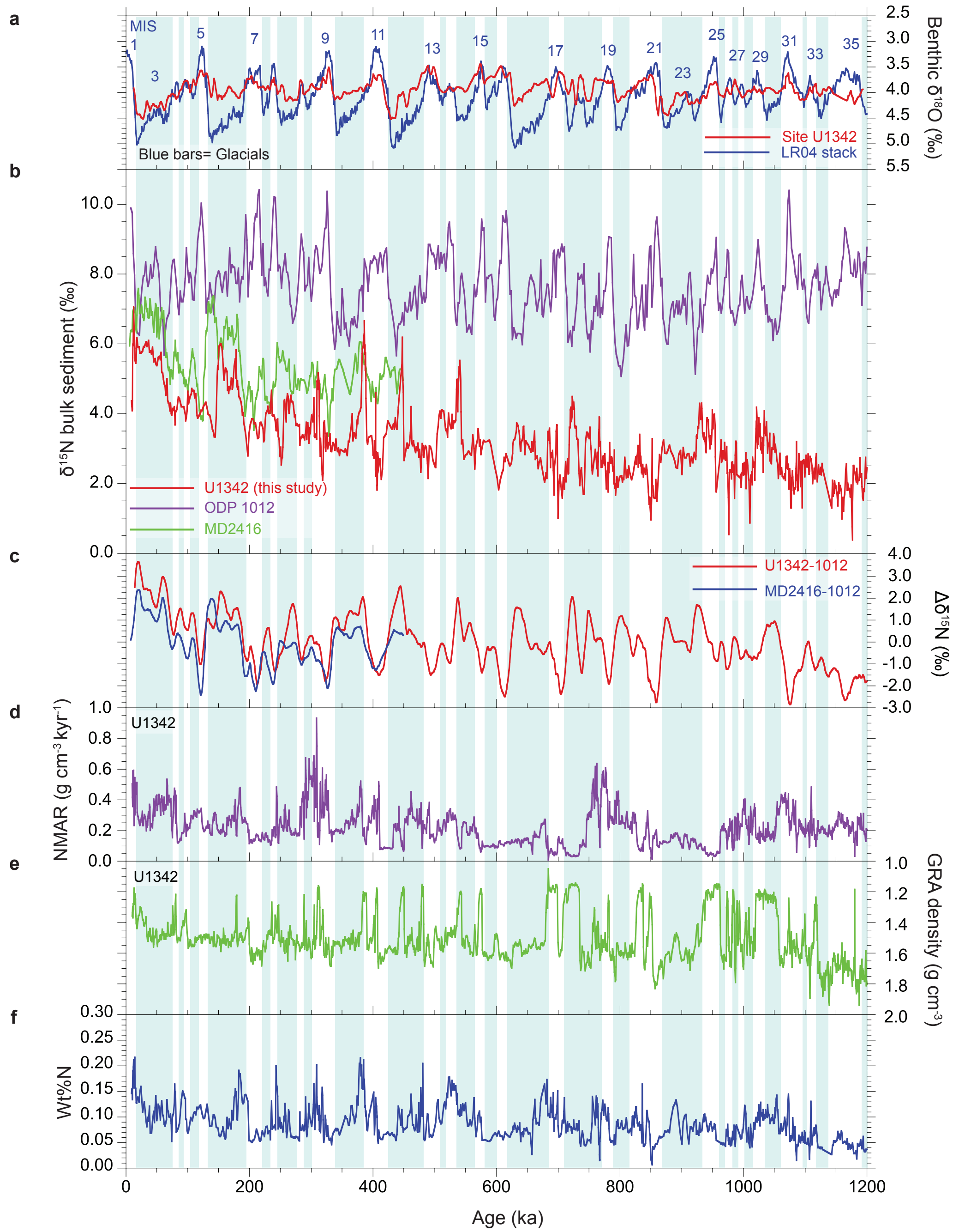

Figure B5. Comparison of nitrogen isotope and productivity records from 1.2 Ma. (a) Records of benthic foraminiferal $\delta^{18}O$ from the LR04 benthic stack (blue) [Lisiecki and Raymo, 2005], reflecting global changes in ice volume and oceanic temperature. Glacial intervals, where LR04 $\delta^{18}O \geq 4.0$‰, are highlighted with blue vertical bars. Marine Isotope Stages (MIS) are marked with blue numbers. Benthic $\delta^{18}O$ stratigraphy from Site U1342 (red) [Knudson and Ravelo, 2015] indicates that the U1342 record was continuous to 1.2 Ma. **(b)** Bulk sedimentary $\delta^{15}N$ records from Bering Sea site U1342 (this study; red line); Eastern Tropical North Pacific site ODP 1012 (violet) from Liu et al. [2005], which is used here to represent a record of $\delta^{15}N_{nitrate}$; and western subarctic Pacific site MD2416 (green) from Galbraith et al. [2008]. **(c)** $\Delta\delta^{15}N$ (nitrate utilization) record at Site U1342 (this study; red), calculated as (U1342 $\delta^{15}N_{bulk}$ – Site 1012 $\delta^{15}N_{bulk}$), shows good agreement with a shorter record of $\Delta\delta^{15}N$ from site MD2416, calculated as (MD2416 $\delta^{15}N_{bulk}$ – Site 1012 $\delta^{15}N_{bulk}$) from Galbraith et al. [2008] (blue). **(d)** Nitrogen mass accumulation rate (NMAR) at Site U1342, representing a local record of primary productivity. **(e)** Sediment density measured by gamma ray attenuation (GRA) at Site U1342 from Expedition 323 Scientists [2011], in which low values indicate the increased presence of biogenic sediments. **(f)** U1342 weight percent N (wt%N), another proxy for local primary productivity. While nitrate utilization ($\Delta\delta^{15}N$) at both U1342 and MD2416 is enhanced during glacials, changes in local primary productivity do not consistently vary with glacial/interglacial changes and nitrate utilization, demonstrating that primary productivity is not primarily responsible for increased glacial nitrate utilization in the subarctic Pacific.

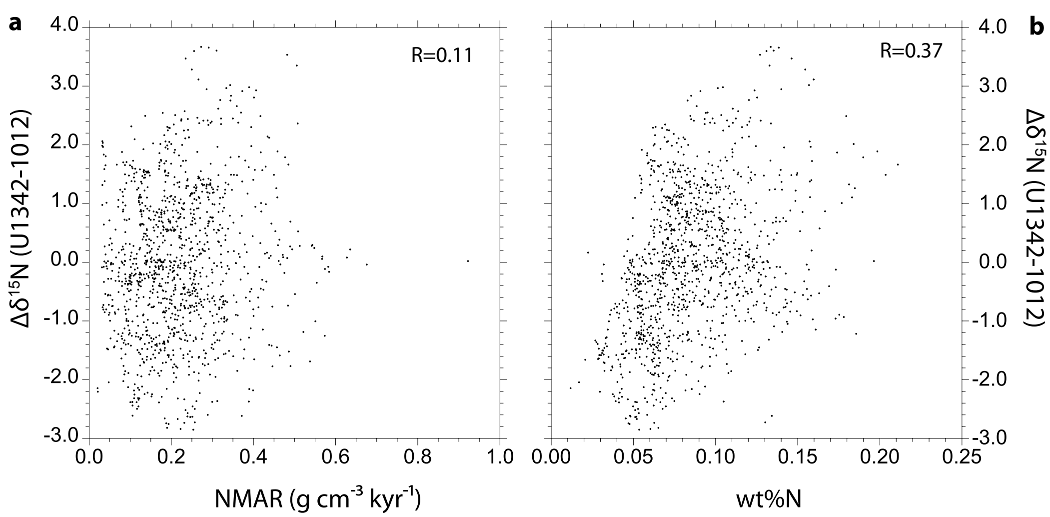

Figure B6. Cross-plot of $\Delta\delta^{15}N$ (U1342 $\delta^{15}N_{bulk}$ – Site 1012 $\delta^{15}N_{bulk}$) versus **(a)** U1342 nitrogen mass accumulation rate (NMAR) and **(b)** U1342 wt%N. Low correlation between nitrate utilization proxy, $\Delta\delta^{15}N$, and productivity proxies, NMAR and wt%N, provide evidence that fluctuations in primary productivity were not the main control over nitrate utilization at Site U1342 over the past 1.2 Myr. These results imply that enhanced physical water column stratification was likely the most important mechanism controlling nitrate utilization.

References Cited

Cooper, L. W., C. Lalande, R. Pirtle-Levy, I. L. Larsen, and J. M. Grebmeier (2009), Seasonal and decadal shifts in particulate organic matter processing and sedimentation in the Bering Strait Shelf region, Deep-Sea Research Part II-Topical Studies in Oceanography, 56(17), 1316-1325.

Expedition 323 Scientists (2011), Site U1342. In Takahashi, K., Ravelo, A.C., Alvarez Zarikian, C.A., and the Expedition 323 Scientists. Proceedings of the Integrated Ocean Drilling Program, 323: Tokyo (Integrated Ocean Drilling Program Management International, Inc.)

Galbraith, E. D., M. Kienast, S. L. Jaccard, T. F. Pedersen, B. G. Brunelle, D. M. Sigman, and T. Kiefer (2008), Consistent relationship between global climate and surface nitrate utilization in the western subarctic Pacific throughout the last 500 ka, Paleoceanography, 23(2).

Guo, L. D., and R. W. Macdonald (2006), Source and transport of terrigenous organic matter in the upper Yukon River: Evidence from isotope ($\delta^{13}C$, $\Delta^{14}C$, and $\delta^{15}N$) composition of dissolved, colloidal, and particulate phases, Global Biogeochemical Cycles, 20(2).

Guo, L. D., T. Tanaka, D. Wang, N. Tanaka, and A. Murata (2004), Distributions, speciation and stable isotope composition of organic matter in the southeastern Bering Sea, Marine Chemistry, 91(1-4), 211-226.

Knudson, K. P., and A. C. Ravelo (2015), North Pacific Intermediate Water circulation enhanced by the closure of the Bering Strait, Paleoceanography (in press).

Laskar, J., P. Robutel, F. Joutel, M. Gastineau, A. C. M. Correia, and B. Levrard (2004), A long-term numerical solution for the insolation quantities of the Earth, Astron. Astrophys., 428(1), 261–285.

Lisiecki, L. E., and M. E. Raymo (2005), A Pliocene-Pleistocene stack of 57 globally distributed benthic $\delta^{18}O$ records, Paleoceanography, 20(1).

Liu, Z. H., M. A. Altabet, and T. D. Herbert (2005), Glacial-interglacial modulation of eastern tropical North Pacific denitrification over the last 1.8-Myr, Geophysical Research Letters, 32(23).

McClelland, J. W., A. Townsend-Small, R. M. Holmes, F. F. Pan, M. Stieglitz, M. Khosh, and B. J. Peterson (2014), River export of nutrients and organic matter from the North Slope of Alaska to the Beaufort Sea, Water Resources Research, 50(2), 1823-1839.

Meyers, P. A. (1994), Preservation of elemental and isotopic source identification of sedimentary organic matter, Chemical Geology, 114(3-4), 289-302.

Paillard, D. L., L. Labeyrie, and P. Yiou (1996), Machintosh program performs time-series analysis, in Eos Trans AGU, edited.

Riethdorf, J. R., B. Thibodeau, M. Ikehara, D. Nurnberg, L. Max, R. Tiedemann, and Y. Yokoyama (2015), Surface nitrate utilization in the Bering Sea since 180 ka BP: Insight from sedimentary nitrogen isotopes, Deep Sea Research II, in press.